Exploration of Aggregation and Multivalency as Viral Inhibition Strategies

by

Swechchha Pradhan

A Dissertation Presented in Partial Fulfillment
of the Requirements for the Degree
Doctor of Philosophy

Approved August 2022 by the
Graduate Supervisory Committee:

Rizal Fajar Hariadi, Chair
Ian B. Hogue
Arvind Varsani
Qiang 'Shawn' Chen

ARIZONA STATE UNIVERSITY

December 2022

ABSTRACT

Scientists are entrusted with developing novel molecular strategies for effective prophylactic and therapeutic interventions. Antivirals are indispensable tools that can be targeted at viral domains directly or at cellular domains indirectly to obstruct viral infections and reduce pathogenicity. Despite their transformative potential in healthcare, to date, antivirals have been clinically approved to treat only 10 out of the greater than 200 known pathogenic human viruses. Additionally, as obligate intracellular parasites, many virus functions are intimately coupled with host cellular processes. As such, the development of a clinically relevant antiviral is challenged by the limited number of clear targets per virus and necessitates an extensive insight into these molecular processes. Compounding this challenge, many viral pathogens have evolved to evade effective antivirals. Therefore, a means to develop virus- or strain-specific antivirals without detailed insight into each idiosyncratic biochemical mechanism may aid in the development of antivirals against a larger swath of pathogens. Such an approach will tremendously benefit from having the specific molecular recognition of viral species as the lowest barrier. Here, I modify a nanobody (anti-green fluorescent protein) that specifically recognizes non-essential epitopes (glycoprotein M-pHluorin chimera) presented on the extra virion surface of a virus (Pseudorabies virus strain 486). The nanobody switches from having no inhibitory properties (tested up to 50 μM) to ~3 nM IC_{50} in *in vitro* infectivity assays using porcine kidney (PK15) cells. The nanobody modifications use highly reliable bioconjugation to a three-dimensional wireframe deoxyribonucleic acid (DNA) origami scaffold. Mechanistic studies suggest that inhibition is mediated by the DNA origami scaffold bound to the virus particle, which obstructs the internalization of the viruses into cells, and that inhibition is enhanced by avidity resulting from multivalent virus and scaffold interactions. The assembled nanostructures demonstrate negligible cytotoxicity (<10 nM) and sufficient stability, further supporting their therapeutic potential. If translatable to other viral species and epitopes, this approach may open a new strategy that leverages existing infrastructures – monoclonal antibody development, phage display, and in vitro evolution - for rapidly developing novel antivirals *in vivo*.

To my family I give everything.

To my mother, Shubhechhya, who embodies strength and grace like the flowing rivers, who instilled in me the value of good education and independence, who encouraged me to have dreams bigger than what defines our life at present, and above all, who taught me to find joys in moments of life that would otherwise just pass by.

To my father, Uttam, and my sister, Sneha, for their outpouring of love, laughter, and emotional support, that kept me afloat on this arduous journey.

To my perfect partner and my biggest cheerleader, Abhishek, for always meeting me where I am and showing me love so calm and fierce that I have nothing but gratitude in my heart.

Be like the flowing river,

Silent in the night.

Be not afraid of the dark.

If there are stars in the sky, reflect them back.

If there are clouds in the sky,

Remember, clouds, like the river, are water,

So, gladly reflect them too,

In your own tranquil depths.

- Manuel Bandeira

ACKNOWLEDGEMENTS

This dissertation would not have been successful without the help of many great people. To begin with, I would like to express my profound appreciation to Dr. Rizal Hariadi, my advisor and committee chair, for his unwavering support and continued guidance. His passion for science and dedication to research and teaching are unassuming and inspirational. He put great faith in me by welcoming me to the Hariadi lab when the world seemed to be shutting down at the beginning of 2020. He has continued to nurture my scientific growth and professional prowess throughout. I thank him for his empathy and kindness, reflected during many occasions and conversations that extended beyond science and research.

I want to extend my sincere thanks to Dr. Ian Hogue, Dr. Arvind Varsani, and Dr. Shawn Chen, my committee members, who generously provided me with knowledge, expertise, and constructive feedback throughout my doctoral journey. Special thanks to Dr. Hogue, with whom I got the chance to collaborate on the virology part of my project, and to Dr. Varsani, with whom I published the first chapter of my dissertation.

I am deeply indebted to Dr. Carter Swanson, my mentor, without whom this endeavor would not have been possible. I have benefited immensely from his wealth of knowledge, critical feedback on all my experimental designs/data, meticulous editing of my manuscripts, and positive outlook at every stage of my research project. Every conversation with him has uplifted my spirit to push for one more experiment and have fun while at it. I have often walked out of our meetings with a clearer understanding of my data. The profound knowledge of science he has is reflected by the interdisciplinary perspectives he brings into our discussions and the clarity of his thoughts, which is something I hope to carry forward throughout my career. I am excited for all future students who will get a chance to be under his mentorship. Carter is not officially my Ph.D. co-advisor, but he may as well be.

Special thanks to my brilliant colleague and friend, Isadonna Tengganu, with whom I built the foundation of this project. We shared countless hours, tears, and laughs while designing and assembling the multivalent systems before proceeding with the *in vitro* work in mammalian cells. I wish her the absolute best in all her endeavors. Similarly, one of the most personally rewarding

experiences of my Ph.D. has been mentoring Chloe Leff and learning from her. She joined my project as an inquisitive and sharp undergraduate student and is now on the path of transforming into a brilliant scientist. There is no doubt in my mind that she has run more agarose gels than me during this project. I would be remiss if I did not mention my friend, Melissa Bergeman from the Hogue lab, who was very generous with her time and energy in teaching me to set up the PRV pathosystem. I would also like to thank Dr. Tarushyam Mukherjee and Tohma Taniguchi from the Hariadi lab, with whom I had the pleasure of collaborating in the final stages of this research project. I want to thank everyone from the Hariadi lab for being fantastic lab mates, constantly boosting peers, lending minds to troubleshoot, hands to help, and ears to unburden stories.

My family and friends deserve endless gratitude. I thank my closest friends, Dr. Farzaneh Moghaddam, Upama Shrestha, and Sapana Shakya, for their love and emotional support over the years and throughout all my highs and lows. I am lucky to know the happiness and excitement their hearts hold to see me arrive at the end of this journey. I am also grateful to my Arizona friends, Dr. David Menn and Hao Hu, who have welcomed me into their home as a family on multiple occasions. Together we have shared the best of food and the funniest of stories.

Lastly, I owe everything in my life to my mother. As far as I can recollect, she modeled passion and sincerity toward her work, giving it, her all, and always striving for more. Through her hard work and courage, I dared to dream of making a better life on my own outside of a small town in Gaindakot, Nepal. And it was her love and support that helped me persevere through the darkest phase of my graduate study. I can only try to learn the grace she armors in navigating through the different chapters of life, personally and professionally. From an early age, my father instilled in me the importance of taking risks and weathering storms, which still resonates with me. My sister is the biggest joy in my life. She inspires me to seek the path of least resistance and draw boundaries, all while being a thorough professional with kindness and compassion. Finally, I thank my best friend, biggest cheerleader, and life partner, Dr. Abhishek Shrestha, for his unconditional love. Thank you for seeing through me and giving me love with profound understanding. Words cannot express the love, respect, and gratitude I have in my heart for you. I couldn't have done this without you.

TABLE OF CONTENTS

CHAPTER Page

Page

APPENDIX

LIST OF TABLES

LIST OF FIGURES

CHAPTER 1

VIRAL AGGREGATION: THE KNOWNS AND UNKNOWNS

Abstract

Viral aggregation is a complex and pervasive phenomenon affecting many viral families. An increasing number of studies have indicated that it can modulate critical parameters surrounding viral infections, and yet its role in viral infectivity, pathogenesis, and evolution is just beginning to be appreciated. Aggregation likely promotes viral infection by increasing the cellular multiplicity of infection (MOI), which can help overcome stochastic failures of viral infection and genetic defects and subsequently modulate their fitness, virulence, and host responses. Conversely, aggregation can limit the dispersal of viral particles and hinder the early stages of establishing a successful infection. The cost-benefit of viral aggregation seems to vary not only depending on the viral species and aggregating factors but also on the spatiotemporal context of the viral life cycle. Here, we review the *knowns* of viral aggregation by focusing on studies with direct observations of viral aggregation and mechanistic studies of the aggregation process. Next, we chart the *unknowns* and discuss the biological implications of viral aggregation in their infection cycle. We conclude with a perspective on harnessing the therapeutic potential of this phenomenon and highlight several challenging questions that warrant further research for this field to advance.

Keywords: viral aggregation; multiplicity of infection; viral transmission; viral infectivity

1.1. Introduction

Although there are no standard definitions of a viral aggregate, historically, it has been used to refer to multi-unit structures such as assemblages of viruses belonging to either the same or different species/families. Over time, researchers have documented such multi-unit structures using different terminologies depending upon their composition and the spatiotemporal context of their occurrence. For instance, outside the host, the insect-infecting baculoviruses (family *Baculoviridae*) [1] and ascoviruses (family *Ascoviridae*) [2] are embedded within highly organized crystalline protein lattices called occlusion bodies (OBs). OBs confer viruses with stability and resistance against adverse environmental conditions for an extended period, particularly considering their host's cyclic and seasonal nature. Additionally, the OBs serve as transmission vehicles that facilitate the host-to-host transfer of multiple virions simultaneously. Similarly, several early studies have reported aggregates of influenza virus (family *Orthomyxoviridae*) [3], vaccinia virus (family *Poxvirus*) [4], poliovirus (family *Picornaviridae*) [5], reovirus (family *Reoviridae*) [5], adenovirus (family *Adenoviridae*) [6], and rotavirus (family *Reoviridae*) [7], primarily in the context of the virus production processes or as occurrences in environmental settings that are relevant to human health. Similarly, several animal-infecting RNA viruses, such as enterovirus (family *Picornaviridae*) [8], rotavirus, and norovirus (family *Caliciviridae*) [9], have been reported to shed inside extracellular vesicles (EVs), like exosomes and microvesicles, in multiple numbers. These viruses can hijack the host extracellular vesicle biogenesis machinery to facilitate their collective assembly, envelopment, and subsequent dissemination through a nonlytic pathway. Finally, tetherin, an interferon-inducible host protein, has been identified as an antiviral factor that inhibits the release of a variety of enveloped viruses from the host cells [10–13]. More recently, Sanjuan coined "collective infectious units" as an umbrella term encompassing several types of structures that mediate the collective delivery of multiple virions/viral genomes to the same cell and often modulate viral infectivity differently than free viruses [14]. Some of these structures, including polyploid virions, occlusion bodies, viral aggregates, and lipid cloaked virions, are described in greater detail in another review [14]. Given the context of this review, we have used the term *viral aggregate* to refer to multi-unit

structures comprising two or more virus particles without discriminating against their composition or causative factors responsible for their assembly.

In this review, we begin by summarizing the *knowns* of viral aggregation by providing a brief synopsis of historical studies that rather one-dimensionally focused on physicochemical parameters surrounding viral aggregation. We discuss the challenges faced by earlier studies and, concurrently, the limitations in our current knowledge of viral aggregation. We then explore the *unknowns* and expand the dimensionality of the field by discussing viral aggregation in light of viral pathogenesis. We critically assess a few studies that provide direct evidence of how viral aggregation affects their infectivity in simulated biological models. Next, to consider the implications of viral aggregation in the broader and largely ignored context of an infectious viral life cycle, we review studies providing correlations between viral aggregation and one or more components of their life cycle. We conclude by shedding light on the therapeutic potential of viral aggregation and formulating several challenging questions that need further investigation for this field to advance.

1.2. A Brief Historical Review of Studies on Viral Aggregation

A quick survey of available literature on viral aggregation reflects its fascinating scientific journey. More than eight decades ago, the first studies reported aggregates of plant-infecting tobacco mosaic virus (TMV, family *Virgaviridae*) [15] and animal-infecting influenza viruses [16] merely as undesirable technical artifacts causing inconsistencies in viral titers and the serum titers required to neutralize them. Studies that came in the 50s and 60s reported how aggregation compromised the “quality” of laboratory-propagated strains of different viruses by reducing their infectious titers as assessed by plaque assays [4,17]. In the environmental context, aggregates of poliovirus, reovirus, and adenovirus caused problems in water decontamination processes because of their enhanced resistance to disinfectants in comparison to monodispersed particles [18-20]. In the two decades that followed, scientific research mainly aimed at preventing or disintegrating viral aggregates to increase the infectious titer of laboratory-grown viral strains, minimize their batch-to-batch variations, and enhance the efficiency of virus neutralization in vitro and disinfection processes in the environment. These studies investigated the physicochemical parameters

influencing viral aggregation and subsequently underscored its role in viral transport, adsorption, and retention, mainly in water bodies and in vitro settings [5,20-27]. We have summarized them in the following two sections of this review.

A few other studies in the 60s and 70s showed the ability of aggregated vaccinia viruses and influenza viruses to overcome genetic defects and enhance their infectivity and survival in cultured cells [3,28]. For instance, the survival curves for vaccinia viruses showed a slower decline in their titers upon UV irradiation when they were in an aggregated state compared to their monodispersed form [28]. Another study showed that aggregation increased the infectious virus titer per genome and rescued the infective potential of mutant influenza viruses with defective genomes [3]. These studies established a potential correlation between viral aggregation and multiplicity reactivation—a phenomenon by which viable viruses are released from cells infected by two or more viruses, each with a uniquely defective genome.

It is important to note that for a long time, viral aggregation was only studied as a consequential phenomenon, with the main determinants being the physicochemical interactions virus particles have at different interfaces. A few studies in the 1980s started challenging this perspective when they reported membranous aggregates of several pathogenic viruses in fecal specimens of patients with gastroenteritis [6,7]. The electron microscopy (EM) images of some of these viruses are given in Table 1. The observed aggregates were neither technical artifacts nor seemed to result from interactions with other biomolecules such as cell debris, proteins, or antibodies. They postulated that these aggregates formed during virus maturation or assembly inside host cells [7]. These studies led the scientific community to question if aggregation could also be an intrinsic viral trait that happens during the viral infection cycle and influences their infectivity and pathogenicity. With the advances made in live-cell imaging and molecular biology, an increasing number of studies have reported the aggregation of different animal-infecting viruses with potential implications in their infectivity, fitness, and evolution. We have discussed them in separate sections of this review. However, since this field of research is relatively new, there is a lack of standard guidelines and definitions for better describing and differentiating viral aggregates.

Table 1. Microenvironments of different animal viruses either collected from biological sources or propagated in laboratories and their corresponding EM images of viral aggregation. Scale bars are indicated wherever possible. Panels a) through i) are republished with permission from the respective journals. All permissions are conveyed through the Copyright Clearance Center, Inc.

Virus	Family	Virus source	Microenvironment of virus and aggregating condition	Image	Ref.
Vaccinia	Poxvirus	Virus propagated in Earle's L cells in vitro	Purified virus particles were resuspended in PBS.	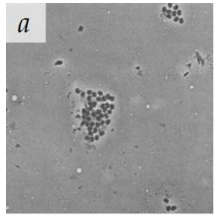	28
Human adenovirus 2	Adenoviridae	Virus propagated in A549 cells in vitro	Cell-associated virus (CAV) particles were resuspended in chlorine demand-free (CDF) grade water.	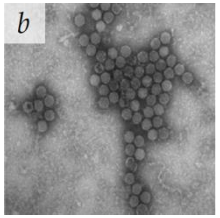	29
Adenovirus	Adenoviridae	Virus present in fecal specimens collected from patients with gastroenteritis	Fecal samples with virus particles were diluted in PBS.	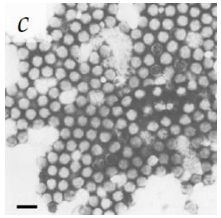 100nm	6

Rotavirus	Reoviridae	Virus present in fecal specimens collected from patients with gastroenteritis	Fecal samples with virus particles were diluted in water. Image shows aggregates of Rotavirus inside membranes.	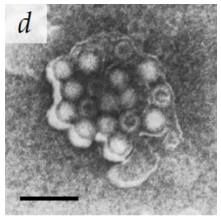 200 nm	7
Parvovirus	Parvoviridae	Virus present in fecal specimens collected from patients with gastroenteritis	Fecal samples with virus particles were diluted in water. Image shows aggregates of Parvovirus inside membranes.	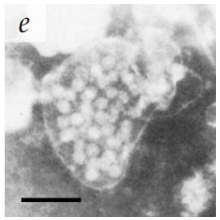 100 nm	7
Norwalk virus	Caliciviridae	Virus present in fecal specimens collected from patients with gastroenteritis	Fecal samples with virus particles were diluted in water. Image shows three Norwalk virus particles associated with a fuzzy membranous element.	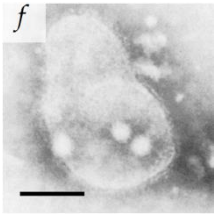 100 nm	7
Poliovirus	Picornaviridae	Virus propagated in HEp-2 cells in vitro	Purified virus particles were diluted in buffers of different pH. Aggregation was observed in buffer with low pH which was reversible when returned to neutral pH.	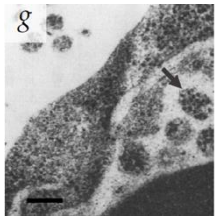 200 nm	30

Reovirus	Reoviridae	Virus propagated in L cells in vitro	Purified virus particles were diluted in buffers of different pH. Aggregation was observed in buffer with low pH which was reversible when returned to neutral pH.	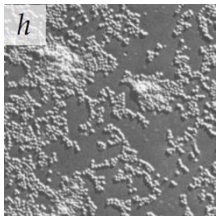	5
West Nile Virus	Picornaviridae	Virus propagated in Vero cells in vitro	Images show WNV particles infecting P388D1 cells. i) Aggregate of WNV observed after binding for 2h at 0ºC. ii) Aggregate of WNV in phagosomes observed 15-30 min after warming to 37 ºC.	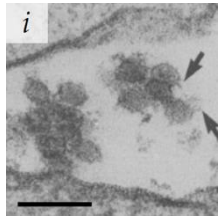 100 nm	31

It is safe to assume that the analyses in many historical studies were technologically challenged, because of which their appeal could be limited to current virologists. Nevertheless, these fundamental concepts laid the foundations for many of the basic laboratory practices in virology followed to date. Furthermore, these studies highlighted that viral aggregation could have crucial public health and biotechnology implications by providing insight into how the virus production processes in laboratory settings emulate natural environments and into the stability of viable viruses following groundwater transport and wastewater treatments.

1.2.1. Factors Influencing Viral Aggregation

The interplay between viruses and different biotic and abiotic factors present in their microenvironment plays a vital role in viral aggregation. In suspension, viral aggregation is affected by several physicochemical parameters of the aqueous medium, including but not limited to pH, ionic strength and composition, and temperature. Some studies investigating these parameters have shown that aggregation can be reversible for some viruses. For some viruses, these parameters also govern the degree of reversibility of viral aggregation [5,21,24,32].

Viruses get their net charge from different functional groups present in their phospho- lipid envelope or capsid proteins. Their isoelectric point (pI) ranges from 1.9 to 8.4 [33], and they tend to aggregate near their pI, where their net neutral charge cancels the electrostatic repulsion between particles [34–36]. Lowering the pH also favors viral aggregation and, for some viruses, this could recapitulate the acidic conditions inside endosomes that trigger their uncoating and subsequent release into the cytoplasm [37,38]. Likewise, ionic strength and composition affect viral aggregation by compressing or expanding the electric double layer (EDL) surrounding viral particles [34,35,39,40].

Cations and cationic polymers complex with the exposed and deprotonated carboxylic groups of polar amino acids on the viral surface and reduce their zeta potential [40]. Divalent cations aggregate viral particles more strongly than monovalent cations due to increased charge shielding and EDL shrinking [34,35,40]. On the other hand, anions and anionic polymers can add to the EDL

and increase the zeta potential by sequestering cations and adsorbing to the viral surfaces, preventing charge shielding and virus aggregation [34,39].

Similarly, temperature influences viral aggregation, with more aggregates forming at higher temperatures. Viruses are colloidal particles, and as such, their Brownian motion and subsequent collision rate rise at higher temperatures leading to more aggregation. Several studies exploring the kinetics of viral aggregation as a function of these physico-chemical parameters show that the process is mainly virus-specific and depends on the surface properties of viral particles. For instance, four genogroups of F-specific RNA bacteriophages, MS2, GA, Qβ, and SP, showed different aggregation behaviors over a broad range of pH (1.5–7.5) and ionic strength (1–100 mM NaNO3) conditions tested [41]. While MS2 only aggregated near their isoelectric point (pH = 4) regardless of the ionic strength, Qβ aggregated at low pH and high ionic strength, and GA and SP both aggregated over the entire range of tested conditions.

Most earlier studies investigated these parameters from a technical standpoint, either to improve the monodispersity of viral particles in purified viral stocks or to improve the inactivation kinetics of viruses in different settings. They have been discussed more extensively in another review [42]. A key challenge for this expanding field of scientific study is to link these primarily in vitro described environmental parameters to those that are likely to be encountered within the viral life cycle in a host. Studies have shown that viral aggregates are a non-negligible fraction of their populations and maybe more frequently prevalent in biological fluids than estimated or known in vitro [9,43]. Therefore, these findings will be critical in determining the nature of interventions needed to contain or eliminate viruses, particularly for those causing the emergence/re-emergence of infectious diseases. Some of the recent work has begun to address that challenge by exploring the aggregation of vesicular stomatitis virus (VSV, family *Rhabdoviridae*) under physiologically relevant conditions [43,44]. VSV is an economically significant livestock virus that primarily infects the oral cavity and is shed in the host saliva. Microscopic analysis of VSV-infected cultures showed two phenotypically distinct genetic variants of VSV, one expressing mCherry and the other expressing GFP, aggregated in the presence of human and cow saliva [43]. Another work revealed that unlike protein-lipid interactions driving VSV aggregation in purified stocks [43], VSV

aggregation in saliva was protein-driven [44]. Proteomic analysis revealed the differential expression of 18 different genes among saliva donors that positively correlated with their aggregating potential. Furthermore, fibrinogen gamma chain (FGG) protein was identified as the molecular factor strongly promoting VSV aggregation in saliva. For most other infectious viruses, the physicochemical and molecular determinants of viral aggregation in environments recapitulating viral hosts remain to be investigated.

1.2.2. The Research Landscape of Viral Aggregation in Comparison to Their Bacterial Counterparts

Analogizing viral aggregation to its bacterial counterpart, aggregation in bacteria has been rather extensively studied. Bacterial aggregation is a corollary defense mechanism against environmental stress and immunological response [45–47]. Distinct genetic processes regulate bacterial aggregation in response to stress factors such as harsh environmental conditions and attacks from predators, primarily bacteriophages. Studies have shown multiple bacterial species including *Escherichia coli* [48], *Pseudomonas aeruginosa* [49], *Legionella pneumophilia* [50], *Staphylococcus aureus* [51], and *Neisseria meningitidis* [52] converge on this strategy. For a more in-depth insight into this area, we refer readers to another review discussing molecular mechanisms underlying bacterial aggregation and its role in bacterial pathogenesis [53].

In contrast, the genetic and molecular mechanisms driving viral aggregation are largely unresolved and unfortunately understudied. Although several studies claim viral aggregation as an intrinsic phenomenon, our understanding of its role in viral population dynamics and evolution is limited. What is striking from the reviewed literature is that aggregation spans across various viral families, including enveloped and non-enveloped viruses, segmented and non-segmented viruses, and DNA and RNA viruses. So, aggregation may be more broadly common than is known and potentially with a fitness advantage to some viruses.

1.3. Viral Aggregation and the Stoichiometry of MOI

Viral populations encounter several viral factors and host barriers as bottlenecks during their infection cycle in the context of both intra- and inter-host transmission. As obligate intracellular parasites, viruses depend entirely on the host cell and use a “Trojan horse” machinery to encode viral proteins and replicate their genetic material. The multiplicity of infection (MOI) is the most critical parameter affecting their infection cycle at the cellular level. MOI, defined as the ratio of infectious virions to susceptible cells, controls the gene copy number and determines the fate of the infected cell. An MOI higher than 1 sets the stage for genetic exchange [54], competition [55], or complementation [56] to occur between co-infecting viral genomes. Viral aggregation is associated with increasing MOI and the subsequent co-transmission of multiple viral genomes to the same cell [4,6,7,28,40,57]. Therefore, it is essential to study how it can regulate these phenomena and impact the broader viral pathogenesis, fitness, diversity, and evolution spectrum.

1.3.1. The Stochasticity in Early Events of Viral Infection Often Leads to Unproductive Infection

Historically, the “one-hit” paradigm in virology views viral particles as independent and optimal infectious units such that one infectious unit is enough to establish a productive infection [58]. According to this theory, at high dilutions of virus particles, one infectious particle gives rise to one plaque, and the number of plaques is directly proportional to the concentration of the virus. Most mammalian viruses show a linear relationship between the number of plaques and dilution of virus plated, holding the framework true in titration assays to determine viral titers and the infectious dose. However, one of the major limitations of this framework stems from its failure to address the stochastic fluctuations that challenge early events of viral infections and render most infections futile.

As with the vast majority of pathosystems, the mere existence of a virus in a suitable microenvironment with many permissible and susceptible host cells is not sufficient to guarantee successful infection. Viral infections are stochastic and discrete events, influenced by several viral factors and host barriers, which pose challenges of thwarted outcomes in each step of their life

cycle. Several studies have reported cell-to-cell variability surrounding different phases of viral infections, including viral endocytosis [59], virus progeny titers, RNA levels [60], and progeny production modes [61]. The variability is attributed to noisy biochemical processes involved in viral infections. For instance, stochastic fluctuations accounted for up to 90% of failed single-hit infections with influenza A virus (IAV) [60]. Apart from different components of the host immune responses which can neutralize them, there are other mechanical, physicochemical, and genetic barriers for viruses to overcome, the permutations and combinations of which can further hinder their infection cycle.

1.3.2. Segmented and Multipartite Viruses Have Low Infection Probability

Although many RNA and DNA viruses show non-infectiousness and low infectivity, they are more prominent in viruses with either segmented genomes [62] or multipartite genomes [63,64]. Segmented viruses have the information required for the infection cycle divided between two or more nucleic acid segments, typically found together in one capsid. However, not all segments are needed for the virus to be infectious. For instance, influenza A virus (IAV) has eight single-stranded RNA segments, each encoding at least one viral protein [65-67]. Studies have shown that single-hit IAV infections predominantly failed to replicate and resulted in semi-infectious viral particles lacking one or more of the essential viral proteins [60,68,69]. Multipartite viruses are slightly different and instead have their genetic information divided into segments packaged into independent viral capsids [70]. The dose-response kinetics of Guaico Culex virus (GCXV, family *Flaviviridae*), a five-segmented RNA virus, showed that establishing a productive infection required at least three different particles [71]. Multipartite genomes underscore the interdependency of viruses in these systems, necessitating the co-transmission of several virus particles into one host cell to form a complete genome set and increase the likelihood of a productive infection. The cost-benefit analysis of these peculiar genome organization systems in viruses has posed some of the most exciting puzzles for virologists concerning the importance of virus genome integrity for successful infection cycles [60,71].

The stochastic, genetic, structural, and host barriers are magnified in low MOI or single-hit infections and may enable viruses to adopt mechanisms more conducive to preserving their genome integrity. Several studies have shown that aggregation increased the cellular MOI and enhanced viral infectivity [3,8,43]. The substantial body of work on collective infectious units in viruses describes several structural systems that support viral co-transmission, including polyploid virions, virion aggregates, viral occlusion bodies, and virions with extracellular vesicles [14,72]. All of these structures assist in increasing cellular MOI and subsequently delivering multiple viral genomes to the same cell, which can help in overcoming the replication barriers mentioned above required

1.4. Viral Aggregation in the Context of Infectious Viral Life Cycle

Viral aggregation impacts different aspects of viral pathogenesis including infectivity, antibody escape, and antiviral resistance. Some studies have demonstrated an enhancement of viral infectivity when viruses were in an aggregated state as opposed to being in a monodispersed state [3,9,73,74]. On the other hand, some studies have demonstrated that viral aggregation compromised the replication, transmission, and survival of viruses [75–77]. We have summarized the impacts of viral aggregation on the viral life cycle and pathogenesis in Table 2. To better understand the apparent discrepancy concerning the cost-benefit of viral aggregation, we have categorized the events in the life cycle of an infectious virus into three distinct stages, including viral motion to find a suitable host, replication inside the host cell, and release from the host cell. Aggregation may favor or oppose the infecting viruses in each stage, subsequently influencing their outcomes and determining their fate.

Table 2. Effects of viral aggregation on the life cycle and pathogenicity of different animal-infecting viruses

Virus	Genetic Material	Enveloped	Family	Size (nm)	Effect of aggregation on infection cycle	Ref.
Baculovirus	DNA	Enveloped	Baculoviridae	200-450	Co-transmission of multiple viral genomes leading to maintenance of genetic diversity [78], enhanced viral protection [79]	[78,79]
Coronavirus	RNA	Enveloped	Coronaviridae	80-120	Correlated with loss of viral infectivity although not determined as the only cause	[77]
Echovirus type 4	RNA	Non-enveloped	Picornaviridae	30	Enhanced protection against neutralizing antibodies	[26]
Enterovirus	RNA	Non-enveloped	Picornaviridae	30	Enhanced protection against neutralizing antibodies [8,26], enhanced infectivity [8]	[8,26]
Hepatitis A virus	RNA	Non-enveloped	Picornaviridae	27	Viral aggregates inside host-derived membranes showed enhanced infectivity and resistance against antibodies	[74]
Human Immunodeficiency virus	RNA	Enveloped	Retroviridae	120	Tetherin-induced viral aggregates showed reduced infectivity due to impairment of their fusion capabilities [75], enhanced cell-to-cell transfer either by mediating the accumulation of virions on the cell surface or by regulating the integrity of the virological synapse [80]	[75,80]
Human T-lymphotropic virus	RNA	Enveloped	Retrovirus	120	Facilitated attachment of virus to target cell surface	[81]
Influenza A virus	RNA	Enveloped	Orthomyxoviridae	80-120	Enhanced infective capacity when aggregated by nucleohistones [3], enhanced opsonization and uptake by neutrophils when aggregated by collectins, defensins, or antiviral peptides [76,82,83], decrease in viral uptake and replication by host cells [84]	[3,76,82-84]
Poliovirus	RNA	Non-enveloped	Picornaviridae	30	Aggregates formed in low pH showed decrease in infectious viral titer [32,85] and promoted coinfection that correlated with the mutation frequency and rescue of heavily mutagenized viruses [85]. Vesicle-enclosed viral aggregates showed non-lytic release, enhanced viral spread in vitro and pathogenicity in vivo [86]	[32,85,86]
Vaccinia virus	DNA	Enveloped	Poxvirus	250-360	Enhanced viral survival via increase in cellular MOI	[28,57]
Rotavirus	RNA	Non-enveloped	Reoviridae	55-70	Vesicle-enclosed aggregates showed enhanced infectivity in vitro and in vivo by overcoming replication barriers associated with low MOI	[9]
Vesicular somatitis virus	RNA	Enveloped	Rhabdoviridae	70	Co-transmission of multiple viral genomes to same cells [43], saliva-induced viral aggregates showed enhanced viral fitness via increase in per capita progeny production [73]	[43,73]
West Nile Virus	RNA	Enveloped	Flaviviridae	40-65	Slower uptake and phagocytosis by macrophage-like cells	[31]

1.4.1. Viral Aggregation Influencing Viral Motion

Viruses are colloidal particles with defined densities and intrinsic half-lives. Owing to the rapid decay rate of viruses, it is a race against time for them to find permissible host cells before they start degrading [87]. Devoid of locomotory organs, viruses travel through diffusion in their microenvironment to establish initial contact with host cells and start their infection cycle. Aggregation slows down diffusion, decreases the surface-to-volume ratio, and lowers the number of effective viral particles (Figure 1 A, B). In addition, it reduces the frequency of viral adsorption onto host cells and their likelihood of reaching the maximum number of host cells.

To traverse the distance to their host cells before degradation, they rely on their Brownian motion and the movement of their surrounding fluid. Upon breaking down the effects of aggregation on the viral life cycle, we think the distribution of viral particles will be consequential based on the following rationale despite this not being tested experimentally. The mean squared displacement $\langle r^2 \rangle$ of viral particles over time t is defined by the equation of mean squared displacement (MSD) for a three-dimensional Brownian motion, given by

$$r^2 = 6Dt, \tag{1}$$

where D is the diffusion coefficient. Assuming a viral particle/aggregate as a sphere of an effective radius r, the diffusion coefficient of the viral assembly is described by the celebrated Stokes–Einstein equation,

$$D = \frac{k_B T}{6\pi\eta r}, \tag{2}$$

where k_B is the Boltzmann constant, T is the absolute temperature in Kelvin, and η is the viscosity of the medium. For example, the diffusion coefficient of a single IAV particle has been measured to be ~800 nm^2/s [88] with a half-life of ~3 h [89]. Using these numbers, Equation (1) yields ~7 μm for the average displacement after 3 h. The calculated mean-squared displacement is less than the typical size of a mammalian cell (10–100 μm). Diffusion is, therefore, one of the limiting factors determining the success of the earliest events in infection. Viral particles with a size of less than 100 nm can form aggregates that are up to 1000 nm [6]. Regarding the excursion to reach the host cell, monodispersed particles diffuse faster than the aggregated particles, and so they will collide with the host cell surfaces more frequently. Assuming host cells as uniform spheres of radius a and

invoking a diffusion-limited reaction, the number of viral particles arriving per unit of time is given by

$$\frac{dN}{dt} = 4\pi Dac, \tag{3}$$

Where c is the concentration of the viral monomers/aggregates. Moreover, the effective number of viral particles reaching more host cells is higher when they are in a monodispersed state than when they are in an aggregated state by a factor of N/n, where n is a positive integer and denotes the mean size of the viral aggregates. Viruses with a shorter half-life will reach even a smaller number of host cells before decay. The poor transduction efficiency of retroviruses has been attributed to their short half-life, limiting the distance they can travel in solution by Brownian motion [90].

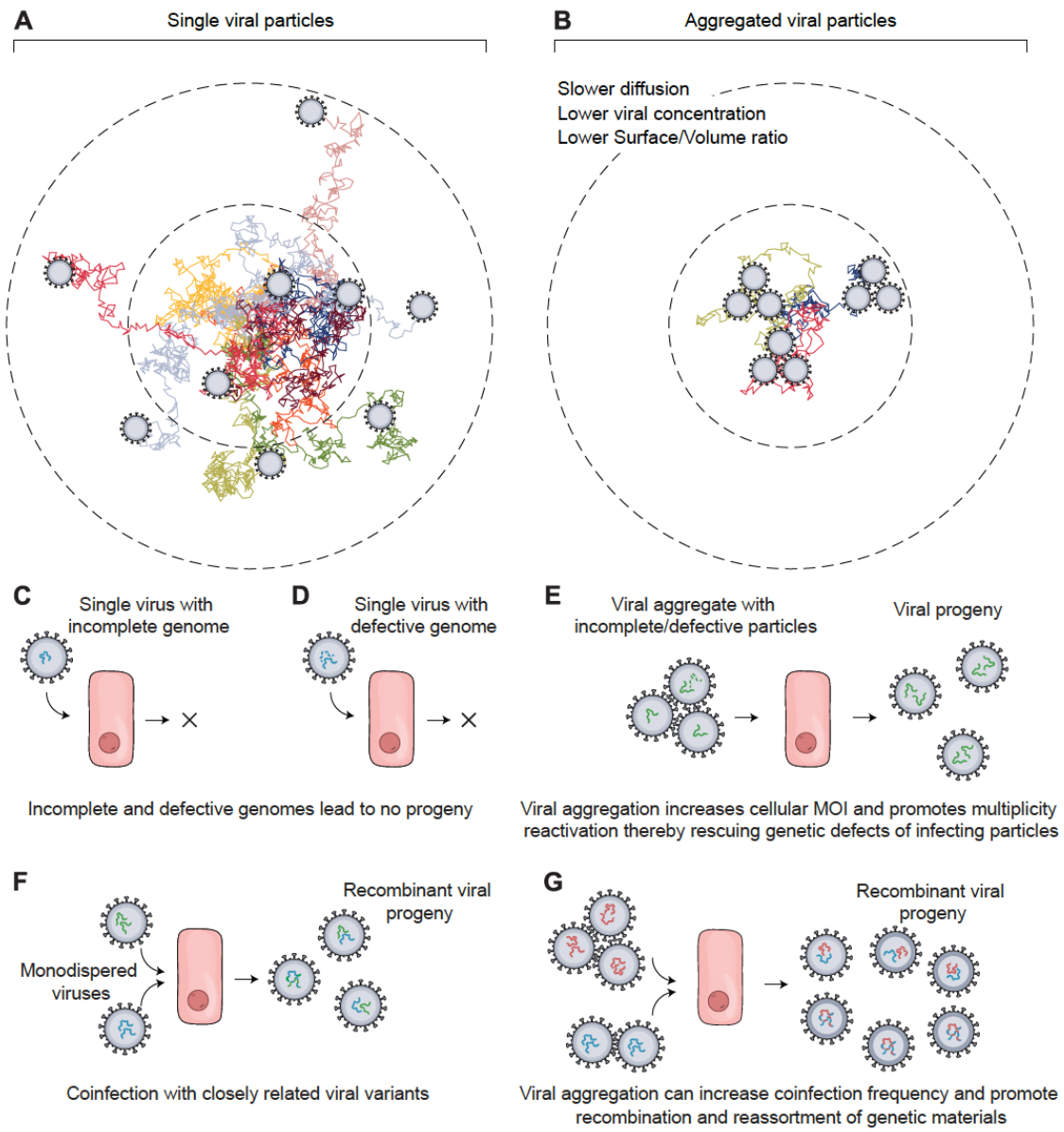

Figure 1. Schematic showing how viral aggregation affects their ability to infect target cells and their evolution. (**A**) A hypothetical arrangement of monodispersed viral particles (N = 9 viral particles) has a relatively faster diffusion, which increases their dissemination and the frequency of adsorption to target cells. (**B**) Aggregated viral particles (N = 3 trimers = 9 viral particles) diffuse more slowly and lead to a lower effective titer, which decreases their association rate with target cells before being deactivated or degraded. (**C**,**D**) In the case of multi-segmented and multipartite viruses, a single virus particle is likely to fail in producing progeny due to several challenges, the most prominent being defective or incomplete genomes. Following virus entry, the viral genome is released inside the host cell to start viral replication. However, the genome is highly likely to be incomplete or defective, particularly with RNA viruses such as influenza. This results in the failure of the virion to transcribe or translate necessary viral factors to produce infectious progeny. (**E**) Invasion of host cells by viral particles in an aggregated state is conducive to increasing cellular

MOI, which releases multiple copies of the viral genome inside the host cell. This sets the stage for genetic complementation and multiplicity reactivation, which facilitates the overcoming of any genetic defect or missing genetic factors. It increases the chances of the virions to replicate and produce viral progeny that will start their infection cycle. (**F**, **G**) Genetic recombination and reassortment between closely related virions in either the monodispersed state (**F**) or the aggregated state (**G**) can produce chimeric progeny with genetic segments derived from each parent. This influences their fitness and contributes to genetic diversity.

Once virus particles adsorb on the surface of a suitable host, they begin the multistep and tightly controlled process of entering the host cell. It starts with the virus binding to specific receptors or attachment factors such as carbohydrates, lipids, and other cellular proteins on the host cell surface [91]. After binding, they enter host cells either by endocytosis or by direct fusion with the host cell plasma membrane. However, regardless of the route taken, the end goal is to release viral genomes in the cytoplasm, where they are processed further for nuclear import [92]. For many years, scientists seeking to decipher the molecular mechanisms driving viral entry studied singular interactions between a virus and a host cell but largely ignored viral aggregates. The dynamics of viral entry for viral aggregates will likely be different than for a single virus particle and depend on the aggregate's size, shape, and composition. However, they remain yet to be investigated and are far from resolved.

1.4.2. Viral Aggregation Influencing Replication Inside Host Cells

Following cell entry, viral genomes are transported to the nucleus or specific sites in the cytoplasm for replication, expression of viral proteins, and assembly [92]. Viral aggregates diffuse more slowly and are likely to infect fewer cells than their monodispersed counterparts. However, for some viruses, aggregation compensates this cost by increasing the MOI, subsequently reducing the risk of stochastic failures. For instance, cells infected with saliva-induced aggregates of VSV and phosphatidylserine (PS)-enclosed aggregates of enteroviruses produced higher progenies than cells infected with an equal number of monodispersed viruses [8,73]. Microscopic analyses of cells infected with VSV aggregates and enterovirus aggregates in these studies showed the transmission of multiple viral genomes to the same cells. Interestingly, VSV aggregation did not compromise their dispersal capacity, and the higher MOI did not rescue genetic defects [73]. Instead, the fitness advantage of VSV aggregates correlated with cellular permissivity to infection and the increased

chances of overcoming initial stochastic barriers. On the other hand, like many other RNA viruses, enteroviruses have high mutation rates and exhibit a great deal of genomic heterogeneity. The enhancement of the replication kinetics of vesicle-enclosed enterovirus aggregates correlated with genetic complementation, reductions in stochastic fluctuations, and the PS-mediated enhanced modulation of antiviral response [8]. In another recent study, vesicle-enclosed aggregates of rotaviruses showed enhanced infectivity in vitro and in vivo in mice compared to freely dispersed viruses [9]. As causative agents of gastroenteritis, rotaviruses infect the intestinal cells and transmit through the fecal-oral route. In this study, vesicle-enclosed rotaviruses overcame the intrinsic replication barrier of RNA viruses by ensuring a more concentrated delivery of viral particles and enhanced their infectivity by providing a higher degree of protection from host immune components as viruses traverse through the GI tract before infecting the intestinal cells.

In addition, during replication, the presence of multiple viral genomes can promote genetic interactions such as recombination, competition, and complementation. These interactions can influence viral fitness, diversity, and evolution (Figure 1C–G). In an early line of work, aggregates of UV irradiated vaccinia viruses showed enhanced survival compared to monodispersed viruses [28]. For RNA viruses, the impact of these interactions could be even more profound. Because of the lack of proofreading activity of their RNA- dependent RNA polymerases, they have high mutation rates and often fail to establish productive infections (Figure 1C,D). For instance, about 90% of influenza viruses failed to express one viral protein [68]. A higher MOI may promote complementing and cooperative interactions among viral genomes, rescuing their lethal/defective mutations and enhancing their infectivity [3,60].

1.4.3. Viral Aggregation Influencing Release from Host Cells

In the canonical route of virus release, enveloped viruses leave the infected cell by budding and secretion [93]. Non-enveloped viruses typically lyse the host cells to exit them. However, some of them escape via secretory pathways. They can bud into intracellular multivesicular bodies (MVB) and leave after fusing with the plasma membrane. Some follow the non-canonical route, subverting cellular autophagy and releasing by secretory mechanisms.

According to the conventional model of viral transmission, viral particles release and spread as free individual particles, and the fate of individual viral genomes is not interdependent during virus trafficking [94]. This concept has been contended by several lines of work, which are discussed in the following sections. Some viruses converge inside or on the host cell surface to form multi-virion structures before release. These structures can modulate vital aspects of viral pathogenesis, including infectivity, virulence, transmission, antibody escape, and fitness.

1.4.3.1. Extracellular Vesicles-Mediated Release of Viral Aggregates

In addition to being carriers of biomolecules (nucleic acids, proteins, lipids) and mediums for cell-cell communication, extracellular vesicles (EV) can also carry virus clusters and function as independent infectious units [93]. The EV-mediated transfer of viral clusters is termed as vesicle-mediated en bloc transmission [93]. Several recent findings showed EV-mediated in vitro release and transmission of clustered enterovirus [8,86,95], hepatitis A viruses (HAV, family *Picornaviridae*) [74], rotavirus and norovirus [9]. Some of them clustered within phosphatidylserine (PS) lipid-enriched vesicles [8,9]. Following the common routes of EV biogenesis, vesicle-enclosed virus clusters can originate intracellularly from autophagosomes and multivesicular bodies (MVBs) or directly from the host cell plasma membrane [74,86,95]. However, vesicle-enclosed viruses always follow the non-lytic mode of virus release, blurring the conventional distinction between enveloped and non- enveloped viruses. A schematic representing different routes of EV-mediated viral release is shown in Figure 2A. A recent review has discussed the advantages of EV-mediated en bloc transmission of several infectious viruses along with the known molecular mechanisms of cargo delivery [96].

Poliovirus demonstrated the lysis-independent release of viral clusters within host- derived vesicles [86]. Quantitative single-cell analysis showed the virus clusters originated from autophagosomes. However, viruses subverted the autophagy pathway by inhibiting the fusion of autophagosomes with lysosomes, followed by their non-lytic release in single-membrane vesicles. This process is called *autophagosome-mediated exit without lysis* (AWOL) [97]. Upregulation of the autophagy pathway enhanced viral spread in vitro and pathogenicity in mice. In another work,

Hepatitis A viruses (HAV, family *Picornaviridae*) demonstrated AWOL-mediated non-lytic release from exosome-like EVs. The vesicle- enclosed viruses showed enhanced infectivity and resistance against antibodies [74]. The formation of these extracellular vesicles relied on the multivesicular body (MVB) components and the autophagy pathways. In another work, the sequential events of infection and viral spread of coxsackievirus B3 (CVB3) were tracked in real-time using a recombinant virus, Timer-CVB3, which expressed a fluorescent timer protein that changed color from green to red over time. The progression of Timer-CVB3 in partially differentiated neural progenitor and stem cells (NPSCs) revealed that the viruses frequently pooled together inside extracellular microvesicles (EMVs) and released in a lysis-independent manner [95]. The study postulated that the EMV-mediated release of viral clusters could enhance viral spread by exploiting the migratory nature of progenitor cells and modulating cellular differentiation to catapult viral egress in the absence of cell lysis.

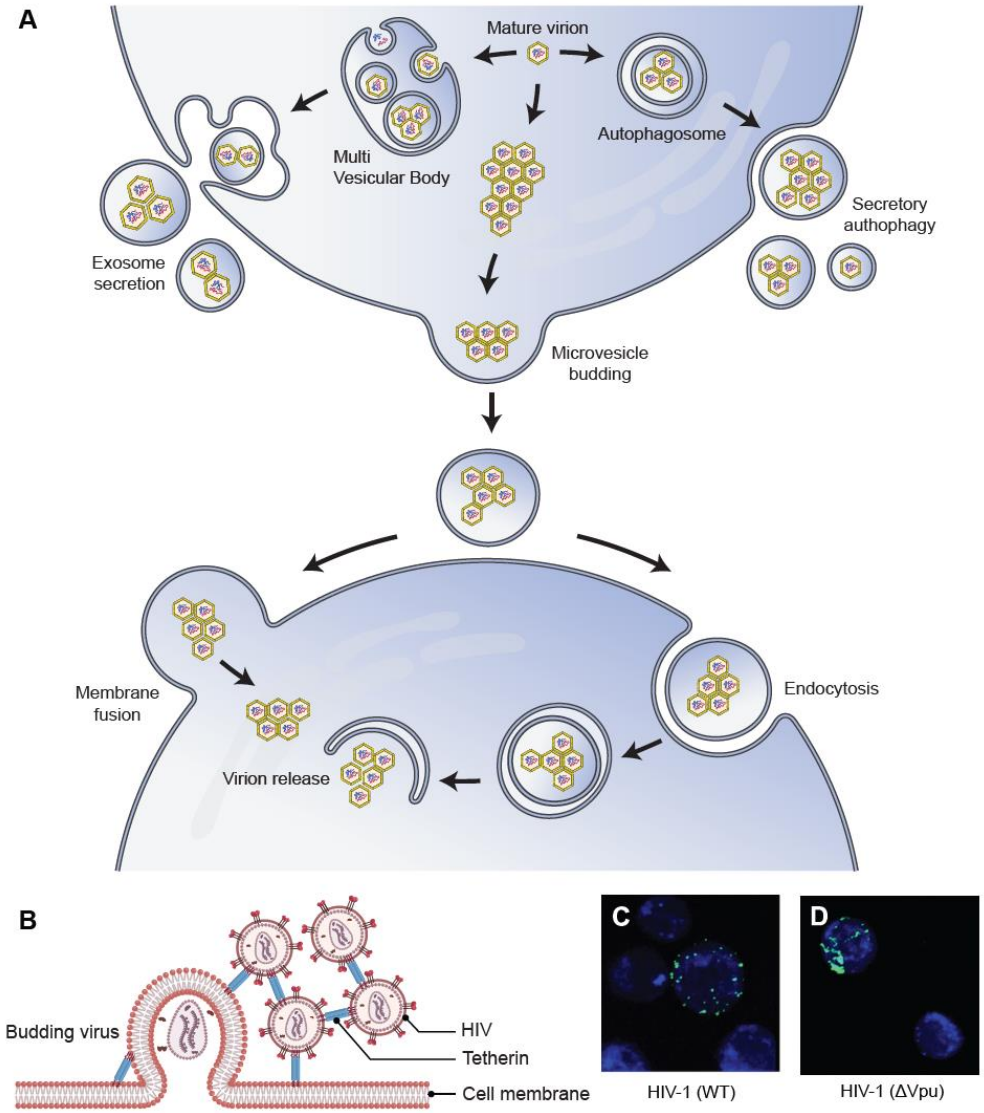

Figure 2. Possible mechanisms by which the aggregation of virus particles affects their transmission ability. (**A**) Virions can aggregate and be subsequently released from their host cells inside extracellular vesicles (EVs). They can aggregate inside microvesicles that are released directly from the plasma membrane using a budding mechanism. They can also bud into multivesicular bodies (MVB) that are trafficked to the plasma membrane and released into the extracellular space by membrane fusion. They can also aggregate inside autophagosomes and be released using the secretory autophagy pathway. After release, the EV-enclosed virions can enter new host cells either by fusion at the cell membrane or by the endocytic route. EVs enhance the transmission ability and the subsequent infectivity of virions by protecting against neutralizing antibodies [74] and promoting the collective delivery of multiple virions [8,74], respectively. (**B**) Schematic representation of tetherin (an interferon- inducible antiviral factor)-mediated aggregation and retention of HIV particles on the surface of the infected cells, which affects the cell-to-cell transmission of the virus. Tetherin colocalizes with Gag protein at the plasma membrane and is antagonized by Vpu protein. (**C**,**D**) Correlative light-scanning electron microscopy (SEM) images showing the distribution of HIV-GagGFP (WT or ΔVpu) particles (green) on target Jurkat cells (blue) [75]. Cells were harvested

after 2 h of cocultivation with WT or ΔVpu HIV-transfected HeLa donor cells. In the presence of Vpu, WT HIV particles were transferred as small clusters (**C**), and in the absence of the antagonist, ΔVpu HIV particles were transferred as larger aggregates (**D**). Parts (**C**,**D**) are republished with permission from [75]. Copyright 2010 under Creative Commons Attribution License 2.0.

1.4.3.2. Tetherin Mediated Viral Aggregation and the Consequent Inhibition of Viral Release

A rather intriguing route of viral aggregation is mediated by tetherin, an interferon- induced cellular restriction factor that acts as an innate antiviral defense against HIV [10,75] and other enveloped viruses, including other retroviruses [98], filoviruses [98], gamma- herpesviruses [99], and rhabdoviruses [100]. Mutational analyses have revealed the autonomous mode of tetherin function is determined by its overall configuration rather than sequence homology [10].

In the case of HIV, tetherin accumulates with viral Gag proteins at cell surfaces. It incorporates itself into assembling virions as a disulfide-linked dimer using either of its two membrane anchors [10]. This simple configuration of tetherin directly tethers virion particles to the cellular membranes of infected cells and retains them (Figure 2B). In response, viruses have also adapted mechanisms to interact with tetherin to impede its function. For instance, the HIV-1 accessory protein, Vpu, acts as a viral antagonist of tetherin [101].

A few studies have shown the tetherin-mediated aggregation and retention of HIV, however, with different implications on the cell-to-cell release of viruses [75,80,102]. In general, mature virions can employ any of the several routes for direct cell-to-cell transmission, including viral synapses, polysynapses [103], filopodial bridges [104,105], and viral biofilms [81]. FACS analyses showed tetherin inhibited the cell-to-cell transfer of HIV from infected donor cells to uninfected target cells [75,102]. Casartelli et al. showed that upon infection, tetherin-expressing cells transferred HIV aggregates as abnormally large patches (Figure 2C,D) that were impaired in their fusion capabilities [75]. In addition, target cells showed lower levels of viral DNA over time when co-cultured with tetherin-expressing donor cells infected with Vpu-defective HIV (ΔVpu). Conversely, Jolly et al. showed that tetherin expression enhanced the cell-to-cell transfer of viruses, most likely by increasing the localized and effective concentration of virions [80]. Contrary to the previous work, viral DNA synthesis in target cells co-cultured with ΔVpu HIV-infected donor cells

increased over time. The increase was not as rapid in target cells co-cultured with WT HIV-infected donor cells, implying enhanced transmission of ΔVpu HIV. In addition, tetherin inhibition did not increase viral spread, and the tethered virions remained fully infectious. While the implications of tetherin-mediated retention of viruses on viral transmission need further investigation, the contrasting findings in these studies potentially reflect the dynamic nature of tetherin modulation that depends on cell type and expression level of other cellular and immune components.

1.5. Viral Aggregation as an Antiviral Response

Host immune responses present a significant barrier for viruses. Throughout their infection cycle, they encounter different components of the immune system, ready to neutralize any incoming pathogen. Depending on the nature of the viral infection, it may activate various components of either the innate immune system or the adaptive immune system or both [106–108]. Innate immune responses are rapid but largely non-specific. As the first line of defense, they neutralize infiltrating viruses directly by macrophage and neutrophil-mediated phagocytosis and indirectly by natural killer cell-mediated apoptosis or complement-mediated lysis. If some viruses evade innate responses, the adaptive immune system kicks in. The adaptive response relies on antigen-presenting cells (APCs), such as dendritic cells and macrophages, to successfully activate cytotoxic T cells (CTLs) that kill infected cells and B cells that synthesize virus-specific antibodies. The distinguishing feature of adaptive immunity is its ability to differentiate between non-self-materials, leading to the development of immunological memory, which causes the immune system to respond more vigorously to re-exposures.

Several lines of evidence suggest that viral aggregates are more resistant to chemical disinfection and antibody neutralization [22,26,74,96,109]. Vesicle-enclosed viral clusters, in particular, can modulate host responses to enhance their infectivity in different ways [96]. Here, we discuss viral aggregation as a common antiviral host response mechanism.

Aggregation is a standard route taken by antiviral agents to neutralize viral infections. We have highlighted some studies showing the aggregation of influenza A virus (IAV) following their interaction with different antiviral components in Table 3. For instance, natural IgM and the

complement system worked synergistically to neutralize viral particles primarily by aggregating them [110]. The IgM-mediated deposition of complement proteins on the viral surface aggregated viruses and subsequently neutralized them by blocking the accessibility of hemagglutinin (HA) receptors for their cellular ligands. HA glycoproteins coordinate the effective membrane fusion of influenza viruses with the host cells. In several other lines of work, soluble innate inhibitors, such as lectin inhibitors and antimicrobial peptides, aggregated viruses and neutralized them [82,83,111–115]. The neutralizing potential of antimicrobial peptides correlated with their aggregating potential [82]. Aggregation reduced the effective virus concentration, promoted their clearance from the airway through mucociliary action, and enhanced phagocytosis. In another study, histone proteins neutralized H3N2 and H1N1 influenza viruses by aggregating them directly and inhibiting their internalization [84]. The arginine-rich histone, H4, had the most potent anti-influenza activity of all core histones tested. In another study, a twenty amino acid EB peptide aggregated H5N1 influenza viruses, resulting in reduced virus binding with host cell receptors and increased opsonization [76]. Incorporating the peptide as adjuvants in H5N1 vaccines reduced influenza-associated morbidity in mice and enhanced viral clearance by improving cell-mediated immune response. These studies set a precedent for harnessing viral aggregation as a tool to develop novel antiviral therapeutics.

Table 3. Aggregation of Influenza A virus (IAV) by different biomolecules.

IAV Strain	Aggregating factor	Ref.
H3N2 A/Philippines/2/82	Arginine-rich histone proteins [H4 image]	[84]
H3N2 A/Philippines/2/82	Beta-amyloid peptides [fragments of Alzheimer-associated beta-amyloid protein, 40k x 2ug/mL BA22-42 image]	[118]
H3N2 A/X-31	IgG antibodies	[116]
H1N1 A/PR/8/34	Mouse serum with complement proteins and virus-specific antibodies	[110]
H1N1 A/PR/8/34	EB peptide [entry blocker antiviral peptide, 20 amino acid peptide derived from fibroblast growth factor-4]	[117]

1.6. Harnessing Viral Aggregation as a Therapeutic Tool

Given the pervasive impact of aggregation on the life cycle, fitness, and the pathogenicity of infectious viruses, we cannot neglect the potential of harnessing this phenomenon as a therapeutic tool. Viruses were discovered as infectious agents and repurposed as gene delivery vehicles over time. Infectious disease research is heavily focused on developing robust and rapid antiviral therapeutics. At the same time, gene therapy studies put considerable effort into engineering viral vectors with higher cargo capacity, inert immunogenicity, and strong transduction efficiency. We understand that the phenomenon of viral aggregation can be repurposed to cater to both dimensions of research focusing on viral infections (Figure 3).

Figure 3. A viral aggregation strategy can potentially be harnessed to decrease viral infectivity (**left**) or to increase cargo capacity and subsequent transduction efficiency of viral vectors (**right**). Viral aggregation can be induced by introducing multivalent viral binders or by modulating their environment.

The synergy between nanomaterials and small molecules (proteins, peptides, aptamers, etc.) has been increasingly exploited to develop nano-enabled solutions that address modeling, diagnostic, and therapeutic challenges in various viral pathosystems. Similar design principles can be used to fabricate nanoscale platforms that aggregate viral particles, subsequently limiting viral diffusion and adhesion onto the host cell surface. For instance, two-dimensional and three-dimensional nanostructures that can cross-link circulating viral particles could be a logical design to aggregate viral particles. Similarly, interfacial nanostructures enabling the physical entrapment of circulating viral particles could also be a potential platform design to aggregate viral particles. Synthetic peptides [76,120], nucleoside analogs, proteins [121], and nucleic acid aptamers [121] can be chemically conjugated as virus binders to a wide variety of biocompatible nanomaterials (DNA-based, carbon- based, polymers, dendrimers, etc.) that can provide the structural

framework/backbone to cross-link or entrap viral particles. Unlike many antivirals that target cellular mechanisms, such platforms can directly target viruses and function autonomously. For instance, the potential of IAV-aggregating EB peptide to work as a vaccine adjuvant has been previously established [76]. The same molecule can be incorporated into multivalent nanostructures and repurposed as an antiviral that aggregates multiple viral particles at once.

Viral aggregation can also be leveraged to engineer enhanced gene delivery vehicles for gene therapy. Viral vectors are the gold standard for in vitro and in vivo gene delivery. Adeno-associated virus (AAV) vectors, with their diverse tissue tropism and low immunogenicity, are the leading gene delivery platforms for gene silencing, editing, and replacement therapeutics [122–124]. However, their therapeutic applications are limited mainly because of their small cargo capacity (4.7 kb). Many studies have focused on engineering the AAV genome and capsid to enhance gene delivery efficiency with minimum immunogenicity. Scientists have developed the split AAV vector approaches that enable the delivery of genetic fragments larger than 4.7 kb [125,126]. These systems utilize genome fragmentation, overlapping, and trans-splicing mechanisms to divide the transgene into multiple fragments and rely on genetic cues post vector co-infection to regenerate the entire transgene. For instance, one study used an overlapping strategy to fragment the alkaline phosphatase gene into two AAV vectors and deliver the gene to airway epithelial cells in mice [125]. Another study used a trans-splicing vector approach to fragment a 6 kb mini-dystrophin gene into two AAV vectors and deliver it to a mouse model of muscular dystrophy [126]. The interdependency between AAV vectors presents a major limitation in these systems. The complete functionality of the transgene within a cell is contingent upon the co-delivery of all AAV vectors in the same cell. Therefore, it is challenging to realize the potential of these platforms until they incorporate modalities to guarantee the co-delivery of all AAV vectors. This gap can be addressed by nano-enabled platforms immobilizing viruses such that the delivery of the platform guarantees co-infection of all viruses. For instance, it is possible to design platforms that can integrate multiple AAV vectors into one functional unit for cellular delivery. Each AAV vector could carry a fragment of the desired transgene or a component of the multi-unit genome editor (for instance, either gRNA or Cas9 or fusion proteins in the context of CRISPR-Cas9). Cells infected with these viral

assemblies would, in principle, have higher co-infections and subsequently better chances at reassembling all the fragments and producing the full-length transgene.

1.7. Concluding Remarks and Prospects

Viral aggregation is a widespread phenomenon affecting different aspects of viral infectivity, survival, and population dynamics. In the initial stages of infection, it can hinder viral spread by limiting the diffusion of viral particles. However, it can compensate for the loss by increasing cellular MOI, reducing stochastic barriers, and enhancing infectivity. In addition, a higher MOI sets the stage for genetic interactions among co-infecting viruses, with potential implications in viral diversity and evolution. Vesicle-enclosed viral aggregates act as optimal infectious units, mediating non-lytic release, en bloc transmission of viruses, and enhanced immune evasion. Aggregation is also the main route taken by antibodies and antiviral compounds to neutralize viruses, and as such, viruses aggregated by antivirals show enhanced opsonization and rapid clearance. However, these outcomes are not absolute and vary depending on the viral species and the spatiotemporal context of viral aggregation.

Live-cell imaging studies coupled with single virus tracking have provided more profound insights into molecular mechanisms underlying virus infection, trafficking, and interactions with cells, antibodies, and antivirals. However, for aggregated viruses, these molecular mechanisms are far from resolved. Given the impact of viral aggregation on different aspects of viral infectivity and survival, it has the potential to be harnessed into therapeutic tools for gene delivery and antiviral interventions. Furthermore, establishing standards for describing, differentiating, and characterizing viral aggregates is essential to assist studies in this rapidly evolving and expanding scientific field. Findings so far suggest that viral aggregation is a dynamic phenomenon with unpredictable outcomes, and as such, several questions remain yet to be answered. Some of them are given below:

a. How commonly do aggregates of pandemic/epidemic/endemic strains of viruses occur in different environments, such as inside a host cell versus a wastewater treatment plant?

b. Are there any genetic determinants of viral aggregation? What factors, genetic and otherwise, influence and distinguish the formation of different kinds of viral aggregates, for instance, vesicle-enclosed viral aggregates versus virus-virus binding aggregates versus aggregates formed by virus binding to other surfaces/molecules?
c. Does the nature of viral aggregates determine their fate regarding immune evasion and clearance? For instance, vesicle-enclosed viral aggregates show enhanced immune evasion. In contrast, aggregates formed by antibodies are more potent immune stimuli triggering enhanced opsonization and immune clearance.
d. How does viral aggregation influence different events of an infectious viral life cycle, including viral adhesion, entry, replication, assembly, and release? What molecular and cellular factors/mechanisms drive those outcomes? Is aggregation conditional on any stage of the viral life cycle?
e. How does viral aggregation influence the infectivity and virulence of different viral species or even different strains of the same viral species? Are there aggregation patterns exhibited by viral strains/species that can be traced back to the similarities and differences in their structural/genetic makeup?
f. How does aggregation contribute to the viral fitness, diversity, and evolution landscape?
g. Can we develop model systems to study viral aggregation? Can we induce viral aggregation in vitro, in vivo, and ex vivo to modulate infectivity, virulence, and neutralization?
h. How does viral aggregation influence the kinetics and efficiency of viral vectors in gene therapy?

Author Contributions: Conceptualization, S.P.; investigation, S.P., R.F.H., A.V., C.J.S. and C.L.; resources, R.F.H.; writing—original draft preparation, S.P.; writing—review and editing, R.F.H., A.V., C.L. and C.J.S.; visualization, S.P.; supervision, R.F.H., A.V. and C.J.S. All authors have read and agreed to the published version of the manuscript.

Funding: The research in Hariadi lab was supported by the National Institutes of Health Director's New Innovator Award (1DP2AI144247), National Science Foundation (2027215), and Arizona Biomedical Research Consortium (ADHS17-00007401).

Acknowledgments: The authors would like to thank Ian Hogue, Brenda Hogue, and Isadonna Tengganu for valuable discussions. We thank Sapto Cahyono for his assistance with the illustrations. We thank Bonfilio Nainggolan for his help with manuscript formatting.

Conflicts of Interest: The authors declare no conflict of interest.

Abbreviations

The following abbreviations are used in this manuscript:

AAV	Adeno-associated virus
AWOL	Autophagosome-mediated exit without lysis EB Entry blocker
EM	Electron microscopy
EMV	Extracellular microvesicles
EV	Extracellular vesicle
FGF-4	Fibroblast growth factor-4
GCXV	Guaico CuleX virus
HA	Hemagglutinin
HAV	Hepatitis A virus
HIV	Human immunodeficiency virus
IAV	Influenza A virus
MOI	Multiplicity of infection
MSD	Mean-squared displacement
MVB	Multivesicular body
NA	Neuraminidase
NET	Neutrophil extracellular trap
OBs	Occlusion bodies
PS	Phosphatidylserine
RSV	Respiratory syncytial virus

TMV Tobacco mosaic virus

VSV Vesicular stomatitis virus

REFERENCES

1. Rohrmann, G.F. Baculovirus structural proteins. *J. Gen. Virol.* **1992**, *73 Pt 4*, 749-761.

2. Federici, B.A.; Vlak, J.M.; Hamm, J.J. Comparative study of virion structure, protein composition and genomic DNA of three ascovirus isolates. *J. Gen. Virol.* **1990**, *71 Pt 8*, 1661-1668.

3. Hirst, G.K.; Pons, M.W. Mechanism of influenza recombination: II. Virus aggregation and its effect on plaque formation by so-called noninfective virus. *Virol. J.* **1973**, *56*, 620-631.

4. Galasso, G.J.; Sharp, J.; Sharp, D.G. The influence of degree of aggregation and virus quality on the plaque titer of aggregated vaccinia virus. *J. Immunol.* **1964**, *92*, 870-878.

5. Floyd, R.; Sharp, D.G. Aggregation of poliovirus and reovirus by dilution in water. *Appl. Environ. Microbiol.* **1977**, *33*, 159-167.

6. Narang, H.K.; Codd, A.A. Frequency of preclumped virus in routine fecal specimens from patients with acute nonbacterial gastroenteritis. *J. Clin. Microbiol.* **1981**, *13*, 982-988.

7. Williams, F.P. Membrane-associated viral complexes observed in stools and cell culture. *Appl. Environ. Microbiol.* **1985**, *50*, 523-526.

8. Chen, Y.H.; Du, W.; Hagemeijer, M.C.; Takvorian, P.M.; Pau, C.; Cali, A.; Brantner, C.A.; Stempinski, E.S.; Connelly, P.S.; Ma, H.C. Phosphatidylserine vesicles enable efficient en bloc transmission of enteroviruses. *Cell* **2015**, *160*, 619-630.

9. Santiana, M.; Ghosh, S.; Ho, B.A.; Rajasekaran, V.; Du, W.L.; Mutsafi, Y.; De Jésus-Diaz, D.A.; Sosnovtsev, S.V.; Levenson, E.A.; Parra, G.I. Vesicle-cloaked virus clusters are optimal units for inter-organismal viral transmission. *Cell Host Microbe* **2018**, *24*, 208-220.e8.

10. Perez-Caballero, D.; Zang, T.; Ebrahimi, A.; McNatt, M.W.; Gregory, D.A.; Johnson, M.C.; Bieniasz, P.D. Tetherin inhibits HIV-1 release by directly tethering virions to cells. *Cell* **2009**, *139*, 499-511.

11. Arnaud, F.; Black, S.G.; Murphy, L.; Griffiths, D.J.; Neil, S.J.; Spencer, T.E.; Palmarini, M. Interplay between ovine bone marrow stromal cell antigen 2/tetherin and endogenous retroviruses. *J. Virol.* **2010**, *84*, 4415-4425.

12. Kaletsky, R.L.; Francica, J.R.; Agrawal-Gamse, C.; Bates, P. Tetherin-mediated restriction of filovirus budding is antagonized by the Ebola glycoprotein. *Proc. Natl. Acad. Sci. USA* **2009**, *106*, 2886-2891.

13. Ilinskaya, A.; Derse, D.; Hill, S.; Princler, G.; Heidecker, G. Cell-cell transmission allows human T-lymphotropic virus 1 to circumvent tetherin restriction. *Virology* **2013**, *436*, 201-209.

14. Sanjuán, R. Collective infectious units in viruses. *Trends Microbiol.* **2017**, *25*, 402-412.

15. Bald, J.G.; Briggs, G.E. Aggregation of Virus Particles. *Nature* **1937**, *140*, 111.

16. Hirst, G.K. Studies of antigenic differences among strains of influenza A by means of red cell agglutination. *J. Exp. Med.* **1983**, *78*, 407-423.

17. Hilleman, M.R. System for measuring and designating antigenic components of influenza viruses with analyses of recently isolated strains. *Proc. Soc. Exp. Biol. Med.* **1951**, *78*, 208-215.

18. Floyd, R. Viral aggregation: Mixed suspensions of poliovirus and reovirus. *Appl. Environ. Microbiol.* **1979**, *38*, 980-986.

19. Sharp, D.G.; Floyd, R.; Johnson, J.D. Nature of the surviving plaque-forming unit of reovirus in water containing bromine. *Appl. Environ. Microbiol.* **1975**, *29*, 94-101.

20. Galdiero, F. Adenovirus aggregation and preservation in extracellular environment. *Arch. Virol.* **1979**, *59*, 99-105.

21. Fiszman, M.; Bucchini, D.; Girard, M. Purification of the Sabin strain of poliovirus type I through treatment with sarkozyl. *J. Virol.* **1971**, *7*, 687-689.

22. Young, D.C.; Sharp, D.G. Poliovirus aggregates and their survival in water. *Appl. Environ. Microbiol.* **1977**, *33*, 168-177.

23. Floyd, R.; Sharp, D.G. Viral aggregation: Effects of salts on the aggregation of poliovirus and reovirus at low pH. *Appl. Environ. Microbiol.* **1978**, *35*, 1084-1094.

24. Totsuka, A.; Ohtaki, K.; Tagaya, I. Aggregation of enterovirus small plaque variants and polioviruses under low ionic strength conditions. *J. Gen. Virol.* **1978**, *38*, 519-533.

25. Floyd, R.; Sharp, D.G. Viral aggregation: Quantitation and kinetics of the aggregation of poliovirus and reovirus. *Appl. Environ. Microbiol.* **1978**, *35*, 1079-1083.

26. Von Zeipel, G. Neutralization of Aggregated Strains of Enterovirus 71 and Echovirus Type 4 in RD and Vero or GMK-AH1 Cells. *Acta Pathol. Microbiol. Scand. B* **1979**, *87*, 71-73.

27. Katouzian-safadi, M.; Favre, A.; Haenni, A. Effect of freezing and thawing on the structure of turnip yellow mosaic virus. *Eur. J. Biochem.* **1980**, *112*, 479-486.

28. Galasso, G.J.; Sharp, D.G. Effect of particle aggregation on the survival of irradiated vaccinia virus. *J. Bacteriol.* **1965**, *90*, 1138-1142.

29. Kahler, A.M.; Cromeans, T.L.; Metcalfe, M.G.; Humphrey, C.D.; Hill, V.R. Aggregation of adenovirus 2 in source water and impacts on disinfection by chlorine. *Food Environ. Virol.* **2016**, *8*, 148-155.

30. Tucker, S.P.; Thornton, C.L.; Wimmer, E.; Compans, R.W. Vectorial release of poliovirus from polarized human intestinal epithelial cells. *J. Virol.* **1993**, *67*, 4274-4282.

31. Gollins, S.W.; Porterfield, J.S. Flavivirus infection enhancement in macrophages: An electron microscopic study of viral cellular entry. *J. Gen. Virol.* **1985**, *66*, 1969-1982.

32. Gassilloud, B.; Gantzer, C. Adhesion-aggregation and inactivation of poliovirus 1 in groundwater stored in a hydrophobic container. *Appl. Environ. Microbiol.* **2005**, *71*, 912-920.

33. Michen, B.; Graule, T. Isoelectric points of viruses. *J. Appl. Microbiol.* **2010**, *109*, 388-397.

34. Wong, K.; Mukherjee, B.; Kahler, A.M.; Zepp, R.; Molina, M. Influence of Inorganic Ions on Aggregation and Adsorption Behaviors of Human Adenovirus. *Environ. Sci. Technol.* **2012**, *46*, 11145-11153.

35. da Silva, A.K.; Kavanagh, O.V.; Estes, M.K.; Elimelech, M. Adsorption and aggregation properties of norovirus GI and GII virus-like particles demonstrate differing responses to solution chemistry. *Environ. Sci. Technol.* **2011**, *45*, 520-526.

36. Langlet, J.; Gaboriaud, F.; Gantzer, C. Effects of pH on plaque forming unit counts and aggregation of MS2 bacteriophage. *J. Appl. Microbiol.* **2007**, *103*, 1632–1638.

37. Zoueva, O.P.; Bailly, J.E.; Nicholls, R.; Brown, E.G. Aggregation of influenza virus ribonucleocapsids at low pH. *Virus Res.* **2002**, *85*, 141–149.

38. Libersou, S.; Albertini, A.A.V.; Ouldali, M.; Maury, V.; Maheu, C.; Raux, H.; de Haas, F.; Roche, S.; Gaudin, Y.; Lepault, J. Distinct structural rearrangements of the VSV glycoprotein drive membrane fusion. *J. Cell Biol.* **2010**, *191*, 199–210.

39. Davis, H.E.; Rosinski, M.; Morgan, J.R.; Yarmush, M.L. Charged Polymers Modulate Retrovirus Transduction via Membrane Charge Neutralization and Virus Aggregation. *Biophys. J.* **2004**, *86*, 1234–1242.

40. Gutierrez, L.; Mylon, S.E.; Nash, B.; Nguyen, T.H. Deposition and aggregation kinetics of rotavirus in divalent cation solutions. *Environ. Sci. Technol.* **2010**, *44*, 4552–4557.

41. Langlet, J.; Gaboriaud, F.; Jérôme, F.; Gantzer, C. Aggregation and surface properties of F-specific RNA phages: implication for membrane filtration processes. *Water Res.* **2008**, *42*, 2769–2777.

42. Gerba, C.P.; Betancourt, W.Q. Viral Aggregation: Impact of virus behavior in the environment. *Environ. Sci. Technol.* **2017**, *51*, 7318–7325.

43. Cuevas, J.M.; Moreno, M.D.; Sanjuán, R. Multi-virion infectious units arise from free viral particles in an enveloped virus. *Nat. Microbiol.* **2017**, *2*, 1–7.

44. Anschau, V.; Sanjuán, R. Fibrinogen Gamma Chain Promotes Aggregation of Vesicular Stomatitis Virus in Saliva. *Viruses* **2020**, *12*, 282.

45. Corno, G.; Coci, M.; Giardina, M.; Plechuk, S.; Campanile, F.; Stefani, S. Antibiotics promote aggregation within aquatic bacterial communities. *Front. Microbiol.* **2014**, *5*, 297.

46. Blom, J.F.; Zimmermann, Y.S.; Ammann, T.; Pernthaler, J. Scent of danger: floc formation by a freshwater bacterium is induced by supernatants from a predator-prey coculture. *Appl. Environ. Microbiol.* **2010**, *76*, 6156–6163.

47. Hahn, M.W.; Moore, E.R.B.; Höfle, M.G. Role of Microcolony Formation in the Protistan Grazing Defense of the Aquatic Bacterium Pseudomonas sp. MWH1. *Microb. Ecol.* **2000**, *39*, 175–185.

48. Sherlock, O.; Schembri, M.A.; Reisner, A.; Klemm, P. Novel roles for the AIDA adhesin from diarrheagenic Escherichia coli: cell aggregation and biofilm formation. *J. Bacteriol.* **2004**, *186*, 8058–8065.

49. O'Toole, G.A.; Kolter, R. Flagellar and twitching motility are necessary for Pseudomonas aeruginosa biofilm development. *Mol. Microbiol.* **1998**, *30*, 295–304.

50. Abdel-Nour, M.; Duncan, C.; Prashar, A.; Rao, C.; Ginevra, C.; Jarraud, S.; Low, D.E.; Ensminger, A.W.; Terebiznik, M.R.; Guyard, C. The Legionella pneumophila collagen-like protein mediates sedimentation, autoaggregation, and pathogen-phagocyte interactions. *Appl. Environ. Microbiol.* **2014**, *80*, 1441–1454.

51. Kuroda, M.; Ito, R.; Tanaka, Y.; Yao, M.; Matoba, K.; Saito, S.; Tanaka, I.; Ohta, T. Staphylococcus aureus surface protein SasG contributes to intercellular autoaggregation of Staphylococcus aureus. *Biochem. Biophys. Res. Commun.* **2008**, *377*, 1102–1106.

52. Arenas, J.; Cano, S.; Nijland, R.; van Dongen, V.; Rutten, L.; van der Ende, A.; Tommassen, J. The meningococcal autotransporter AutA is implicated in autoaggregation and biofilm formation. *Environ. Microbiol.* **2015**, *17*, 1321–1337.

53. Trunk, T.; Khalil, H.S.; Leo, J.C. Bacterial autoaggregation. *AIMS Microbiol.* **2018**, *4*, 140.

54. Jung, A.; Maier, R.; Vartanian, J.P.; Bocharov, G.; Jung, V.; Fischer, U.; Meese, E.; Hobsor, S.W.; Meyerhans, A. Multiply infected spleen cells in HIV patients. *Nature* **2002**, *418*, 144–144.

55. Sanjuán, R.; Cuevas, J.M.; Furió, V.; Holmes, E.C.; Moya, A. Selection for Robustness in Mutagenized RNA Viruses. *PLoS Genet.* **2007**, *3*, e93.

56. Novella, I.S.; Reissig, D.D.; Wilke, C.O. Density-dependent selection in vesicular stomatitis virus. *J. Virol.* **2004**, *78*, 5799–5804.

57. Kim, K.S.; Sharp, D.G. Electron microscopic observations on the nature of vaccinia virus particle aggregation. *J. Immunol.* **1966**, *97*, 197–202.

58. Flint, S.J.; Enquist, L.W.; Racaniello, V.R.; Skalka, A.M. *Principles of Virology*, 3rd ed.; John Wiley & Sons, Inc.: Hoboken, NJ, USA, 2009.

59. Snijder, B.; Sacher, R.; Rämö, P.; Damm, E.M.; Liberali, P.; Pelkmans, L. Population context determines cell-to-cell variability in endocytosis and virus infection. *Nature* **2009**, *461*, 520–523.

60. Heldt, F.S.; Kupke, S.Y.; Dorl, S.; Reichl, U.; Frensing, T. Single-cell analysis and stochastic modelling unveil large cell-to-cell variability in influenza A virus infection. *Nat. Commun.* **2015**, *6*, 1–12.

61. Pearson, J.E.; Krapivsky, P.; Perelson, A.S. Stochastic theory of early viral infection: continuous versus burst production of virions. *PLoS Comput. Biol.* **2011**, *7*, e1001058.

62. Patton, J.T.; Spencer, E. Genome replication and packaging of segmented double-stranded RNA viruses. *J. Virol.* **2000**, *277*, 217–225.

63. Reijnders, L. The origin of multicomponent small ribonucleoprotein viruses. In *Advances in Virus Research*; Elsevier: Amsterdam, The Netherlands, 1978; Volume 23, pp. 79–102.

64. Jaspars, E.M.J. Plant viruses with a multipartite genome. In *Advances in Virus Research*; Elsevier: Amsterdam, The Netherlands, 1974; Volume 19, pp. 37–149.

65. Palese, P.; Schulman, J.L. Mapping of the influenza virus genome: Identification of the hemagglutinin and the neuraminidase genes. *Proc. Natl. Acad. Sci. USA* **1976**, *73*, 2142–2146.

66. Palese, P.; Ritchey, M.B.; Schulman, J.L. Mapping of the influenza virus genome II. Identification of the P1, P2, and P3 genes. *J. Virol.* **1977**, *76*, 114–121.

67. Ritchey, M.B.; Palese, P.; Schulman, J.L. Mapping of the influenza virus genome. III. Identification of genes coding for nucleoprotein, membrane protein, and nonstructural protein. *J. Virol.* **1976**, *20*, 307-313.

68. Brooke, C.B.; Ince, W.L.; Wrammert, J.; Ahmed, R.; Wilson, P.C.; Bennink, J.R.; Yewdell, J.W. Most influenza a virions fail to express at least one essential viral protein. *J. Virol.* **2013**, *87*, 3155-3162.

69. Jacobs, N.T.; Onuoha, N.O.; Antia, A.; Steel, J.; Antia, R.; Lowen, A.C. Incomplete influenza A virus genomes occur frequently but are readily complemented during localized viral spread. *Nat. Commun.* **2019**, *10*, 1-17.

70. Varsani, A.; Lefeuvre, P.; Roumagnac, P.; Martin, D. Notes on recombination and reassortment in multipartite/segmented viruses. *Curr. Opin. Virol.* **2018**, *33*, 156-166.

71. Ladner, J.T.; Wiley, M.R.; Beitzel, B.; Auguste, A.J.; Dupuis, A.P., II; Lindquist, M.E.; Sibley, S.D.; Kota, K.P.; Fetterer, D.; Eastwood, G. A multicomponent animal virus isolated from mosquitoes. *Cell Host Microbe* **2016**, *20*, 357-367.

72. Sanjuán, R. Collective properties of viral infectivity. *Curr. Opin. Virol.* **2018**, *33*, 1-6.

73. Andreu-Moreno, I.; Sanjuán, R. Collective infection of cells by viral aggregates promotes early viral proliferation and reveals a cellular-level Allee effect. *Curr. Biol.* **2018**, *28*, 3212-3219.e4.

74. Feng, Z.; Hensley, L.; McKnight, K.L.; Hu, F.; Madden, V.; Ping, L.; Jeong, S.H.; Walker, C.; Lanford, R.E.; Lemon, S.M. A pathogenic picornavirus acquires an envelope by hijacking cellular membranes. *Nature* **2013**, *496*, 367-371.

75. Casartelli, N.; Sourisseau, M.; Feldmann, J.; Guivel-Benhassine, F.; Mallet, A.; Marcelin, A.G.; Guatelli, J.; Schwartz, O. Tetherin restricts productive HIV-1 cell-to-cell transmission. *PLoS Pathog.* **2010**, *6*, e1000955.

76. Jones, J.C.; Settles, E.W.; Brandt, C.R.; Schultz-Cherry, S. Virus aggregating peptide enhances the cell mediated response to influenza virus vaccine. *Vaccine* **2011**, *29*, 7696-7703.

77. Sturman, L.S.; Ricard, C.S.; Holmes, K.V. Conformational change of the coronavirus peplomer glycoprotein at pH 8.0 and 37 degrees C correlates with virus aggregation and virus-induced cell fusion. *J. Virol.* **1990**, *64*, 3042-3050.

78. Clavijo, G.; Williams, T.; Mun, D.; Caballero, P.; Lopez-Ferber, M. Mixed genotype transmission bodies and virions contribute to the maintenance of diversity in an insect virus. *Proc. Biol. Sci.* **2010**, *277*, 943-951.

79. Sajjan, D.B.; Hinchigeri, S.B. Structural Organization of Baculovirus Occlusion Bodies and Protective Role of multilayered polyhedron envelope protein. *Food Environ. Virol.* **2016**, *8*, 86-100.

80. Jolly, C.; Booth, N.J.; Neil, S.J.D. Cell-cell spread of human immunodeficiency virus type 1 overcomes tetherin/BST-2-mediated restriction in T cells. *J. Virol.* **2010**, *84*, 12185-12199.

81. Correia, A.M.P. Biofilm-Like Extracellular Viral Assemblies Mediate HTLV-1 (Human T Cell Leukemia Virus Type-1) Cell-to-Cell Transmission at Virological Synapses. *Nat. Med.* **2010**, *16*, 83-89.

82. Tecle, T.; White, M.R.; Gantz, D.; Crouch, E.C.; Hartshorn, K.L. Human neutrophil defensins increase neutrophil uptake of influenza A virus and bacteria and modify virus-induced respiratory burst responses. *J. Immunol.* **2007**, *178*, 8046–8052.

83. Doss, M.; White, M.R.; Tecle, T.; Gantz, D.; Crouch, E.C.; Jung, G.; Ruchala, P.; Waring, A.J.; Lehrer, R.I.; Hartshorn, K.L. Interactions of α-, β-, and θ-defensins with influenza A virus and surfactant protein D. *J. Immunol.* **2009**, *182*, 7878–7887.

84. Hoeksema, M.; Tripathi, S.; White, M.; Qi, L.; Taubenberger, J.; van Eijk, M.; Haagsman, H.; Hartshorn, K.L. Arginine-rich histones have strong antiviral activity for influenza A viruses. *Innate Immun.* **2015**, *21*, 736–745.

85. Aguilera, E.R.; Erickson, A.K.; Jesudhasan, P.R.; Robinson, C.M.; Pfeiffer, J.K. Plaques Formed by Mutagenized Viral Populations Have Elevated Coinfection Frequencies. *mBio* **2017**, *8*, e02020-16.

86. Bird, S.W.; Maynard, N.D.; Covert, M.W.; Kirkegaard, K. Nonlytic viral spread enhanced by autophagy components. *Proc. Natl. Acad. Sci. USA* **2014**, *111*, 13081–13086.

87. Andreadis, S.; Lavery, T.; Davis, H.E.; Le Doux, J.M.; Yarmush, M.L.; Morgan, J.R. Toward a more accurate quantification of the activity of recombinant retroviruses: Alternatives to titer and multiplicity of infection. *J. Virol.* **2000**, *74*, 3431–3439.

88. Vahey, M.D.; Fletcher, D.A. Influenza A virus surface proteins are organized to help penetrate host mucus. *Elife* **2019**, *8*, e43764.

89. Baccam, P.; Beauchemin, C.; Macken, C.A.; Hayden, F.G.; Perelson, A.S. Kinetics of influenza A virus infection in humans. *J. Virol.* **2006**, *80*, 7590–7599.

90. Chuck, A.S.; Clarke, M.F.; Palsson, B.O. Retroviral infection is limited by Brownian motion. *Hum. Gene Ther.* **1996**, *7*, 1527–1534.

91. Marsh, M.; Helenius, A. Virus entry: Open sesame. *Cell* **2006**, *124*, 729–740.

92. Cohen, S.; Au, S.; Pante, N. How viruses access the nucleus. *Biochim. Biophys. Acta Mol. Cell Res.* **2011**, *1813*, 1634–1645.

93. Altan-Bonnet, N.; Perales, C.; Domingo, E. Extracellular vesicles: Vehicles of en bloc viral transmission. *Virus Res.* **2019**, *265*, 143–149.

94. Brandenburg, B.; Zhuang, X. Virus trafficking-learning from single-virus tracking. *Nat. Rev. Microbiol.* **2007**, *5*, 197–208.

95. Robinson, S.M.; Tsueng, G.; Sin, J.; Mangale, V.; Rahawi, S.; McIntyre, L.L.; Williams, W.; Kha, N.; Cruz, C.; Hancock, B.M. Coxsackievirus B exits the host cell in shed microvesicles displaying autophagosomal markers. *PLoS Pathog.* **2014**, *10*, e1004045.

96. Kerviel, A.; Zhang, M.; Bonnet, N.A. A new infectious unit: extracellular vesicles carrying virus populations. *Annu. Rev. Cell Dev. Biol.* **2021**, *37*, 171–197.

97. Jackson, W.T.; Giddings, T.H., Jr.; Taylor, M.P.; Mulinyawe, S.; Rabinovitch, M.; Kopito, R.R. Subversion of Cellular Autophagosomal Machinery by RNA Viruses. *PLoS Biol.* **2005**, *3*, e156.

98. Jouvenet, N.; Neil, S.J.D.; Zhadina, M.; Zang, T.; Kratovac, Z.; Lee, Y.; McNatt, M.; Hatziioannou, T.; Bieniasz, P.D. Broad-spectrum inhibition of retroviral and filoviral particle release by tetherin. *J. Virol.* **2009**, *83*, 1837–1844.

99. Pardieu, C.; Vigan, R.; Wilson, S.J.; Calvi, A.; Zang, T.; Bieniasz, P.; Kellam, P.; Towers, G.J.; Neil, S.J.D. The RING-CH Ligase K5 Antagonizes Restriction of KSHV and HIV-1 Particle Release by Mediating Ubiquitin-Dependent Endosomal Degradation of Tetherin. *PLoS Pathog.* **2010**, *6*, e1000843.

100. Weidner, J.M.; Jiang, D.; Pan, X.B.; Chang, J.; Block, T.M.; Guo, J.T. Interferon-Induced Cell Membrane Proteins, IFITM3 and Tetherin, Inhibit Vesicular Stomatitis Virus Infection via Distinct Mechanisms. *J. Virol.* **2010**, *84*, 12646–12657.

101. Miyagi, E.; Andrew, A.J.; Kao, S.; Strebel, K. Vpu enhances HIV-1 virus release in the absence of Bst-2 cell surface down-modulation and intracellular depletion. *Proc. Natl. Acad. Sci. USA* **2009**, *106*, 2868–2873.

102. Kuhl, B.D.; Sloan, R.D.; Donahue, D.A.; Bar-Magen, T.; Liang, C.; Wainberg, M.A. Tetherin restricts direct cell-to-cell infection of HIV-1. *Retrovirology* **2010**, *7*, 115.

103. Rudnicka, D.; Feldmann, J.; Porrot, F.; Wietgrefe, S.;Guadagnini, S.; Prévost, M.C.; Estaquier, J.; Haase, A.T.; Sol-Foulon, N.; Schwartz, O. Simultaneous cell-to-cell transmission of human immunodeficiency virus to multiple targets through polysynapses. *J. Virol.* **2009**, *83*, 6234–6246.

104. Sherer, N.M.; Lehmann, M.J.; Jimenez-Soto, L.F.; Horensavitz, C.; Pypaert, M.; Mothes, W. Retroviruses can establish fiopodial bridges for efficient cell-to-cell transmission. *Nat. Cell Biol.* **2007**, *9*, 310–315.

105. Sowinski, S.; Jolly, C.; Berninghausen, O.; Purbhoo, M.A.; Chauveau, A.; Köhler, K.; Oddos, S.; Eissmann, P.; Brodsky, F.M.; Hopkins, C. Membrane nanotubes physically connect T cells over long distances presenting a novel route for HIV-1 transmission. *Nat. Cell Biol.* **2008**, *10*, 211–219.

106. Braciale, T.J.; Hahn, Y.S. Immunity to viruses. *Immunol. Rev.* **2013**, *255*, 5–12.

107. Mueller, S.N.; Rouse, B.T. Immune responses to viruses. *Clin. Immunol.* **2008**, *2008*, 421.

108. Rouse, B.T.; Sehrawat, S. Immunity and immunopathology to viruses: what decides the outcome? *Nat. Rev. Immunol.* **2010**, *10*, 514–526.

109. Wallis, C.; Melnick, J.L. Virus aggregation as the cause of the non-neutralizable persistent fraction. *J. Virol.* **1967**, *1*, 478–488.

110. Jayasekera, J.P.; Moseman, E.A.; Carroll, M.C. Natural antibody and complement mediate neutralization of influenza virus in the absence of prior immunity. *J. Virol.* **2007**, *81*, 3487–3494.

111. Qi,L.; Kash, J.C.; Dugan, V.G.; Jagger, B.W.; Lau, Y.F.; Sheng, Z.M.; Crouch, E.C.; Hartshorn, K.L.; Taubenberger, J.K. The ability of pandemic influenza virus hemagglutinins to induce lower respiratory pathology is associated with decreased surfactant protein D binding. *Virology* **2011**, *412*, 426–434.

112. Doss, M.; Ruchala, P.; Tecle, T.; Gantz, D.; Verma, A.; Hartshorn, A.; Crouch, E.C.; Luong, H.; Micewicz, E.D.; Lehrer, R.I.; et al. Hapivirins and diprovirins: novel *θ*-defensin analogs with potent activity against influenza A virus. *J. Immunol.* **2012**, *188*, 2759–2768.

113. Hartshorn, K.L.; White, M.R.; Crouch, E.C. Contributions of the N-andC-terminal domains of surfactant protein d to the binding, aggregation, and phagocytic uptake of bacteria. *Infect. Immun.* **2002**, *70*, 6129–6139.

114. Hartshorn, K.L.; White, M.R.; Tecle, T.; Holmskov, U.; Crouch, E.C. Innate defense against influenza A virus: activity of human neutrophil defensins and interactions of defensins with surfactant protein D. *J. Immunol.* **2006**, *176*, 6962–6972.

115. Hartshorn, K.L.; Webby, R.; White, M.R.; Tecle, T.; Pan, C.; Boucher, S.; Moreland, R.J.; Crouch, E.C.; Scheule, R.K. Role of viral hemagglutinin glycosylation in anti-influenza activities of recombinant surfactant protein D. *Respir. Res.* **2008**, *9*, 65.

116. Williams, J.A.; Gui, L.; Hom, N.; Mileant, A.; Lee, K.K. Dissection of epitope-specific mechanisms of neutralization of influenza virus by intact IgG and Fab fragments. *J. Virol.* **2017**, *92*, e02006-17.

117. Jones, J.C.; Settles, E.W.; Brandt, C.R.; Schultz-Cherry, S. Identification of the Minimal Active Sequence of an Anti-Influenza Virus Peptide. *Antimicrob. Agents Chemother.* **2011**, *55*, 1810–1813.

118. White, M.R.; Kandel, R.; Hsieh, I.N.; De Luna, X.; Hartshorn, K.L. Critical role of C-terminal residues of the Alzheimer's associated *β*-amyloid protein in mediating antiviral activity and modulating viral and bacterial interactions with neutrophils. *PLoS ONE* **2018**, *13*, e0194001.

119. Outlaw, M.C.; Dimmock, N.J. Mechanisms of neutralization of influenza virus on mouse tracheal epithelial cells by mouse monoclonal polymeric IgA and polyclonal IgM directed against the viral haemagglutinin. *J. Gen. Virol.* **1990**, *71*, 69–76.

120. Jones, J.C.; Turpin, E.A.; Bultmann, H.; Brandt, C.R.; Schultz-Cherry, S. Inhibition of influenza virus infection by a novel antiviral peptide that targets viral attachment to cells. *J. Virol.* **2006**, *80*, 11960–11967.

121. Kwon, P.S.; Ren, S.; Kwon, S.J.; Kizer, M.E.; Kuo, L.; Xie, M.; Zhu, D.; Zhou, F.; Zhang, F.; Kim, D. Designer DNA architecture offers precise and multivalent spatial pattern-recognition for viral sensing and inhibition. *Nat. Chem.* **2020**, *12*, 26–35.

122. Gao, G.; Vandenberghe, L.H.; Alvira, M.R.; Lu, Y.; Calcedo, R.; Zhou, X.; Wilson, J.M. Clades of Adeno-associated viruses are widely disseminated in human tissues. *J. Virol.* **2004**, *78*, 6381–6388.

123. Boutin, S.; Monteilhet, V.; Veron, P.; Leborgne, C.; Benveniste, O.; Montus, M.F.; Masurier, C. Prevalence of serum IgG and neutralizing factors against adeno-associated virus (AAV) types 1, 2, 5, 6, 8, and 9 in the healthy population: implications for gene therapy using AAV vectors. *Hum. Gene Ther.* **2010**, *21*, 704–712.

124. Zincarelli, C.; Soltys, S.; Rengo, G.; Rabinowitz, J.E. Analysis of AAV serotypes 1-9 mediated gene expression and tropism in mice after systemic injection. *Mol. Ther.* **2008**, *16*, 1073–1080.

125. Halbert, C.L.; Allen, J.M.; Miller, A.D. Efficient mouse airway transduction following recombination between AAV vectors carrying parts of a larger gene. *Nat. Biotechnol.* **2002**, *20*, 697-701.

126. Lai, Y.; Yue, Y.; Liu, M.; Ghosh, A.; Engelhardt, J.F.; Chamberlain, J.S.; Duan, D. Efficient in vivo gene expression by trans-splicing adeno-associated viral vectors. *Nat. Biotechnol.* **2005**, *23*, 1435-1439.

CHAPTER 2

3D DNA ORIGAMI-BASED MULTIVALENT ANTIVIRAL PLATFORM TARGETING NON-ESSENTIAL VIRAL EPITOPES

2.1. Introduction

Vaccines are the ultimate long-term solutions for infectious diseases. However, the inherent structural, genetic, and pathophysiological complexities of some viral pathogens make it challenging to develop effective vaccines against them. For instance, the exceptional genomic variability and quasispeciation of chronic RNA viruses like human immunodeficiency virus (HIV) and hepatitis C virus (HCV), with mutation rates as high as 10^{-3} and 10^{-4} per base per replication, respectively, armor them with ingenious immune evasion mechanisms, thereby complicating the development of vaccines capable of providing effective cross-genotype immunity (1-3). In contrast, despite the slow molecular evolution of DNA viruses, efforts to develop vaccines against herpes simplex viruses (HSV), for instance, have met with limited success. Following primary infection, HSVs often establish latency with a limited expression of viral proteins and only sporadically reactivate to resume their normal lytic cycle and cause diseases (4). Unfortunately, prophylactic treatments against HSVs that can prevent active infections and latency reactivation have not moved past animal trials. The recent coronavirus disease 2019 (COVID-19) pandemic has been an exception on many fronts. It is caused by the highly infectious and transmissible respiratory virus, severe acute respiratory syndrome coronavirus 2 (SARS-CoV-2). Moderna Therapeutics and Pfizer/BioNTech made history in 2020 by developing their SARS-CoV-2 mRNA vaccine candidates for human trials in less than two months since the outbreak and receiving emergency authorization for clinical use in less than a year (5-7). To date, 23 vaccines have been authorized for public use globally, and hundreds more are in various stages of clinical trials (8). This achievement has been deemed the "quantum leap" in vaccine research and development, made possible by the decades-long experience of previous viral epidemics, tremendous infrastructure backing, and state-of-the-art molecular technologies, including gene sequencing and structure-based in silico screening of targets (9). However, over two million lives were already lost before the first vaccine was made

available to the public in 2020. As of July 2022, it has caused more than 500 million infections and over 6 million deaths (10).

Since its inception in the 1960s, antiviral therapy has been substituting for vaccines and addressing problems associated with vaccine inaccessibility (11). It has revolutionized treatments for infectious diseases, as demonstrated by the significant decline in mortality and morbidity associated with Hepatitis, Herpes, and HIV/AIDS, which is no longer characterized as a terminal illness (12). For reference, to date, there are about 47 anti-HIV, 14 anti-HCV, and 9 anti-HSV licensed antiviral drugs in use, and together they save millions of lives every year (13). Likewise, 9 antiviral treatments, including 6 monoclonal antibodies treatments and 3 small molecule drug treatments, have been authorized for the treatment of COVID-19 (14). They have effectively reduced hospitalizations, improved patient care, and unloaded pressure on public health systems. The intensive search for antiretroviral inhibitors during the HIV/AIDS epidemic in the 80s and 90s had partly fueled the soaring discovery of antivirals in the past three decades (13). However, the authorization timeline for antiviral drugs is a far cry from the rate of drug discovery and synthetic productivity. The current arsenal of antiviral treatments has only about 118 FDA-licensed antiviral drugs that treat ten human infectious diseases (15). It comprises predominantly small molecules and a small fraction of oligomeric compounds, including proteins, peptides, carbohydrates, and oligonucleotides, grouped under the umbrella term "biologics". Small molecules and biologics vastly differ in their physiochemical properties and clinical development trajectories. Small molecules are chemically synthesized and, as their name implies, have low molecular weights (less than 1 kDa). Their simple and well-defined structures give them an attractive pharmacological profile that favors oral bioavailability, immune tolerance, predictable side effects, and a superior ability to permeate cell membranes (16). On the other hand, biologics are derived from biological systems and have relatively higher molecular weights, making them impervious to cell membranes and higher structural complexity, making their characterization difficult and clinical outcomes less predictable and tolerable (17). The virus infection cycle is a multistep process involving a series of tightly controlled sequential stages orchestrated by various virus and cellular factors. In principle, antiviral treatments can target any of these stages. However, rather than neutralizing viruses directly, they

inhibit molecular components needed by viruses to progress the infection cycle. Most antiviral drugs target virus-specific cellular machinery such as virus-encoded enzymes or virus-specific structural domains, though some also target host-specific cellular machinery such as host cell protein receptors.

Therapeutic drug development is a complicated process with several challenges unique to small molecules or biologics. However, the bottlenecks of lengthy development timelines, exorbitant costs, and immense infrastructure prerequisites hinder them without bias. Even more concerning is the possibility that post-authorization, the lifetime of these drugs will be severely cut short due to the intractable problem of drug resistance. The large population size of viruses, their high mutation rates, and the often-unchecked exposure of animal reservoirs to antiviral drugs work together to accelerate virus adaptation toward resistance (18). For instance, amantadine and rimantadine are two small molecules belonging to the adamantane family of antiviral drugs that block the M2 ion channels of influenza A viruses (IAV), subsequently preventing virus uncoating. They received clinical authorization in 1966 and 1993, respectively, and were used after that to prevent and treat IAV infections. However, in early 2000, they were discontinued following the rapid and worldwide adamantane resistance caused by a single S31N amino acid substitution within the transmembrane domain of the M2 protein (19, 20). Drug resistance has been reported for six of the ten human virus infections currently being treated with antiviral drugs, including HIV/AIDS, HBV, HCV, herpes, influenza, and SARS-CoV-2/COVID-19. Antiviral selective pressures start working right from the moment of drug administration to compromise its clinical potential. For instance, acyclovir is a small molecule nucleoside analog that acts as a DNA polymerase inhibitor and is widely used to treat herpes infection and encephalitis. Acyclovir-resistant HSV strains were first reported in 1982, shortly after the drug's clinical authorization and initial systemic administration (21). Similarly, multiple variants of concerns (VOC) have already been reported in the last two years since the COVID-19 pandemic (22-26). In particular, with the rise of the omicron variant and sub-variants, the US FDA has already limited the use of three of the six anti-SARS-CoV-2 monoclonal antibody treatments for mild to moderate COVID-19, including REGEN-CoV (casirivimab and imdevimab, administered together), bamlanivab and etesemivab administered together, and

sotromivab (14, 27-29). These limitations have reemphasized COVID-19 vaccine authorization and distribution for all age groups. Additionally, as obligate intracellular parasites, viruses depend on the host-cell biosynthetic machinery to replicate and advance their infection cycle. So, antivirals have limited virus-specific metabolic functions to target without collateral damage to the host. This fact, coupled with the considerable structural and functional differences among viral families, makes developing broad-spectrum antivirals even more challenging.

Therefore, our current repertoire of antiviral drugs and global preparedness fall short of the level needed to deal with novel, reemerging, and persistent infectious diseases. Considering the pressing need for better antivirals and the challenges surrounding clinical drug development pathways, researchers have substantially shifted their focus toward repurposing drugs, especially in the case of viral diseases lacking specific treatments. This strategy provides a "shortcut" to developing effective therapeutic interventions, such as novel drug targets and molecular pathways, by adapting existing (pre-clinical or clinical) drugs into ready-to-run standardized platforms (30). Compared to *de novo* drug discovery, it can reduce development timelines, costs, and potential risks while improving drug predictability and efficacy. Its clinical potential has been demonstrated by an increasing number of studies identifying promising drug candidates for numerous viral infectious diseases, some of which have advanced to clinical trials and received FDA authorization within a few years (31-33). They are described in greater detail elsewhere (30).

A critical element of drug repurposing studies is controlling the effective doses required for antiviral activity, which could be higher than those in clinically approved regimens. One way to increase the effective concentration of antiviral drugs without compromising their therapeutic index is by leveraging multivalency. Multivalent interactions are pervasive phenomena underlying several biological processes, particularly at the molecular, microbial, and cellular levels (34). They can be exemplified by interfacial interactions such as membrane receptors cross-linking different cells or cells with other molecules for signaling, transcription factors binding to DNA for gene regulation, and bacteria and viruses adhering to cell surfaces for infection. They result in enhanced binding and exhibit more distinctive properties than their monovalent counterparts; hence, they can be manipulated to enhance or obstruct collective interactions. For instance, in the early stage of

infection, pathogenic viruses and bacteria adhere to host cell surfaces, typically via multivalent protein-carbohydrate interactions (35-36). Many pathogens employ more than one type of protein-carbohydrate interaction. A summary of viral and bacterial surface ligands and their corresponding receptors is given in this review (34). Individually, the protein-carbohydrate interactions are weak, characterized by dissociation constants (K_D) ranging from uM to mM concentrations, and fail to progress the infection cycle to the next step (37, 38). However, their collective binding strength, also referred to as avidity, is remarkably stronger and subsequently orchestrates the internalization of pathogens inside host cells. For instance, during influenza viral infection, it is estimated that multiple hemagglutinin (HA) ligands of a virus bind to sialic acid (SA) surface receptors of an erythrocyte with an affinity of 10^{13} M^{-1}, but the association constant for a single SA-HA interaction is 10^3 M^{-1} (34).

Conventional antiviral treatments employ monovalent drugs, which require high dosages to outcompete multivalent interactions between viruses and host cells and carry an elevated risk of triggering antiviral resistance mechanisms (39, 40). Therefore, multivalent architectures with different spatial arrangements of ligands are intensively investigated as prophylactic and therapeutic intervention strategies to probe various microbial pathosystems (34, 41). As antivirals, they can competitively inhibit host-pathogen interactions and prevent pathogen adhesion to the host cells during the initial stages of infection. Alternatively, they can be used to display antigenic epitopes that mimic the unique glycoconjugates present on the surface of pathogens, subsequently eliciting or enhancing immune responses as vaccines and immunomodulators (42, 43).

Viral surfaces are decorated with repeating units of proteins, carbohydrates, and lipids, which are responsible for early molecular interactions that attach them to the cell surface before locking into specific entry receptors (35, 36). These domains can serve as pharmaceutically relevant targets depending on their spatial distribution and accessibility. Recent examples of optimized multivalent inhibitors include the structure-based designs of sialic acid (SA) glycoconjugates on dendrimer and icosahedral bacteriophage (Qβ) backbones that enable modulation of ligand density and spacing to mimic native virus epitope geometry and enhance binding efficiency (44, 45). The multivalent ligands bind to hemagglutinin (HA) trimers on the

influenza virus surface with high affinity and block HA interaction with SA receptors on the host cell glycocalyx, preventing cellular entry. Similarly, studies investigating multivalent ligand architectures for HIV include gold nanoparticles displaying oligomannoside ligands, mimicking the high-mannose-type glycans of viral envelope glycoprotein gp120, and obstructing DC-SIGN-mediated HIV infection (46). Another example comprises peptide-triazoles (PT) ligands arranged on gold nanoparticles that bind to HIV-1 envelope gp120 with high affinity and antagonize interactions between the HIV envelope and CCR5/CXCR4 receptors on CD4+ cells, thereby inhibiting virus infection (47). Similarly, for SARS-CoV-2, a few recent studies have reported multivalent designs with proteins and nanobodies that mimic the host angiotensin-converting enzyme 2 (ACE2) receptors and bind to the receptor binding domains (RBD) of the viral spike proteins to block virus entry into cells (48).

A rational design of multivalent inhibitors requires careful consideration of the intrinsic affinity between the virus binding ligands and their receptors on the virus surface, as well as the spatial distribution, density, and accessibility of receptors on the virus surface (41, 49). Additionally, to appeal as broad-spectrum antiviral platforms, they must be modular and adaptable to incorporate different functional domains and accommodate precise spatial configurations that can effectively address the target pathogen. Most of the earlier multivalent inhibitor designs seem to have failed in this aspect, most likely owing to the structural limitations stemming from their choice of scaffold material. The scaffold choice in multivalent systems seems to be the predominant deterministic factor for addressing spatial and temporal control issues such as the geometry, valency, and density of ligands and the avidity, selectivity, flexibility, stability, and biocompatibility of the assembled constructs. In the past, studies investigating multivalent architectures for competitively and effectively inhibiting viral infections primarily focused on the influenza virus and utilized various scaffold materials, including proteins, polymers, dendrimers, nanoparticles, liposomes, and quantum dots, with varying degrees of success. However, to further elucidate their role in functional multivalent systems, systematic studies that compare diverse scaffold architectures synthesized from the same material or that compare different scaffold materials making similar designs are lacking. The intrinsic mechanical features of many of these materials hinder designs that

incorporate modularity, self-assembly, flexibility, and reproducibility, which may explain why multivalent inhibitors have not concretely realized their enormous therapeutic potential. In addition, some of them present non-negotiable problems at biological interfaces, such as high toxicity, poor biocompatibility, and low in vivo efficacy. Together, these challenges present a unique landscape for structural nanotechnology and molecular medicine to occupy.

Structural DNA nanotechnology, with its unique features of molecular self-assembly, nanofabrication, programmability, and nanometer-scale addressability, has emerged as a breakthrough technology enabling the engineering of sophisticated diagnostic, therapeutic, and theranostic tools capable of addressing the aforementioned concerns. The DNA origami (DO) method, pioneered by Rothemund, enables the folding of one long single-stranded scaffold DNA by a set of complementary short strands, resulting in the assembly of highly sophisticated and customizable 2D and 3D nanostructures with well-defined geometry in a homogenous, reproducible, and scalable manner (50). As a biological material, DNA is biocompatible and biodegradable with minimal cytotoxicity. As a construction material, DNA can be modified to incorporate various active domains, such as molecular cargos and targeting ligands, that can cater to the various functionalities of the assembled nanostructures. In addition, DNA nanostructures (DN) can develop dynamic capabilities in response to different physiological or non-physiological stimuli by incorporating responsive components (51).

From a therapeutic perspective, DNA origami nanostructures (DONs) have been extensively investigated as multivalent carriers of molecular cargoes like drugs, antibodies, and therapeutic nucleic acids. DONs such as DO tetrahedra (DT), DO triangles, and DO nanotubes have been successfully used to deliver doxorubicin (Dox), resulting in optimal drug internalization and antitumor effects assessed by increased apoptosis of cancerous cells in vitro and reduced tumor growth *in vivo* (52, 53). Additionally, owing to their modularity and ease of bioconjugation, DONs have been successfully used as multiplexing platforms. Some examples of DO-based multifunctional delivery systems include DO triangles for the co-delivery of Dox with two short hairpin RNAs (shRNA) targeting tumor-associated genes to combat multidrug-resistant tumors (MCF-7R) and DO triangles for the co-delivery of Dox with aptamer-tagged gold nanorods for

effective circumvention of tumor drug resistance (54, 55). To improve targeted drug delivery, DONs can be assembled with ligands that target pathological cues or biomarkers specific to diseases. An early example of DO-based targeted drug delivery includes a dynamic logic-gated nanorobot assembled as a hexagonal barrel, which was used as a vehicle to deliver antibody fragments to cells. Antibody fragments were loaded onto the nanorobot in a closed configuration using an aptamer "lock," which can only be opened upon binding with a specific antigen "key", expressed by target cells (56). The enhanced delivery, uptake, and efficacy of DO-carrier drugs with negligible systemic toxicity demonstrated in these multivalent systems as opposed to monovalent drugs serve as excellent examples of DN-based drug repurposing pipelines. On the diagnostic end, DONs can be assembled with targeting probes like aptamers in dynamic configurations that can give readable outputs upon binding/sensing targets. Studies investigating DON-based sensing, imaging, and genotyping applications have been summarized in greater detail in this review (57).

More recently, DN and DONs have been used to probe different pathosystems as sensors and inhibitors of viral infections (58-61). Kwon et al. developed a 2D star-shaped DNA nanostructure with a unique multivalent display of virus-targeting aptamers that matched the spatial patterning of dengue virus envelope domains (ED3) clusters with nanometer precision (58). The bifunctional DNA nanodevice acted as a sensor with fluorescent output upon binding to dengue virus in human serum and plasma and as an inhibitor that obstructed viral entry into cells. The sensitivity of virus detection in serum samples was 10-fold superior to the standard RT-qPCR-based method. Similarly, the half-maximum effective concentration (EC_{50}) of virus inhibition showed an improvement of 7500-fold compared to the monovalent aptamer inhibitor. In yet another recent study, using the DO technique, Sigl et al. developed different sizes of 3D icosahedral shells made with triangular subunits and functionalized with antibodies for trapping viruses and subsequently inhibiting them (59). The shells were adapted to the architectural symmetry principles of viral capsids and behaved like traps with hollow interiors. Unlike the previous 2D DNA star design, in which the positioning of binders mirrored the spatial patterning of viral epitopes, the shell system incorporated virus binders at set anchor points in the shell interior. By incorporating antiviral antibodies into shells, they demonstrated the trapping of hepatitis B virus (HBV) and neutralization

of adeno-associated virus (AAV) with a modest improvement of half-maximal inhibitory concentration (IC_{50}) by a factor of 3 compared to that of the antiviral antibody. Principally, both designs can work with other candidate virus binders, including antibodies, proteins, peptides, and aptamers. However, for viral specificity, the scaffold architecture in the 2D DNA star paper would also need to be modified along with the virus binders to accommodate the spatial patterning of viral epitopes. On the contrary, the DNA shell system can be customized for any virus by only altering the virus-specific binders. In another recent study by the Wang lab, the authors changed their design architecture to accommodate the differences in the spatial distribution and intrinsic nature of the glycoprotein targets on the virus surface (61). In this work, they developed rational 2D DNA net designs with spatially-patterned aptamers that matched and targeted spike proteins of SARS-CoV2 viruses. Similar to their previous design, the DNA net design incorporated fluorophore-quencher pairs that provided a fluorescent readout upon binding to the target. The detection limit of the sensor was comparable to that of the standard RT-PCR-based methods. However, the half-maximum effective concentration (EC_{50}) of virus inhibition showed an improvement of 1000-fold compared to the monovalent aptamer inhibitor.

In this chapter, we have demonstrated the development of a highly potent 3D DNA origami-based multivalent antiviral platform targeting non-essential viral domains. We demonstrate our strategy by directly targeting the recombinant pseudorabies virus (PRV) 486 through nanobody-conjugated snub cube DNA origami (SC-nbGFP). nbGFP targets pHluorin domains attached to the PRV 486 envelope gM. Among the six nonessential PRV glycoproteins, gM is the only one that is conserved throughout the members of the *Herpesviridae* family, which makes it a potential immunological target (62, 63). Although studies suggest differential roles of glycoproteins across alphaherpesviruses (64), PRV gM is not actively involved in the entry and replication events of viral infection (63, 65). This architecture was strategically designed to multivalently present virus binders in 3D while considering the size differences between the virus and snub cube for maximum interaction with negligible cellular impact and off-target effects. Although previous studies have investigated multivalent interactions and platforms to inhibit viral infections, to our knowledge, the therapeutic potential of non-essential viral targets has not been explored. On the therapeutic front,

antivirals targeting essential viral domains often face the challenge of finding structure-dependent molecular targets and the risk of being short-lived due to the tendency of viruses to mutate those domains more frequently. As such, modular and multivalent scaffold strategies capable of incorporating non-essential but virus-specific binders independent of structural characterization may address these issues on both fronts.

2.2. System Overview

All previous studies on multivalent inhibitors are based on binders with some degree of antiviral activity. In this work, to investigate the potential of non-essential viral epitopes to serve as therapeutic targets, we first assembled our model system, comprising an infectious virus strain and virus binders that target external virus domains.

We selected Pseudorabies virus (PRV) as the prototypical pathosystem in this study. The average PRV virion particle size is ~200 nm in diameter. As the causative agent of swine infectious diseases, PRV is responsible for enormous economic losses in the swine industry worldwide. Even though they have been mostly overlooked as human pathogens, several isolated cases of animal-to-human transmissions have been reported. In the absence of PRV-specific antiviral, the problem is exacerbated by the rise of novel PRV variants which seem to evade immunity provided by the only commercially available attenuated vaccine. We took advantage of the strain PRV 486 that expresses pHluorin (a pH sensitive GFP variant) on the glycoprotein M (gM) domains of the viral envelope (Fig. 1A). By targeting pHluorin domains on the virus directly, we could assess changes in the viral infectivity as a measure of the fluorescence output. PRV 486 is derived from the wild-type PRV Becker strain in which the wild-type gM locus is replaced with the gM-pHluorin coding sequence (66). gM is the only non-essential glycoprotein conserved throughout the *Herpesviridae* family (62). It is a 45 kDa type III transmembrane protein comprising eight membrane-spanning domains and expressed as a heterodimer with gN (65). Functional in vitro and in vivo studies employing gM mutant strains have established the role of gM in the virus replication cycle, particularly in virus secondary envelopment and the membrane trafficking of proteins (63, 67-69). In addition, we explore a most-extreme application of our system by targeting a chimeric epitope

that is not involved in viral infection, and which is embedded within a non-essential protein for PRV virulence.

Considering the ease of synthesis and amenability to modifications and bioconjugation, we selected two distinct sets of binders to target the pHluroin domains of the PRV 486 viruses. First, we selected anti-GFP single-domain antibody fragments, also called VHHs or nanobodies. Nanobodies (nb) offer several advantages over conventional antibodies including their general amenability to be recombinantly expressed, a single binding valency, smaller size, and ability to make fusion proteins to aid in bioconjugation, all of which are favorable for our present study (Fig. 1B). nbs are small monomers with molecular weights of 12-15 kDa, as opposed to ~150 kDa for antibodies. Despite their small size, they retain high binding specificities and affinities in the picomolar to nanomolar range. Although conventionally derived from camelids and sharks, they can be recombinantly produced with high purity and stability in different expression systems. They can be modified with customized tags, including fluorophores, affinity tags, and epitope tags, without compromising their affinity and specificity. In biological systems, they show low immunogenicity and excellent tissue penetration characteristics. In our study, we selected GFP-nanobody (nbGFP), a 35 kDa protein, modified with a His-tag for protein purification and a SNAP-tag for additional conjugation (70). It recognizes GFP and pHluorin and has a one-to-one stoichiometric binding to GFP with a K_D < 2 nM (71-73). The binding affinity of nanobody GFP to PRV 486 was previously unknown.

We selected GFP aptamers (apt-GFP) for our next set of binders. Aptamers are short ssDNA or ssRNA nucleic acid sequences (5-25 kDa; < 100 bases) that form unique secondary and tertiary structures. They show highly selective binding to their targets, with K_D in the picomolar to nanomolar range. They are synthesized by an *in vitro* technology called the Systematic Evolution of Ligands by Exponential Enrichment (SELEX), which involves iterative cycles of target binding with a pool of sequences, separation of bound sequences, and amplification for the next round. Similar to nanobodies, they are easy to synthesize and can be easily modified to incorporate different tags with nanometer precision. For these reasons, they are increasingly used as optical and electrochemical sensors and, more recently, as antiviral agents. The GFP aptamer we have

used in this study has a high binding affinity to EGFP, with K_D < 4nM. Like nbGFP, the binding affinity of aptGFP to PRV 486 was previously unknown.

2.3. Results

2.3.1. nbGFP binds to PRV 486 specifically

Previous studies have reported the binding affinity of nbGFP to EGFP to be K_D < 2 nM (71-73). nbGFP has also been successfully used to detect pHluorin-tagged proteins after exocytosis from synaptic vesicles (74). Similarly, PRV 486 viruses have been detected using anti-GFP antibodies for immunofluorescence (IF) studies (66). However, the binding dynamics of nbGFP to PRV 486 have not been investigated independently. Therefore, we decided to analyze interactions between nbGFP and PRV 486 before the assembly of the multivalent platform.

First, we qualitatively confirmed nbGFP binding to PRV 486 using a super-resolution fluorescence microscopy-based imaging assay (Supp Fig. 2). Next, we performed a semi-quantitative ELISA assay to determine the relative affinity of nbGFP to PRV 486. In brief, we coated 96 well ELISA plates with PRV 486 and incubated nbGFP at concentrations ranging from 10 pM to 1 uM. The virus-bound nbGFP was detected with an anti-histidine horseradish peroxidase that catalyzed a colorimetric reaction upon adding TMB substrate. The representative ELISA binding curves are shown in Fig. 1C. The nbGFP molecules were able to bind to the viruses and showed concentration-dependent changes in virus binding. Compared to the virus, nbGFP bound more strongly to EGFP, which we used as a positive control. Although absolute K_D values could not be determined since we used semi-purified viral stocks, we estimated the relative binding affinities using standard curve-fitting for the binding curves. Semi-purified viral stocks were chosen because they more accurately reflect the biologically relevant milieu of intact viral particles and partially formed viral particles that are likely present when an antiviral is to be presented. The relative binding affinities of PRV 486 to nbGFP and EGFP were ~14 nM and ~0.5 nM, respectively. The lower affinity of nbGFP binding to PRV 486 than EGFP is most likely due to the three amino acid changes, at positions 147, 204, and 206, in pHluorin epitopes that bind to the complementarity determining regions (CDRs) of the nbGFP (Fig 1D).

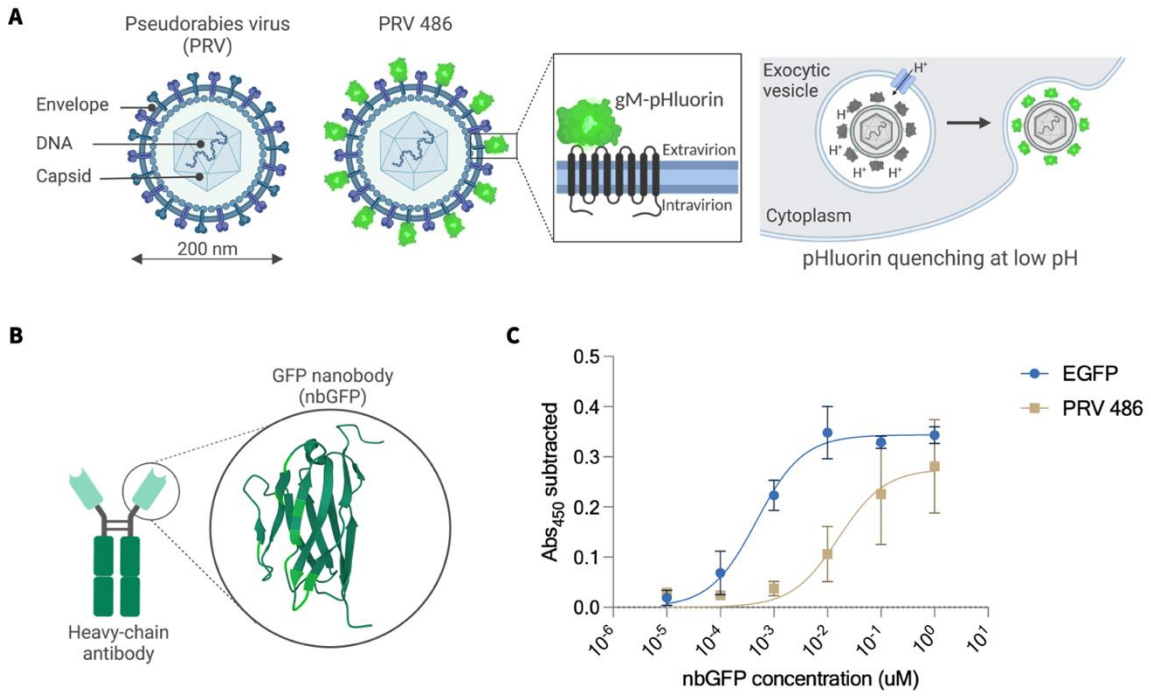

D

Protein	Epitopes of nbGFP
EGFP	E142, N144, N146, **S147**, K166, R168, N170, D173, G174, V176, **Q204**, **A206**, F223
pHluorin	E142, N144, N146, **D147**, K166, R168, N170, D173, G174, V176, **T204**, **T206**, F223

Fig. 1| Characterization of nbGFP binding activity. **A,** Schematic illustrating the structural components of Pseudorabies virus (PRV). PRV 486 expresses pHluorin on the virus envelope which gets quenched in low pH, typically found inside intracellular vesicles. **B,** Schematic illustrating nanobody structure. Ribbon diagram of nbGFP highlighting the amino acids that directly contact GFP. **C,** ELISA binding curves of nbGFP to PRV 486 and EGFP. The absorbance values represent the specific binding of nbGFP. Absorbance resulting from non-specific interactions without the virus or EGFP was subtracted at every tested concentration. Data are presented as mean ± S.E.M., N = 2 biologically independent experiments. **D,** Table showing epitopes of nbGFP on EGFP and pHluorin. The three amino acids that are different between the two molecules are highlighted in bold. nbGFP ribbon diagram created using Mol* (D. Sehnal, S. Bittrich, M. Deshpande, R. Svobodová, K. Berka, V. Bazgier, S. Velankar, S.K. Burley, J. Koča, A.S. Rose (2021) Mol* Viewer: modern web app for 3D visualization and analysis of large biomolecular structures. Nucleic Acids Research).

2.3.2. Design, assembly, and characterization of the multivalent platform

DNA origami (DO) technology enables the synthesis of 3D molecular scaffolds for the spatial presentation of biomolecules with defined nanometer-level precision to build functional molecular

devices (50, 60, 76). To investigate the effect of multivalency on virus binding and subsequent infectivity, we used DNA origami to spatially distribute virus binders, resulting in the formation of the multivalent platform. Previous studies have shown that the size, shape, and complexity of DNA nanostructures affect their stability, pharmacokinetics, and interactions at biological interfaces *in vitro* and *in vivo* (77-84). Like other Herpes viruses, PRV is about ~200 nm in diameter. Studies demonstrating a size-dependent effect on multivalent interactions have shown a higher degree of viral inhibition with inhibitor sizes slightly smaller or similar to the virus (85, 86). Increasing the size of the DNA origami scaffold to match the size of the virus may increase the antiviral efficacy of the multivalent system and provide a higher surface area to increase the valency without clustering of ligands (85). However, a larger DNA origami nanostructure is likely to compromise its immunotolerance and necessitate a higher Mg^{2+} ion concentration to maintain its structural integrity which is not typical in physiological environments (77, 78). In an effort to rationally design the DO scaffold considering the size range of virus particles while maintaining the structural integrity of the assembled multivalent system and a low surface area to volume ratio, we opted for wireframe DNA origami scaffolds, ~50-100 nm diameter size.

To this end, we adapted the snub cube (SC), a 3D wireframe DNA origami, ~60 nm diameter-size, with 60 edges, 24 vertices, and 38 faces, including 6 squares and 32 equilateral triangles (87). For multimerization of SC with virus binders, we site-specifically conjugated 60 copies of nbGFP per SC (one on each edge of the SC) via benzyl guanine (BG) linkers. We named this construct SC60H-nbGFP, where H is the number of handles. The formation of SC60H-nbGFP was accomplished in three steps: i) synthesis of SC60H scaffold, ii) incorporation of complementary linker strands into SC60H, and iii) conjugation of nbGFP to the linker strands-attached SC60H. The SC60H was assembled by hybridizing a 7249-nucleotide M13mp18 ssDNA with a ten-fold molar excess of 192 staple strands in a one-pot thermal annealing reaction followed by purification with 100 kDa molecular weight cut-off filtration (Fig 2A). The staple sequences making up each of the 60 edges were modified from the original SC design to include 20 nucleotides-long single-stranded DNA (ssDNA) overhangs that complement the linker strands (Fig. 2B). Using this approach, we can vary the copy number of virus binders in the SC scaffold from 1 to 60. Next, the sixty ssDNA

overhangs of the SC60H were hybridized with complementary ssDNA linker strands tagged with BG domains (BG-ssDNA). Finally, the BG-tagged SC60H molecules were conjugated to SNAP-tagged nbGFP. We maintained a 12.5 mM Mg^{2+} concentration throughout all preparation and purification steps to retain the structural integrity of the 3D DNA nanostructures. We characterized the formation of SC60H, SC60H-BG-DNA, and SC60H-nbGFP after each step using 1% AGE (Fig. 2C). The gel shift assay showed distinct bands, validating the formation of DO nanostructures (Fig. 2). The reduced electrophoretic mobility of bands aligned with their relatively increasing molecular weights, confirming the correct formation of nanostructures after each synthesis step. The final SC-nbGFP were the heaviest nanostructures showing the lowest mobility in AGE, followed by SC-BG-DNA intermediate nanostructures with the complementary ssDNA attached to the BG-linker and finally by the SC constructs with 60 ssDNA overhangs corresponding to their valency.

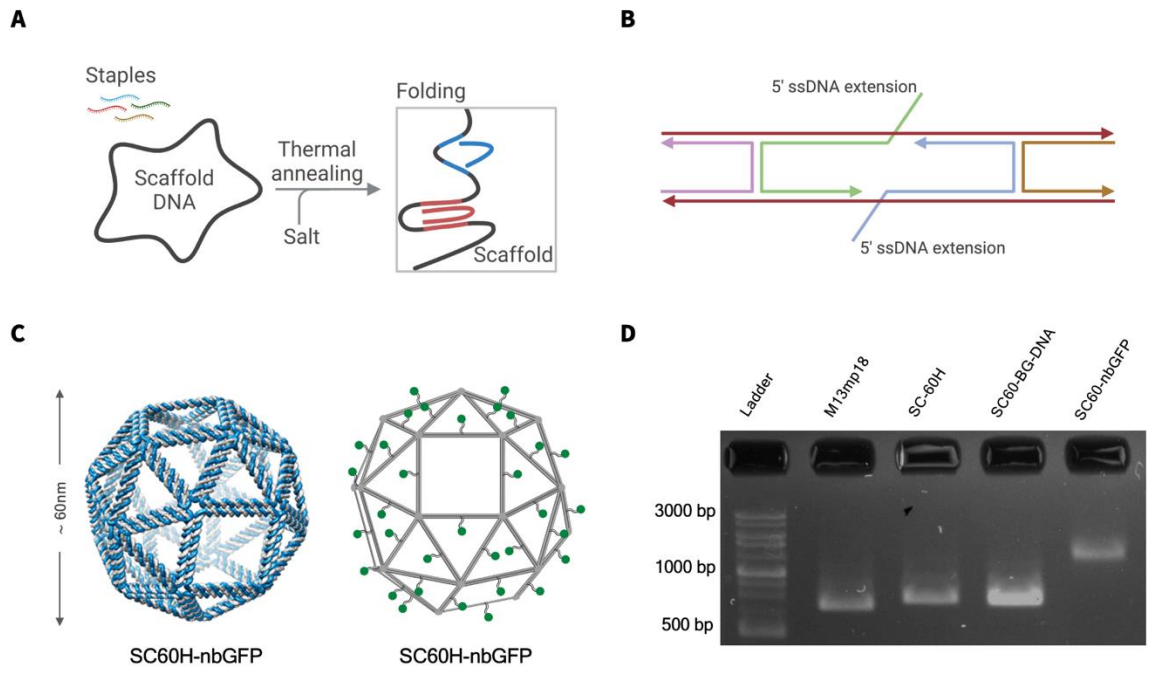

Fig. 2| Characterization of the multivalent system. **A,** Schematic of the DNA origami technology. The technique involves folding the M13mp18 ssDNA using short staple strands in the presence of cations such as Mg^{2+}. **B,** Secondary structure of an edge of the snub cube (SC) with ssDNA overhang. **C**, Schematic of the 3D structure of the SC with 24 vertices and 60 edges and SC-nbGFP displaying multiple copies of nbGFP. **D,** Gel shift assay using 1% AGE showing the successive formation of SC60H, SC60H-BG-DNA, and SC60H-nbGFP. The unfolded M13mp18 strand is used as a reference.

2.3.3. SC60H-nbGFP enhances virus binding avidity

To address the functionality of the multivalent system, we first analyzed the impact of SC60H-nbGFP valency on virus binding using a semi-quantitative ELISA assay. We coated 96 well ELISA plates with PRV 486 and incubated the virus binders, nbGFP, and SC60H-nbGFP, at different concentrations. We quantified the extent of binding of nbGFP and SC60H-nbGFP using an orthogonal nbGFP-specific reporter antibody coupled to horseradish peroxidase (HRP). Residual nbGFP and SC60-nbGFP that were bound to the wells were detected by HRP-catalyzed colorimetric reaction upon the addition of TMB substrate.

The data from the ELISA binding assay are normalized to reflect specific binding values (Fig 3). We used AbGFP as a positive control for nbGFP-associated binders. All binders showed concentration-depended changes in the absorbance values, suggesting specific binding activity. The low binding of nbGFP at concentrations < 10nM is attributable to inefficient passivation of virus surfaces to prevent non-specific interactions. However, the virus binding avidity was enhanced in the presence of the multivalent binder, SC60H-nbGFP. Although we could not quantify the absolute binding affinities using ELISA since we did not account for the batch-to-batch variations in nbGFP and semi-purified virus stocks, the relative KD showed a 1000-fold enhancement in the binding affinity of SC60H-nbGFP (~14 pM) compared to the monomeric nbGFP (~16 nM)

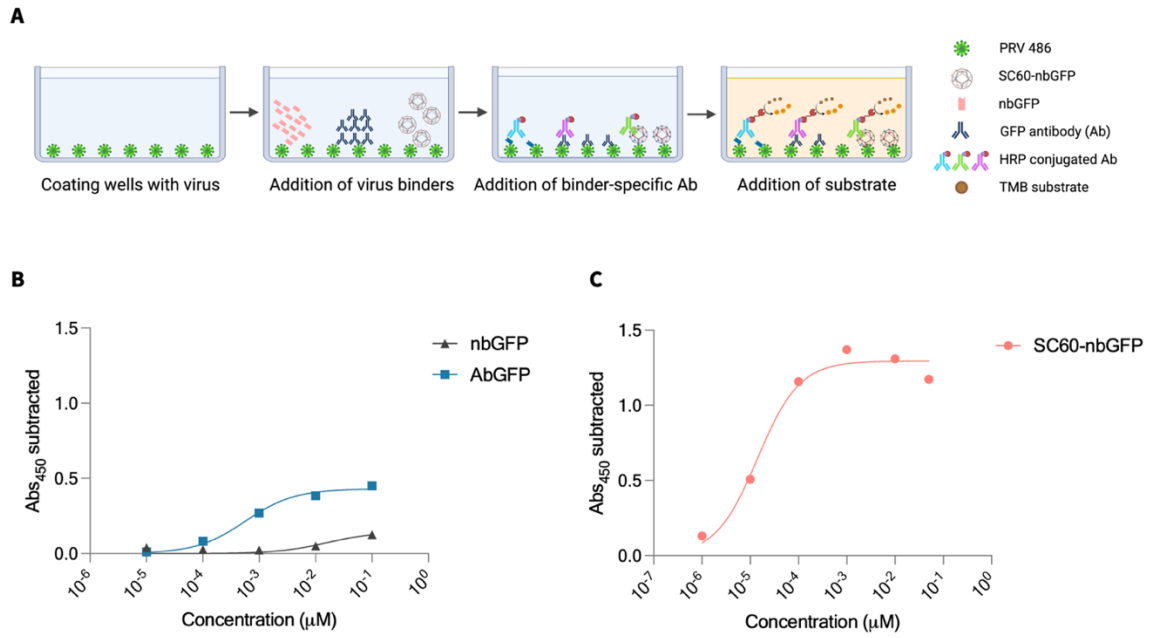

Fig. 3| Characterization of SC60H-nbGFP binding activity. **A,** Schematic of ELISA assay. **B and C,** ELISA binding curves of PRV 486 to nbGFP, AbGFP, and SC60H-nbGFP. Graphs are separated to reflect the x-axis protein concentrations (left) and DNA concentrations (right). Absorbance values resulting from non-specific interactions without the virus or EGFP were subtracted. Data are presented as the average of two technical replicates.

2.3.4. SC60H-nbGFP compromises PRV 486 infectivity *in vitro*

Encouraged by our previous results, we investigated if enhancement of virus binding avidity can influence viral infectivity by performing a plaque reduction assay *in vitro*. To this end, we incubated PRV 486 viral particles with a 1000-fold molar excess (100 nM) of SC60H-nbGFP and determined the residual infectivity by infecting PK15 cells. Viral infectivity is calculated as the ratio of the number of plaques formed in the treatment group to the number of plaques formed in the control group with no binders. We found that incubation of PRV 486 with SC60H-nbGFP significantly reduced viral infectivity by ~50% (Fig 4A). In comparison, the presence of just the scaffold, SC60H, or the monomeric binder, nbGFP, had negligible effects on PRV 486 infectivity.

Next, to assess the antiviral efficacy of SC60H-nbGFP, we performed a dose-response analysis (Fig 4B). We incubated PRV 486 particles with increasing concentrations of the multivalent binder and performed plaque reduction assays on PK15 cells. As controls, we examined the inhibition of the virus by the scaffold, SC60H, and the binder, nbGFP. The group infected with PRV

486 alone is used as the reference to determine viral infectivity of other groups treated with the multivalent binder or its individual components. The representative images from plaque assays are shown in Fig 4C. According to our data, SC60H-nbGFP demonstrated dose-dependent inhibition of PRV 486 with an estimated half maximal inhibitory concentration (IC_{50}) of ~3 nM. In contrast, the viral infectivity remained unchanged upon treatment with the control groups comprising either the scaffold, SC60H, or the binder, nbGFP.

These results indicate that the enhancement of virus binding achieved with SC60H-nbGFP effectively impeded the virus infection cycle. The data also establish that multimerization of non-inhibitors such as the gM-pHluorin targeting nbGFP on rational DNA origami scaffolds such as the snub cube can be effective strategies for probing viral pathosystems and developing effective interventions.

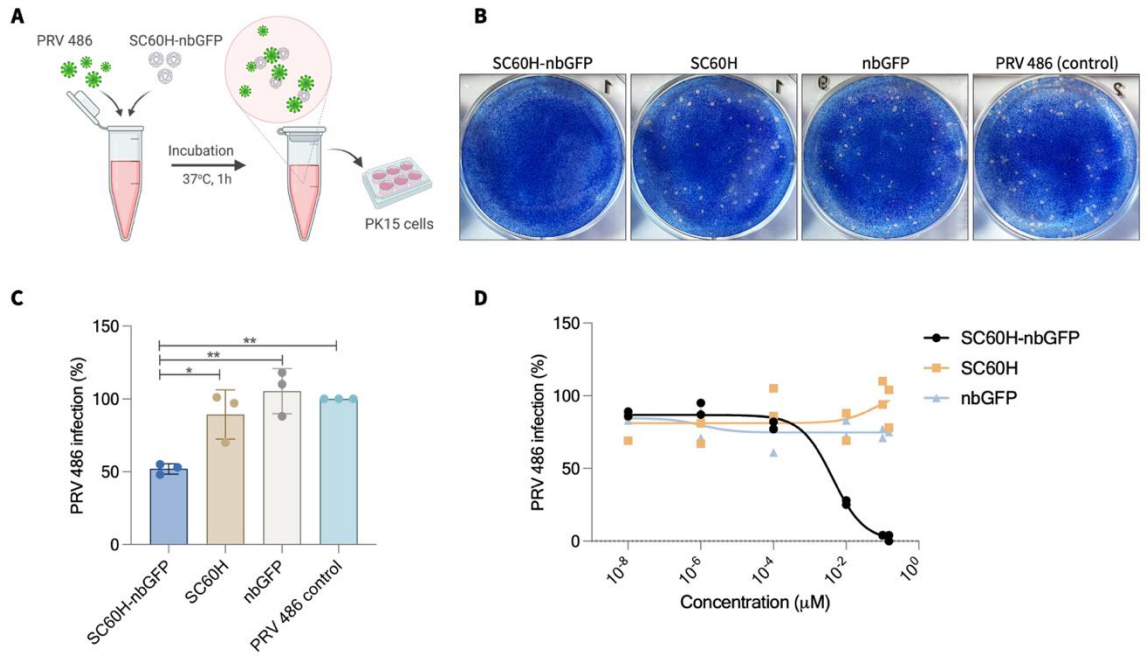

Fig. 4| Effect of SC60-nbGFP on PRV infectivity *in vitro.* **A,** Schematic illustrating infectivity assays. **B,** Comparison of residual infectivity of PRV 486 after treatment with different groups. Data are presented as mean ± S.E.M., N = 3 biologically independent experiments. A two-tailed *t*-test was performed to test significance against the PRV-only group (***P* < 0.005; **P* < 0.05). The infectivity of PRV only group is used as the reference for calculating percent infectivity. C, Representative plaque assays corresponding to the maximum concentration of SC60-nbGFP, SC60, and nbGFP at 150nM. PRV 486 group is shown for reference. **D,** Dose-dependent, plaque-reducing inhibition

curves for the SC60-nbGFP, SC60 (scaffold only), and nbGFP (binder only). Data are presented to show individual replicates.

2.3.5. The IC_{50} is nontoxic to cells *in vitro*

An ideal drug should have a relatively high therapeutic index (TI), i.e., it should be effective at low concentrations and toxic only at very high concentrations (88). Previous studies have attested to the minimal toxicity of DNA-based molecular devices, which makes them attractive therapeutic tools. Here, to further substantiate the therapeutic efficacy of our antiviral platform, we investigated the cytotoxicity of SC60H-nbGFP in PK15 cells using an LDH assay. In brief, we incubated cells with different concentrations of SC60H-nbGFP for 24 hours and processed the cell supernatant to quantify cytotoxicity levels. The LDH assay measures lactate dehydrogenase (LDH) enzyme released by cells upon damage to the plasma membrane in response to cytotoxic components in the cell culture medium.

The data that we obtained are summarized in Fig 5. For the range of concentrations that we tested, we observed no apparent cytotoxicity with SC60H-nbGFP at concentrations < 10 nM. This is consistent with previous studies employing 2D, and 3D DO nanostructures (59, 89). At concentrations > 10 nM, SC60H-nbGFP exhibited a cytotoxic effect on the PK15 cells that was similar to that of SC60H and M13 controls, which indicates that the observed cytotoxicity is due to the DNA component of the multivalent assembly. At the highest DNA concentration of 150 nM, the viability dropped to ~80-90% for SC60H-nbGFP and SC60H. For M13, the drop in cell viability was comparatively higher at ~70-80%. The IC_{50} value of ~3nM falls below the toxicity threshold of SC60H-nbGFP. However, additional experiments are needed to understand how this data fits into the broader context of the SC60H-nbGFP pharmacological profile.

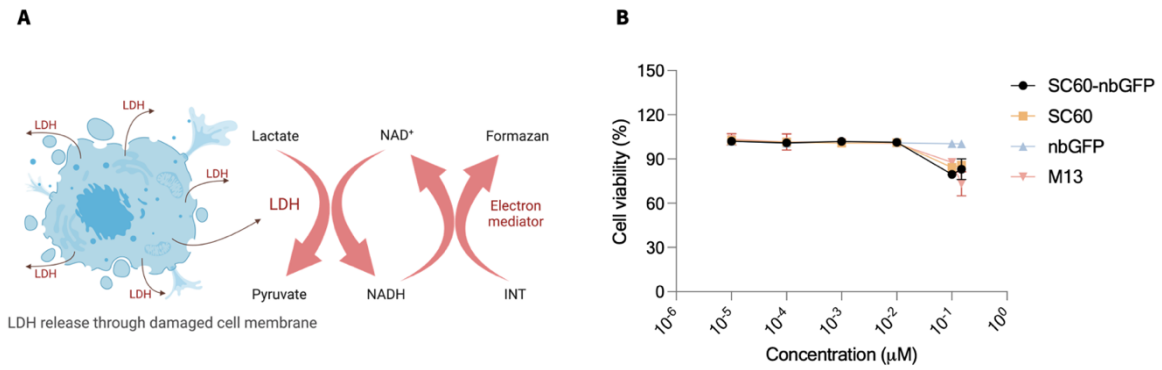

Fig. 5| *In vitro* cytotoxicity assay. **A,** Schematic illustrating the release of lactate dehydrogenase (LDH) enzyme after damage to the cell membrane. **B**, Cell viability after treatment with SC60-nbGFP for 24h. Data are presented as mean ± S.E.M., N = 2 biologically independent experiments.

2.4. Discussion

In this chapter, we have demonstrated the development of a 3D DNA origami-based multivalent antiviral platform. In doing so, we have argued that multivalency can be leveraged to expand the repertoire of antiviral targets to include non-essential viral domains. As the prototypical pathosystem in our study, we chose the recombinant Pseudorabies virus 486, expressing pHluorin domains on the gM of the virus envelope. We targeted the virus using nanobody GFP (nbGFP) binders conjugated at a one-to-one stoichiometric ratio to the 60 edges of the 3D wireframe snub cube (SC) scaffold.

Our multivalent scaffold showed an IC_{50} in the lower nanomolar range, consistent with a few recent studies using multivalent DNA-based 2D and 3D scaffolds for antiviral applications (58, 59, 61). Since no antivirals are available for PRV, we could not directly compare our system's efficacy. However, a recent paper reported an IC_{50} of 15.2 - 31.6 μg/mL (100 - 600 nM) with monoclonal antibodies developed against gB of different PRV strains (90). More importantly, in contrast to all the previous multivalent inhibitor designs that rely on binders targeting essential viral domains, our multivalent system targeted the PRV gM, the only non-essential gene conserved throughout the *Herpesviridae* family, which does not actively participate in virus entry processes (65). To our knowledge, the therapeutic potential of non-essential viral targets has not been explored. For instance, the aptamer binders in the recent DNA star study targeted the envelope protein domain

III (ED3) clusters of the Dengue virus that interact with the primary and secondary cell surface receptors (91, 92). Similarly, the aptamer binders in the recent DNA net study targeted the receptor binding domains of the trimeric spike proteins of SARS-CoV2. Similarly, numerous studies on influenza viruses have utilized protein, peptides, and aptamers targeting the hemagglutinin (HA) epitopes that bind to the cell surface receptors and mediate the virus entry processes (45, 93-95). As expected, by targeting these essential domains, the monovalent binders demonstrated antiviral activity as well, although poorly. The monomeric aptamers in the DNA star and the DNA net papers showed IC_{50} of ~10 μM and ~15 μm, respectively. In comparison, the multivalent inhibitors enhanced the IC_{50} values by three orders of magnitude. The enhancement was mainly attributed to their design strategy to display the binders matching the spatial pattern of virus epitopes with nanometer-scale precision. DNA nanostructures seem to be the perfect scaffold for the rational design of multivalent inhibitors, a challenge that has remained largely unaddressed by the conventional polymeric and inorganic scaffolds. However, in contrast to these studies, the monomeric nbGFP binders in our study failed to inhibit PRV 486 viruses even at a concentration of 50 μM (the highest concentration that we tested), while the multivalent SC-nbGFP demonstrated an IC_{50} ~3 nM. We demonstrated the switch of a non-inhibitor targeting non-essential viral domains to a highly potent one by conjugating it to the 3D DNA origami scaffold and leveraging multivalency for its spatial distribution across the SC surface.

A possible explanation for this could lie in the spatial proximity of gM to other glycoproteins, such as gB, gC, gD, and gH/gL, which are responsible for PRV attachment and binding with cell surface receptors (96). Although the spatial distribution of PRV envelope glycoproteins has not been resolved yet, studies on Herpesviruses, a close counterpart of PRV, have shown that glycoproteins, gB, gC, and gH/gL, are evenly distributed on the virus envelope. The dynamic gD seems to reorganize from functional clustering to a more even distribution during virus binding, subsequently triggering gB and gH/gL mediated membrane fusion (97). In our study, virus-bound SC60H-nbGFP could sterically block the interactions of entry-associated glycoproteins with the cell surface receptors. Another explanation for this is that virus-bound SC60H-nbGFP could increase the molecular weight of the virus particles and compromise their passive mobility achieved via

Brownian motion. Based on our findings, we argue that factors such as steric shielding and virus mobility can be equally effective in modulating key deterministic events of viral infection. This opens the prospect of expanding binder choice to include non-essential targets as long as they are accessible and expressed in sufficient copy numbers.

The performance of the SC-nbGFP in the cytotoxicity assay further substantiates the therapeutic potential of DNA-based multivalent platforms. Investigating the toxicity of DNA nanostructures is essential to realize their clinical translational potential. Interactions and uptake of DNA nanostructures at cellular interfaces can exert cytotoxic effects by activating pathways generating reactive oxygen species, caspase activity, and damage to intracellular organelles. Studies have shown that DNA nanostructures of different shapes are uptaken by scavenger receptors via endocytic pathways (80, 98) and that the uptake depends on their size, shape, compactness, aspect ratio, and the cell type exposed to them (80, 99). As 3D wireframe DNA origami nanostructures with a negatively charged backbone, we anticipated the SC60H-nbGFP remain relatively inert to cellular interactions owing to the negative membrane potential of cells. According to our findings, SC60H-nbGFP demonstrated no cytotoxicity in PK15 cells up to 10 nM concentrations, which is consistent with studies assessing *in vitro* cytotoxicity of DO nanostructures, including a wireframe 3D DNA icosahedron (~43 nm), a solid 3D octahedral half shell (~90 nm) and a hollow 3D DNA triangle (~50 nm) (59, 89, 100). Although these studies did not test cytotoxicity at DNA nanostructure concentrations > 10 nM, the cell viability dropped to ~80-90% at 150 nM in our study. We observed a similar effect with SC60H and M13 but not with nbGFP control groups. This suggests that the observed cytotoxicity is due to the DNA component of the multivalent assembly. However, since we did not independently investigate the cellular uptake of our DNA nanostructures, we cannot confirm if the observed cytotoxicity resulted from the uptake of intact DNA nanostructures or their degradation products over time (101). Furthermore, the cytotoxicity of SC-nbGFP nanostructures may vary *in vivo*, where they are more likely to encounter different cell types, such as epithelial cells, endothelial cells, and immune cells, with different endocytosis profiles.

2.5. Conclusion

Viral infectious diseases are among the biggest threats to human health, including viruses we know of now and future viruses that may spill over from animal reservoirs. We studied PRV because it is a good model system for the HERPES complex 1 and 2 that impact humans and because it is a virus that impacts the global food supply by limiting the swine industry. In particular, viruses such as PRV and Herpes present a unique challenge in their treatment and prevention because they tend to establish lifelong latent infections. So far, no antivirals have been developed for PRV, and the only vaccine against the PRV Bartha strain seems ineffective at providing cross-genotype immunity. These limitations underscore the need to develop new anti-PRV agents with antiviral activity based on alternative mechanisms of action.

In response to the increasing need for new and improved antiviral drugs, the functionality of multivalent interactions has been recognized in many therapeutic applications, including antiviral interventions. In this chapter, using 3D DNA origami as a platform for the spatial presentation of virus binders, we demonstrated the inhibition of PRV 486 viruses. Building on the fundamental principle of multivalent interactions to enhance functional avidity, we demonstrated how it could be leveraged to develop potent antiviral platforms by targeting non-essential virus domains. This study is perhaps the first to explore and highlight the potential of non-essential virus domains to serve as therapeutic targets, many of which remain conserved among viral families. Our strategy can be implemented with other pathosystems and viral vectors to modulate infectivity with negligible impact on the cells. This strategy can also be instrumental in targeting viral pathogens that are novel, emerging, and understudied. Unlike rational design strategies to match spatial epitope patterns that rely on extensive knowledge of the molecular nature of host-pathogen interactions, our strategy can be implemented with limited information on the spatial distribution of virus epitopes and with non-essential targets; many of which remain highly conserved among virus families. The SC60H-nbGFP platform can be implemented to modulate the infectivity of other recombinant viruses expressing GFP/pHluorin domains, particularly in gene therapy studies that employ fluorescently tagged-AAV and lentivirus systems. In addition, the SC scaffold can be adapted to include pre-characterized virus binders such as virus-specific peptides, aptamers, nanobodies, and antibodies, with weak to

moderate binding affinities but great pharmacodynamic/pharmacokinetic profiles to enhance their virus binding avidity and inhibition efficacy. Furthermore, with the advancement of high-throughput screening technologies such as *in vitro* evolution of nucleic acids and microarrays for carbohydrates, proteins, and peptides, it is possible to quickly identify candidate virus-specific binders without requiring exhaustive virus structural characterization.

To establish this system as a proof-of-concept, additional work is needed to validate the system in other pathosystems, starting with recombinant viral vectors with fluorescently tagged envelope domains. Future implementations of this work should include investigations into correlations between valency and stoichiometric binding ratios to identify minimum binder valency to achieve maximal inhibition efficacy. It would also be helpful to examine underlying inhibition mechanisms in relation to targeting non-essential viral domains. Since PRV is known to establish latency with sub-clinical infection and sporadic activation, it would be interesting to know if such antiviral platforms can help to reduce viral load after the onset of symptoms. Finally, to enhance the therapeutic potential of such platforms, an in-depth analysis of stability, cytotoxicity, and immunogenicity is essential. The ultimate test, of course, is validating safety and efficacy *in vivo*.

REFERENCES

1. Cuevas JM, Geller R, Garijo R, López-Aldeguer J, Sanjuán R. Extremely high mutation rate of HIV-1 in vivo. PLoS biology. 2015;13(9):e1002251.

2. Ribeiro RM, Li H, Wang S, Stoddard MB, Learn GH, Korber BT, et al. Quantifying the diversification of hepatitis C virus (HCV) during primary infection: estimates of the in vivo mutation rate. 2012.

3. Cuevas JM, González-Candelas F, Moya A, Sanjuán R. Effect of ribavirin on the mutation rate and spectrum of hepatitis C virus in vivo. Journal of virology. 2009;83(11):5760-4.

4. Dropulic LK, Cohen JI. The challenge of developing a herpes simplex virus 2 vaccine. Expert review of vaccines. 2012;11(12):1429-40.

5. **Moderna's Work on a Potential Vaccine Against COVID-19**. Available from: https://www.sec.gov/Archives/edgar/data/1682852/000119312520074867/d884510dex991.htm#:~:text=On%20January%2013%2C%202020%2C%20the,vaccine%20against%20the%20novel%20coronavirus.

6. Walsh EE, Frenck Jr RW, Falsey AR, Kitchin N, Absalon J, Gurtman A, et al. Safety and immunogenicity of two RNA-based Covid-19 vaccine candidates. New England Journal of Medicine. 2020;383(25):2439-50.

7. Jackson LA, Anderson EJ, Rouphael NG, Roberts PC, Makhene M, Coler RN, et al. An mRNA vaccine against SARS-CoV-2—preliminary report. New England journal of medicine. 2020.

8. The COVID-19 vaccine race. Available from: https://www.gavi.org/vaccineswork/covid-19-vaccine-race.

9. Ball P. The lightning-fast quest for COVID vaccines - and what it means for other diseases. 2020.

10. WHO Coronavirus (COVID-19) Dashboard [Available from: https://covid19.who.int/.

11. Bauer D, St Vincent L. Prophylactic Treatment of Smallpox Contacts with N-Methylisatin (β-Thiosemicarbazone (Compound 33T57, Marboran). Lancet. 1963:494-6.

12. Hoy-Ellis C, Fredriksen-Goldsen K. Is AIDS chronic or terminal? The perceptions of persons living with AIDS and their informal support partners. AIDS care. 2007;19(7):835-43.

13. De Clercq E, Li G. Approved antiviral drugs over the past 50 years. Clinical microbiology reviews. 2016;29(3):695-747.

14. Antiviral Drugs That Are Approved, Authorized, or Under Evaluation for the Treatment of COVID-192022. Available from: https://www.covid19treatmentguidelines.nih.gov/therapies/antiviral-therapy/summary-recommendations/.

15. Tompa DR, Immanuel A, Srikanth S, Kadhirvel S. Trends and strategies to combat viral infections: A review on FDA approved antiviral drugs. International journal of biological macromolecules. 2021;172:524-41.

16. Li Q, Kang C. Mechanisms of action for small molecules revealed by structural biology in drug discovery. International Journal of Molecular Sciences. 2020;21(15):5262.

17. Declerck PJ. Biologicals and biosimilars: a review of the science and its implications. GaBI J. 2012;1(1):13-6.

18. Kumar M, Kuroda K, Dhangar K, Mazumder P, Sonne C, Rinklebe J, et al. Potential emergence of antiviral-resistant pandemic viruses via environmental drug exposure of animal reservoirs. Environmental science & technology. 2020;54(14):8503-5.

19. Bright RA, Medina M-j, Xu X, Perez-Oronoz G, Wallis TR, Davis XM, et al. Incidence of adamantane resistance among influenza A (H3N2) viruses isolated worldwide from 1994 to 2005: a cause for concern. The Lancet. 2005;366(9492):1175-81.

20. Deyde VM, Xu X, Bright RA, Shaw M, Smith CB, Zhang Y, et al. Surveillance of resistance to adamantanes among influenza A (H3N2) and A (H1N1) viruses isolated worldwide. The Journal of infectious diseases. 2007;196(2):249-57.

21. Crumpacker CS, Schnipper LE, Marlowe SI, Kowalsky PN, Hershey BJ, Levin MJ. Resistance to antiviral drugs of herpes simplex virus isolated from a patient treated with acyclovir. New England Journal of Medicine. 1982;306(6):343-6.

22. McCallum M, Bassi J, De Marco A, Chen A, Walls AC, Di Iulio J, et al. SARS-CoV-2 immune evasion by the B. 1.427/B. 1.429 variant of concern. Science. 2021;373(6555):648-54.

23. Dejnirattisai W, Zhou D, Supasa P, Liu C, Mentzer AJ, Ginn HM, et al. Antibody evasion by the P. 1 strain of SARS-CoV-2. Cell. 2021;184(11):2939-54. e9.

24. Chen RE, Zhang X, Case JB, Winkler ES, Liu Y, VanBlargan LA, et al. Resistance of SARS-CoV-2 variants to neutralization by monoclonal and serum-derived polyclonal antibodies. Nature medicine. 2021;27(4):717-26.

25. Diamond M, Chen R, Winkler E, Case J, Aziati I, Bricker T, et al. In vivo monoclonal antibody efficacy against SARS-CoV-2 variant strains. Research square. 2021.

26. McCallum M, Walls A, Sprouse K, Bowen J, Rosen L, Dang H, et al. Molecular basis of immune evasion by the delta and kappa SARS-CoV-2 variants. bioRxiv [Preprint]. 2021 Aug 12: 2021.08. 11.455956. doi: 10.1101/2021.08. 11.455956. PMID.

27. Cameroni E, Bowen JE, Rosen LE, Saliba C, Zepeda SK, Culap K, et al. Broadly neutralizing antibodies overcome SARS-CoV-2 Omicron antigenic shift. Nature. 2022;602(7898):664-70.

28. VanBlargan LA, Errico JM, Halfmann PJ, Zost SJ, Crowe JE, Purcell LA, et al. An infectious SARS-CoV-2 B. 1.1. 529 Omicron virus escapes neutralization by therapeutic monoclonal antibodies. Nature medicine. 2022;28(3):490-5.

29. Case JB, Mackin S, Errico JM, Chong Z, Madden EA, Whitener B, et al. Resilience of S309 and AZD7442 monoclonal antibody treatments against infection by SARS-CoV-2 Omicron lineage strains. Nature communications. 2022;13(1):1-11.

30. Mercorelli B, Palù G, Loregian A. Drug repurposing for viral infectious diseases: how far are we? Trends in microbiology. 2018;26(10):865-76.

31. Sissoko D, Laouenan C, Folkesson E, M'lebing A-B, Beavogui A-H, Baize S, et al. Experimental treatment with favipiravir for Ebola virus disease (the JIKI Trial): a historically controlled, single-arm proof-of-concept trial in Guinea. PLoS medicine. 2016;13(3):e1001967.

32. Haffizulla J, Hartman A, Hoppers M, Resnick H, Samudrala S, Ginocchio C, et al. Effect of nitazoxanide in adults and adolescents with acute uncomplicated influenza: a double-blind, randomised, placebo-controlled, phase 2b/3 trial. The Lancet Infectious diseases. 2014;14(7):609-18.

33. Arabi YM, Alothman A, Balkhy HH, Al-Dawood A, AlJohani S, Al Harbi S, et al. Treatment of Middle East respiratory syndrome with a combination of lopinavir-ritonavir and interferon-β1b (MIRACLE trial): study protocol for a randomized controlled trial. Trials. 2018;19(1):1-13.

34. Mammen M, Choi SK, Whitesides GM. Polyvalent interactions in biological systems: implications for design and use of multivalent ligands and inhibitors. Angewandte Chemie International Edition. 1998;37(20):2754-94.

35. Imberty A, Varrot A. Microbial recognition of human cell surface glycoconjugates. Current opinion in structural biology. 2008;18(5):567-76.

36. Karlsson K-A. Pathogen-host protein-carbohydrate interactions as the basis of important infections. The Molecular Immunology of Complex Carbohydrates—2. 2001:431-43.

37. TAKEMOTO DK, SKEHEL JJ, WILEY DC. A surface plasmon resonance assay for the binding of influenza virus hemagglutinin to its sialic acid receptor. Virology. 1996;217(2):452-8.

38. Sauter NK, Bednarski MD, Wurzburg BA, Hanson JE, Whitesides GM, Skehel JJ, et al. Hemagglutinins from two influenza virus variants bind to sialic acid derivatives with millimolar dissociation constants: a 500-MHz proton nuclear magnetic resonance study. Biochemistry. 1989;28(21):8388-96.

39. Moscona A. Medical management of influenza infection. Annu Rev Med. 2008;59:397-413.

40. Schirmer P, Holodniy M. Oseltamivir for treatment and prophylaxis of influenza infection. Expert opinion on drug safety. 2009;8(3):357-71.

41. Bhatia S, Camacho LC, Haag R. Pathogen inhibition by multivalent ligand architectures. Journal of the American Chemical Society. 2016;138(28):8654-66.

42. Dinleyici EC, Yargic ZA. Pneumococcal conjugated vaccines: impact of PCV-7 and new achievements in the postvaccine era. Expert review of vaccines. 2008;7(9):1367-94.

43. Lauer KB, Borrow R, Blanchard TJ. Multivalent and multipathogen viral vector vaccines. Clinical and Vaccine Immunology. 2017;24(1):e00298-16.

44. Lauster D, Klenk S, Ludwig K, Nojoumi S, Behren S, Adam L, et al. Phage capsid nanoparticles with defined ligand arrangement block influenza virus entry. Nature nanotechnology. 2020;15(5):373-9.

45. Kwon S-J, Na DH, Kwak JH, Douaisi M, Zhang F, Park EJ, et al. Nanostructured glycan architecture is important in the inhibition of influenza A virus infection. Nature nanotechnology. 2017;12(1):48-54.

46. Varga N, Sutkeviciute I, Ribeiro-Viana R, Berzi A, Ramdasi R, Daghetti A, et al. A multivalent inhibitor of the DC-SIGN dependent uptake of HIV-1 and Dengue virus. Biomaterials. 2014;35(13):4175-84.

47. Bastian AR, Nangarlia A, Bailey LD, Holmes A, Sundaram RVK, Ang C, et al. Mechanism of multivalent nanoparticle encounter with HIV-1 for potency enhancement of peptide triazole virus inactivation. Journal of Biological Chemistry. 2015;290(1):529-43.

48. Hunt AC, Case JB, Park Y-J, Cao L, Wu K, Walls AC, et al. Multivalent designed proteins neutralize SARS-CoV-2 variants of concern and confer protection against infection in mice. Science translational medicine. 2022;14(646):eabn1252.

49. Haag R. Multivalency as a chemical organization and action principle. Beilstein-Institut; 2015. p. 848-9.

50. Rothemund PW. Folding DNA to create nanoscale shapes and patterns. Nature. 2006;440(7082):297-302.

51. Zhang Y, Pan V, Li X, Yang X, Li H, Wang P, et al. Dynamic DNA structures. Small. 2019;15(26):1900228.

52. Zhao Y-X, Shaw A, Zeng X, Benson E, Nystrom AM, Högberg Br. DNA origami delivery system for cancer therapy with tunable release properties. ACS nano. 2012;6(10):8684-91.

53. Wiraja C, Zhu Y, Lio DCS, Yeo DC, Xie M, Fang W, et al. Framework nucleic acids as programmable carrier for transdermal drug delivery. Nature communications. 2019;10(1):1-12.

54. Song L, Jiang Q, Liu J, Li N, Liu Q, Dai L, et al. DNA origami/gold nanorod hybrid nanostructures for the circumvention of drug resistance. Nanoscale. 2017;9(23):7750-4.

55. Liu J, Song L, Liu S, Zhao S, Jiang Q, Ding B. A tailored DNA nanoplatform for synergistic RNAi-/chemotherapy of multidrug-resistant tumors. Angewandte Chemie International Edition. 2018;57(47):15486-90.

56. Douglas SM, Bachelet I, Church GM. A logic-gated nanorobot for targeted transport of molecular payloads. Science. 2012;335(6070):831-4.

57. Keller A, Linko V. Challenges and perspectives of DNA nanostructures in biomedicine. Angewandte Chemie International Edition. 2020;59(37):15818-33.

58. Kwon PS, Ren S, Kwon S-J, Kizer ME, Kuo L, Xie M, et al. Designer DNA architecture offers precise and multivalent spatial pattern-recognition for viral sensing and inhibition. Nature chemistry. 2020;12(1):26-35.

59. Sigl C, Willner EM, Engelen W, Kretzmann JA, Sachenbacher K, Liedl A, et al. Programmable icosahedral shell system for virus trapping. Nature Materials. 2021:1-9.

60. Veneziano R, Moyer TJ, Stone MB, Wamhoff E-C, Read BJ, Mukherjee S, et al. Role of nanoscale antigen organization on B-cell activation probed using DNA origami. Nature nanotechnology. 2020;15(8):716-23.

61. Chauhan N, Xiong Y, Ren S, Dwivedy A, Magazine N, Zhou L, et al. Net-shaped DNA nanostructure designed for rapid/sensitive detection and potential inhibition of SARS-CoV-2 virus (preprint). 2022.

62. Dijkstra JM, Visser N, Mettenleiter TC, Klupp BG. Identification and characterization of pseudorabies virus glycoprotein gM as a nonessential virion component. Journal of Virology. 1996;70(8):5684-8.

63. Brack AR, Dijkstra JM, Granzow H, Klupp BG, Mettenleiter TC. Inhibition of virion maturation by simultaneous deletion of glycoproteins E, I, and M of pseudorabies virus. Journal of virology. 1999;73(7):5364-72.

64. Browne H, Bell S, Minson T. Analysis of the requirement for glycoprotein m in herpes simplex virus type 1 morphogenesis. Journal of virology. 2004;78(2):1039-41.

65. Jöns A, Dijkstra JM, Mettenleiter TC. Glycoproteins M and N of pseudorabies virus form a disulfide-linked complex. Journal of virology. 1998;72(1):550-7.

66. Hogue IB, Bosse JB, Hu J-R, Thiberge SY, Enquist LW. Cellular mechanisms of alpha herpesvirus egress: live cell fluorescence microscopy of pseudorabies virus exocytosis. PLoS pathogens. 2014;10(12):e1004535.

67. Crump CM, Bruun B, Bell S, Pomeranz LE, Minson T, Browne HM. Alphaherpesvirus glycoprotein M causes the relocalization of plasma membrane proteins. Journal of General Virology. 2004;85(12):3517-27.

68. Dijkstra JM, Gerdts V, Klupp BG, Mettenleiter TC. Deletion of glycoprotein gM of pseudorabies virus results in attenuation for the natural host. Journal of General Virology. 1997;78(9):2147-51.

69. Nixdorf R, Klupp BG, Mettenleiter TC. Role of the cytoplasmic tails of pseudorabies virus glycoproteins B, E and M in intracellular localization and virion incorporation. Journal of General Virology. 2001;82(1):215-26.

70. Sommese R, Hariadi R, Kim K, Liu M, Tyska M, Sivaramakrishnan S. Patterning protein complexes on DNA nanostructures using a GFP nanobody. Protein Science. 2016;25(11):2089-94.

71. Kubala MH, Kovtun O, Alexandrov K, Collins BM. Structural and thermodynamic analysis of the GFP: GFP-nanobody complex. Protein Science. 2010;19(12):2389-401.

72. Kirchhofer A, Helma J, Schmidthals K, Frauer C, Cui S, Karcher A, et al. Modulation of protein properties in living cells using nanobodies. Nature structural & molecular biology. 2010;17(1):133-8.

73. Rothbauer U, Zolghadr K, Tillib S, Nowak D, Schermelleh L, Gahl A, et al. Targeting and tracing antigens in live cells with fluorescent nanobodies. Nature methods. 2006;3(11):887-9.

74. Seitz KJ, Rizzoli SO. GFP nanobodies reveal recently-exocytosed pHluorin molecules. Scientific reports. 2019;9(1):1-10.

75. Sehnal D, Bittrich S, Deshpande M, Svobodová R, Berka K, Bazgier V, et al. Mol* Viewer: modern web app for 3D visualization and analysis of large biomolecular structures. Nucleic Acids Research. 2021;49(W1):W431-W7.

76. Seeman NC. Nanomaterials based on DNA. Annual review of biochemistry. 2010;79:65.

77. Hahn J, Wickham SF, Shih WM, Perrault SD. Addressing the instability of DNA nanostructures in tissue culture. ACS nano. 2014;8(9):8765-75.

78. Ahmadi Y, De Llano E, Barišić I. (Poly) cation-induced protection of conventional and wireframe DNA origami nanostructures. Nanoscale. 2018;10(16):7494-504.

79. Mei Q, Wei X, Su F, Liu Y, Youngbull C, Johnson R, et al. Stability of DNA origami nanoarrays in cell lysate. Nano letters. 2011;11(4):1477-82.

80. Wang P, Rahman MA, Zhao Z, Weiss K, Zhang C, Chen Z, et al. Visualization of the cellular uptake and trafficking of DNA origami nanostructures in cancer cells. Journal of the American Chemical Society. 2018;140(7):2478-84.

81. Liang L, Li J, Li Q, Huang Q, Shi J, Yan H, et al. Single-particle tracking and modulation of cell entry pathways of a tetrahedral DNA nanostructure in live cells. Angewandte Chemie International Edition. 2014;53(30):7745-50.

82. Lee H, Lytton-Jean AK, Chen Y, Love KT, Park AI, Karagiannis ED, et al. Molecularly self-assembled nucleic acid nanoparticles for targeted in vivo siRNA delivery. Nature nanotechnology. 2012;7(6):389-93.

83. Perrault SD, Shih WM. Virus-inspired membrane encapsulation of DNA nanostructures to achieve in vivo stability. ACS nano. 2014;8(5):5132-40.

84. Bhatia D, Surana S, Chakraborty S, Koushika S, Krishnan Y. A Synthetic Icosahedral DNA-Based Host-Cargo Complex for Functional. Vivo; 2011.

85. Vonnemann J, Sieben C, Wolff C, Ludwig K, Böttcher C, Herrmann A, et al. Virus inhibition induced by polyvalent nanoparticles of different sizes. Nanoscale. 2014;6(4):2353-60.

86. Papp I, Sieben C, Sisson AL, Kostka J, Böttcher C, Ludwig K, et al. Inhibition of influenza virus activity by multivalent glycoarchitectures with matched sizes. ChemBioChem. 2011;12(6):887-95.

87. Zhang F, Jiang S, Wu S, Li Y, Mao C, Liu Y, et al. Complex wireframe DNA origami nanostructures with multi-arm junction vertices. Nature nanotechnology. 2015;10(9):779-84.

88. Katzung B, Masters S, Trevor A. Basic and clinical pharmacology. 12. New York: Companies. Inc; 2012.

89. Zeng Y, Liu J, Yang S, Liu W, Xu L, Wang R. Time-lapse live cell imaging to monitor doxorubicin release from DNA origami nanostructures. Journal of Materials Chemistry B. 2018;6(11):1605-12.

90. Li X, Yang F, Hu X, Tan F, Qi J, Peng R, et al. Two classes of protective antibodies against Pseudorabies virus variant glycoprotein B: Implications for vaccine design. PLoS pathogens. 2017;13(12):e1006777.

91. Pattnaik P, Babu JP, Verma SK, Tak V, Rao PL. Bacterially expressed and refolded envelope protein (domain III) of dengue virus type-4 binds heparan sulfate. Journal of Chromatography B. 2007;846(1-2):184-94.

92. Kaufmann B, Rossmann MG. Molecular mechanisms involved in the early steps of flavivirus cell entry. Microbes and infection. 2011;13(1):1-9.

93. Lauster D, Glanz M, Bardua M, Ludwig K, Hellmund M, Hoffmann U, et al. Multivalent Peptide-Nanoparticle Conjugates for Influenza-Virus Inhibition. Angewandte Chemie International Edition. 2017;56(21):5931-6.

94. Papp I, Sieben C, Ludwig K, Roskamp M, Böttcher C, Schlecht S, et al. Inhibition of influenza virus infection by multivalent sialic-acid-functionalized gold nanoparticles. Small. 2010;6(24):2900-6.

95. Ogata M, Umemura S, Sugiyama N, Kuwano N, Koizumi A, Sawada T, et al. Synthesis of multivalent sialyllactosamine-carrying glyco-nanoparticles with high affinity to the human influenza virus hemagglutinin. Carbohydrate polymers. 2016;153:96-104.

96. Pomeranz LE, Reynolds AE, Hengartner CJ. Molecular biology of pseudorabies virus: impact on neurovirology and veterinary medicine. Microbiology and molecular biology reviews. 2005;69(3):462-500.

97. Beilstein F, Cohen GH, Eisenberg RJ, Nicolas V, Esclatine A, Pasdeloup D. Dynamic organization of Herpesvirus glycoproteins on the viral envelope revealed by super-resolution microscopy. PLoS pathogens. 2019;15(12):e1008209.

98. Raniolo S, Croce S, Thomsen RP, Okholm AH, Unida V, Iacovelli F, et al. Cellular uptake of covalent and non-covalent DNA nanostructures with different sizes and geometries. Nanoscale. 2019;11(22):10808-18.

99. Bastings MM, Anastassacos FM, Ponnuswamy N, Leifer FG, Cuneo G, Lin C, et al. Modulation of the cellular uptake of DNA origami through control over mass and shape. Nano letters. 2018;18(6):3557-64.

100. Zhang J, Xu Y, Huang Y, Sun M, Liu S, Wan S, et al. Spatially patterned neutralizing icosahedral DNA nanocage for efficient SARS-CoV-2 blocking. Journal of the American Chemical Society. 2022.

101. Lacroix AI, Vengut-Climent E, de Rochambeau D, Sleiman HF. Uptake and fate of fluorescently labeled DNA nanostructures in cellular environments: a cautionary tale. ACS central science. 2019;5(5):882-91.

CHAPTER 3

Mechanistic studies of viral inhibition mediated by multivalent DNA origami scaffolding nanostructures

3.1. Introduction

Multivalency is a ubiquitous phenomenon underlying several physiological and biochemical processes like recognition, signaling, and self-organization. In multivalent systems, multiple simultaneous interactions between ligands and receptors enhance the cumulative binding strength and specificity, resulting in a functional cascading of successive events. For instance, in pathogenic systems, multivalency drives the early events of infection when pathogens adhere to the target cell surfaces, typically using low-affinity protein-carbohydrate interactions, and subsequently gain entry into cells (1, 2). Therefore, blocking the early stages of infection, like attachment and entry of viruses, can be an effective broad-spectrum antiviral strategy. The conventional approach employing monovalent drugs often necessitates high doses to outcompete the higher binding affinities of viruses to the multiple binding sites on cell surfaces, which is not feasible *in vivo* (3). In comparison, a multivalent inhibitor can competitively bind to viruses and effectively suppress their interactions with target cells.

However, leveraging multivalency to develop antiviral platforms is not a novel concept. The conventional research landscape in developing multivalent inhibitors is based on scaffold materials, including but not limited to natural/synthetic polymers, gold nanoparticles, proteins, and lipids. As evidenced in many studies, the scaffold choice is crucial in determining the optimum platform configurations, primarily by modulating the valency (4, 5), flexibility (6), and spacing between ligands (7), as well as the overall bioavailability (5), stability (3), toxicity (8, 9), and immunogenicity (9) of the assembled system. A rational design of multivalent inhibitors requires careful consideration of the intrinsic affinity between the virus binding ligands and their receptors on the virus surface, as well as the spatial patterning, density, and accessibility of those receptors (10, 11). Ligand architecture in multivalent systems can influence their functional efficacy by specifying their collective binding modes. Hence, functional enhancements could result from more than one

type of effect: higher binding avidity, steric shielding, receptor clustering, and statistical rebinding (12).

In literature, systematic studies exploring the influence of architectural factors on the strength of multivalent interactions are limited. However, there are a few isolated studies comparing the effects of valency, flexibility, size, and composition on the inhibitory potential of multivalent platforms and their physiological applicability. Studies demonstrating a size-dependent effect on multivalent interactions have shown a higher degree of viral inhibition with inhibitor sizes slightly smaller or similar to the virus (13, 14). This effect is attributable to contact area-dependent enhancement of the virus-inhibitor binding, i.e., with a larger inhibitor, the contact area for interaction also increases. Cryo-TEM studies revealed that inhibitors far smaller than viruses decorated the viral surfaces but were not as effective in blocking virus adhesion to the cell surface. In contrast, larger inhibitors competitively blocked virus-cell binding and formed virus-inhibitor clusters, resulting in superior viral inhibition. Interestingly, the inhibition potential plateaued upon further increasing the inhibitor size, i.e.,> virus, since it was not accompanied by an increase in the contact area between the virus and nanoparticles (13). To further distinguish the effects of multivalency and steric shielding on virus inhibition, Vonnemann et al. employed different sizes of functionalized nanoparticles as virus decoys and investigated their interactions with multivalent ligands based on ligand/receptor pairs with strong and weak binding (15). Using a modified Cheng-Prusoff's equation to account for multivalency and steric shielding, the IC_{50} was calculated based on the equation: $IC_{50} = K_d^{multi} + 0.5P[B]$, where K_d^{multi} is the dissociation constant of the multivalent inhibitor, P is the number of inhibitors required to shield the nanoparticle sterically, and [B] is the virus/nanoparticle concentration. As demonstrated previously, K_d^{multi} exponentially depends on the contact area, and the contribution of steric shielding to IC_{50} is only noticeable if all inhibitors are bound to the virus. For larger inhibitors, K_d^{multi} is far below the virus concentrations typically encountered in body fluids, and as such, steric shielding predominates over multivalency. Based on their analyses, globular inhibitors smaller than the pathogen size are favorable for optimal competitive inhibition in most cases.

Similarly studies investigating the effect of valency on inhibition efficacy of multivalent platforms have underscored the importance of balancing ligand valency with inter-ligand spacing to match the receptor topology unique to target viruses (4, 5, 7). The concept of a higher valency enhancing binding affinities and improving pathogen inhibition holds as long as the valency does not impose any entropic or conformational penalties on pathogen binding. Other factors most likely work in conjunction with valency to modulate multivalent interactions. For instance, a maximum inhibition (~80%) of IAV infection was achieved with 50 nm SA-conjugated nanogels with only 12% ligand density (14). Another study showed a 90% maximum inhibition of IAV infection with 18 nm and 28 nm antiviral peptide-conjugated polymers with just 9% and 10% ligand functionalization, respectively (5). In this section, we have only considered studies modulating ligand valency using scaffolds of the same size. A study investigating structure-independent designs of multivalent inhibitors for pseudotyped Ebola viruses with a statistical distribution of mannose ligands on glycofullerene scaffolds (size ~ < 4 nm) showed a loss of inhibitory potential upon increasing the ligand valency from n = 12 to n = 36 (16). Similarly, complete loss of inhibition potential was observed upon increasing the ligand valency from 20 to 40 with 6'-sialyllactose ligands on polyamidoamine (6SL-PAMAM) dendrimer scaffolds (size = 4.5 nm) to inhibit IAV infection (4). In both of these studies, a higher valency resulted in penalties associated with crowding and steric hindrance between sugar residues, preventing their access to target receptors. As such, in the study with the pseudotyped Ebola viruses, the inhibition potential was rescued with n = 36 valency by incorporating longer spacers that enhanced access of the ligands to their receptors. In the study with 6SL-PAMAM inhibitors, the authors were able to modulate IC_{50} by manipulating the spacing between 6SL ligands. The authors demonstrated higher inhibition efficacies at lower ligand densities with inter-ligand spacings closely mimicking the HA trimer patterning on the IAV envelope.

With advances in structure-based designs, some studies have adopted a more rational approach to designing multivalent inhibitors with ligand placement precisely matching their corresponding receptor patterning on viral surfaces resulting in optimal binding and enhanced IC50 concentrations (6, 7, 17, 18). An early example in the series of such studies includes the trivalent inhibitor comprising *in silico*-designed SA ligands on alkylated peptide backbones with an aromatic

core that demonstrated a 4000-fold increase in binding affinity for H5 of avian influenza (6). The rigid peptide backbone resulted in a reduced entropic loss from conformational flexibility during binding, and flexible alkyl side chains flanking the peptide region compensated for a non-perfect steric match between the ligands and receptors. Another study revealed the limitations of PEG-based flexible backbone as opposed to DNA-based rigid backbone in bivalent interactions between distance-matched SA-based ligands and HA trimers on IAV surface (7). A rational design strategy was adopted to develop planar pentavalent, octavalent and decavalent inhibitors mimicking the receptor topology to inhibit bacterial toxins like cholera and Shiga (19-22). In the first of its kind of studies using DNA scaffolds, a decavalent 2D star-shaped nanostructure displaying pattern-matched aptamers targeting Dengue virus epitopes was recently developed. The bifunctional device primarily acted as a virus sensor with a comparable limit of detection (LoD) as that of gold-standard ELISA and RT-qPCR-based techniques and as an inhibitor with an IC_{50} value in the lower nanomolar range (17).

All these studies show that structure-based multivalent designs facilitate an intelligent way to manipulate different factors such as valency, flexibility, and spatial patterning of ligands to achieve optimum inhibition with minimum ligand redundancy. However, this approach requires nanometer-scale resolution of the molecular nature of host-pathogen interactions. Unfortunately, such information may not always be readily available, particularly for the novel, emerging, evolving, and understudied pathogens. Under such circumstances, an effective technical approach would be to select modular multivalent designs that can be easily adapted to incorporate different ligand types and manipulate ligand valencies, densities, and patterning. As discussed in the sections above, structure-dependent and -independent studies investigating multivalent inhibitors have generally employed protein, polymer, or particle scaffolds with limited modularity, programmability, and adaptability. In addition, the challenges associated with the synthesis, scalability, and biocompatibility of these scaffolds remain largely unresolved.

In this work, we investigate the mechanisms underlying viral inhibition by 3D DNA origami-based multivalent scaffolds targeting non-essential viral domains by exploiting the programmability and modularity of DNA nanostructures. Previously, we developed SC60H-nbGFP, a ~60 nm 3D

DNA origami-based nano-platform to display multiple protein-based virus binding domains, which we refer to as 'binders'. We functionalized the snub cube (SC) scaffold by conjugating 60 copies of GFP nanobodies (nbGFP) binders to target pHluorin domains tagged onto envelope gM of the recombinant Pseudorabies virus (PRV) 486. We demonstrated the superior ability of the assembled nanoconstruct, SC60H-nbGF, to sense and inhibit PRV 486 in a dose-dependent manner with an IC_{50} of ~3 nM. In this work, we use the SC scaffolds to systematically probe the effect of ligand type, valency, and flexibility in relation to their binding modes with the viruses and offer preliminary data suggesting an interplay between avidity and obstruction of virus internalization as the predominant inhibition mechanisms. In addition, as a testament to the biocompatibility of DNA, we assess the stability of the nanostructures in physiologically relevant conditions.

3.2. Results

3.2.1. Design, assembly, and characterization of SC-nbGFP nanostructures with different valency

SC is a 3D wireframe Archimedean structure with 6 squares and 12 triangles making up its 60 edges. Cryo-EM analyses in the original SC paper revealed that SC has a ~60 nm diameter with ~20 nm long edges (23). In the previous chapter, we described the design and synthesis of the SC60H-nbGFP nanoconstruct, in which we functionalized SC to present 60 copies of nbGFP. SC60H-nbGFP presented the maximum valency we could get considering a 1-to-1 stoichiometry of conjugating virus binders to the edges of the wireframe scaffold. Furthermore, it is designed to present an even distribution of nbGFP across the surface of the SC scaffold, which we opted for, considering the limited information available on the precise spatial distributions and protein structures of PRV envelope glycoproteins.

We systematically investigated the effect of valency on PRV 486 inhibition by incorporating lower valencies of nbGFP bioconjugation sites across the surface of the SC. We used the Tiamat program to design candidate DO nanostructures based on our previous design of SC60H-nbGFP (Williams et al. 2009). We modified the SC design to incorporate four different valencies, including n = 1, n = 12, n = 24, and n = 36, in addition to our previous design with n = 60. For n = 60, we used all 6 square and 12 triangle edges for bioconjugation, giving 24 square handles (24SH) and 36

triangle handles (36TH). We modified the sequences of edge strands to include ssDNA overhangs that can be conjugated with complementary ssDNA attached to nbGFP via a benzyl guanine (BG) linker. For n = 36, we used all 12 triangle edges in SC, giving 36 triangle handles (36TH) for bioconjugation. Similarly, for n = 24, we used all 6 square edges in SC, giving 24 square handles (24SH) for bioconjugation. For n = 12, we used two opposite edges of each of the 6 squares in SC, giving 12 square handles (12SH) for bioconjugation. Finally, for n = 1, we used only 1 edge of 1 square in SC, giving 1 square handle (1SH) for bioconjugation.

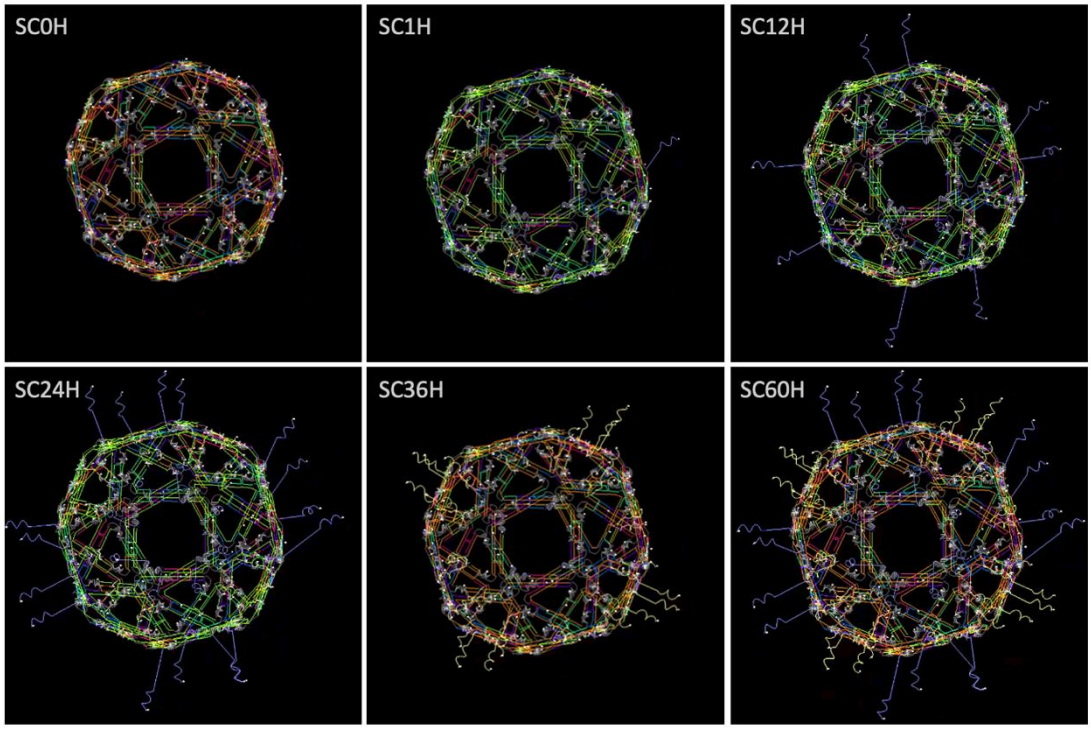

Fig. 1| Tiamat simulation of the snub cube (SC) 3D DNA origami nanostructure of different valencies.

The assembly of SC-nbGFP with different valencies followed the same protocol described in the previous chapter. It was accomplished in three steps: i) synthesis of SC scaffolds with different valencies (n = 1, 12, 24, 36, and 60), ii) incorporation of complementary strands conjugated to benzyl guanine linkers into the SC nanostructures, and iii) conjugation of nbGFP to the linker strands-attached SC nanostructures. The synthesis was carried out in individual one-pot reactions with M13mp18 ssDNA and a ten-fold molar excess of staple strands corresponding to the different

valencies of the SC-nbGFP and in the presence of Mg^{2+} salt. We maintained a 12.5 mM Mg^{2+} concentration throughout all preparation and purification steps to retain the structural integrity of the 3D DNA nanostructures. We characterized the formation of SC, SC-BG-DNA, and SC-nbGFP of different valencies after each step using 1% agarose gel electrophoresis (AGE). We quantified the yield of the assembled SC-nbGFP by measuring their DNA concentrations.

The gel shift assay showed distinct bands, validating the formation of DO nanostructures (Fig. 2). The reduced electrophoretic mobility of bands aligned with their relatively increasing molecular weights, confirming the correct formation of nanostructures after each synthesis step. As expected, within each valency group of the nanostructure assembly, the final SC-nbGFP were the heaviest nanostructures showing the lowest mobility in AGE, followed by SC-BG-DNA intermediate nanostructures with the complementary ssDNA attached to the BG-linker and finally by the SC constructs with the number of handle strands corresponding to their specific valency. Similarly, comparing different valency groups, the electrophoretic mobility decreased with increasing valency of SC, SC-BG-DNA, and SC-nbGFP nanostructures, further confirming the formation of nanostructures with their corresponding valencies.

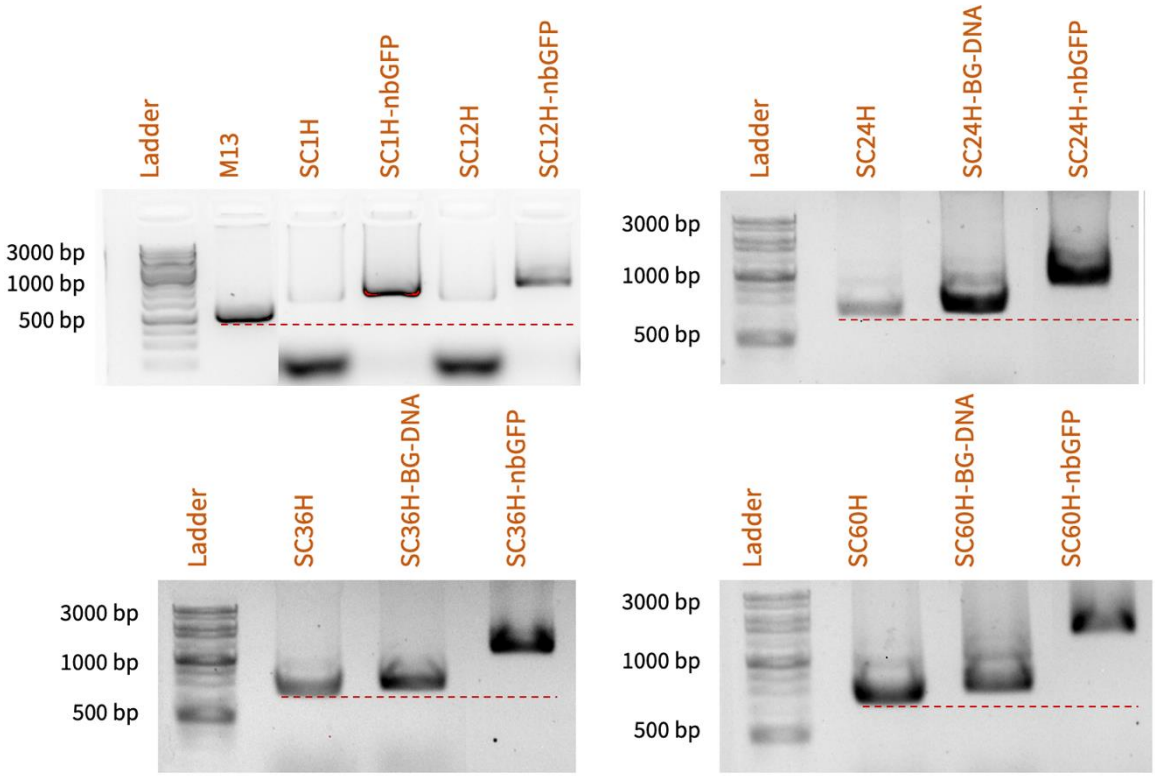

Fig. 2| Characterization of SC-nbGFP of different valencies. The gel shift assay with 1% AGE shows the successive formation of SC, SC-BG-DNA, and SC-nbGFP nanostructures with valency, n = 1, 12, 24, 36, and 60. The red dotted lines are shown as references to compare the electrophoretic mobility of different nanostructures.

3.2.2. Phase I: Effect of valency on virus inhibition

In the previous chapter, we demonstrated the dose-dependent inhibition of PRV 486 with SC60H-nbGFP with an IC_{50} of ~3 nM. Here, we analyzed the impact of SC-nbGFP valency on PRV 486 inhibition in two distinct phases. In the first phase, we compared two valencies in the lower range, including n = 1 and n = 12 with n = 60. SC12H-nbGFP and SC60H-nbGFP present 12-fold and 60-fold higher copy numbers of nbGFP, respectively, compared to SC1H-nbGFP.

First, we performed a semi-quantitative ELISA assay to assess the effect of modulating valency on virus binding. We coated 96-well ELISA plates with PRV 486 and incubated different concentrations of nbGFP, SC1H-nbGFP, SC12H-nbGFP, and SC60H-nbGFP. We quantified the extent of binding of nbGFP and SC-nbGFP using an orthogonal nbGFP-specific reporter antibody coupled to

horseradish peroxidase. Residual nbGFP and SC-nbGFP bound to the wells were detected by HRP-catalyzed colorimetric reaction upon adding TMB substrate.

Once again, the data from the ELISA binding assay are normalized to reflect specific binding values (Fig. 3A). We used an anti-GFP antibody (AbGFP) as a positive control for nbGFP and all SC-nbGFP nanostructures. Similar to our previous observations, all constructs showed concentration-dependent changes in virus binding and their corresponding absorbance values, suggesting their specific binding activities. Since we used semi-purified virus stocks, we could not quantify the absolute binding affinities using this assay. However, the approximate K_D showed a 90-fold and a 150-fold enhancement in binding affinity of SC12H-nbGFP and SC60H-nbGFP, respectively, over SC1H-nbGFP (Fig. 3B). Similar to the monomeric nbGFP, the binding curve of SC1H-nbGFP, with a single nbGFP on the SC, also exhibited poor binding throughout the range of concentrations tested. However, multimerization of nbGFP onto SC enhanced the cumulative binding strength of SC-nbGFP nanostructures. We observed a monotonic increase in binding affinities with rising valency of SC-nbGFP as reflected by the relative K_D ~2.2 nM for SC1H-nbGFP, K_D ~24 pM for SC12H-nbGFP and K_D ~14 pM for SC60H-nbGFP.

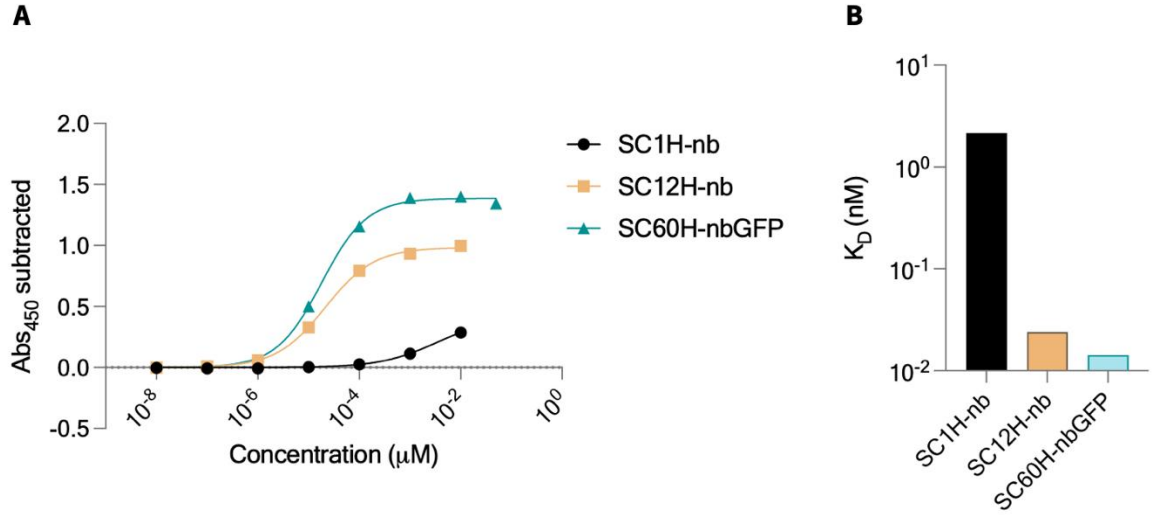

Fig. 3| Modulating valency in Phase I showed enhancement of binding affinities with increasing valency of SC-nbGFP. **A**, Representative ELISA binding curves of PRV 486 to SC-nbGFP of valency, n = 1, 12, and 60. Absorbance values resulting from non-specific interactions without the virus were subtracted. Data are presented as the average of two technical replicates. **B**, Approximate binding affinities (K_D) of SC1H-nbGFP, SC12H-nbGFP, and SC60H-nbGFP were

determined using non-linear regression analysis from the ELISA data. Data are presented as the average of two technical replicates.

Next, to investigate the effect of modulating valency on virus inhibition, we performed dose-response analyses by incubating PRV 486 with increasing concentrations of SC1H-nbGFP, SC12H-nbGFP, and SC60H-nbGFP. The virus and inhibitor cocktails were used to infect PK15 cells, and the residual infectivity was analyzed using flow cytometry as opposed to plaque reduction assays that we used previously. Since PRV 486 is tagged with pHluorin, the virus-infected cells become pHluorin positive as well; therefore, PRV 486 infectivity can be quantified as the percentage of pHluorin-positive cells within a given cell population (Fig. 4A). The group infected with PRV 486 alone was used to normalize the data of virus infectivity for all other groups treated with the multivalent nanostructures or their components.

As expected, SC without nbGFP and nbGFP alone failed to inhibit the virus (Fig. 4D). In contrast, SC-nbGFP constructs of all three valencies showed dose-dependent inhibition of the virus with exceptional half-maximal inhibitory concentration (IC_{50}) values, where a lower IC_{50} demonstrates a more potent inhibition (Fig. 4B). The inhibition efficacies increased monotonically with the rising valency of SC-nbGFP nanostructures, which positively correlates with their corresponding binding affinities (Fig. 4B). Non-linear regression analyses on the dose-response inhibition curves demonstrated the IC_{50} values of 150 nM for SC1H-nbGFP, 38 nM for SC12H-nbGFP and 1.4 nM for SC60H-nbGFP. SC60H-nbGFP enhanced virus inhibition by 27-fold compared to SC12H-nbGFP and by 107-fold compared to SC1H-nbGFP (Fig. 4C). These results, together with our data from phase I, demonstrate the prospect of enhancing the therapeutic potential of SC-nbGFP nanostructures by modulating their valency. The avidity of having multiple nbGFP/SC enhances binding and enables higher potency inhibitory properties. However, a valency of one nbGFP/SC suggests that the platform does not simply function by increasing avidity, but instead, the presence of SC, or rather the 'tagging' of PRV with a single SC, is the primary driver of the antiviral properties, as nbGFP demonstrates no antiviral activity itself.

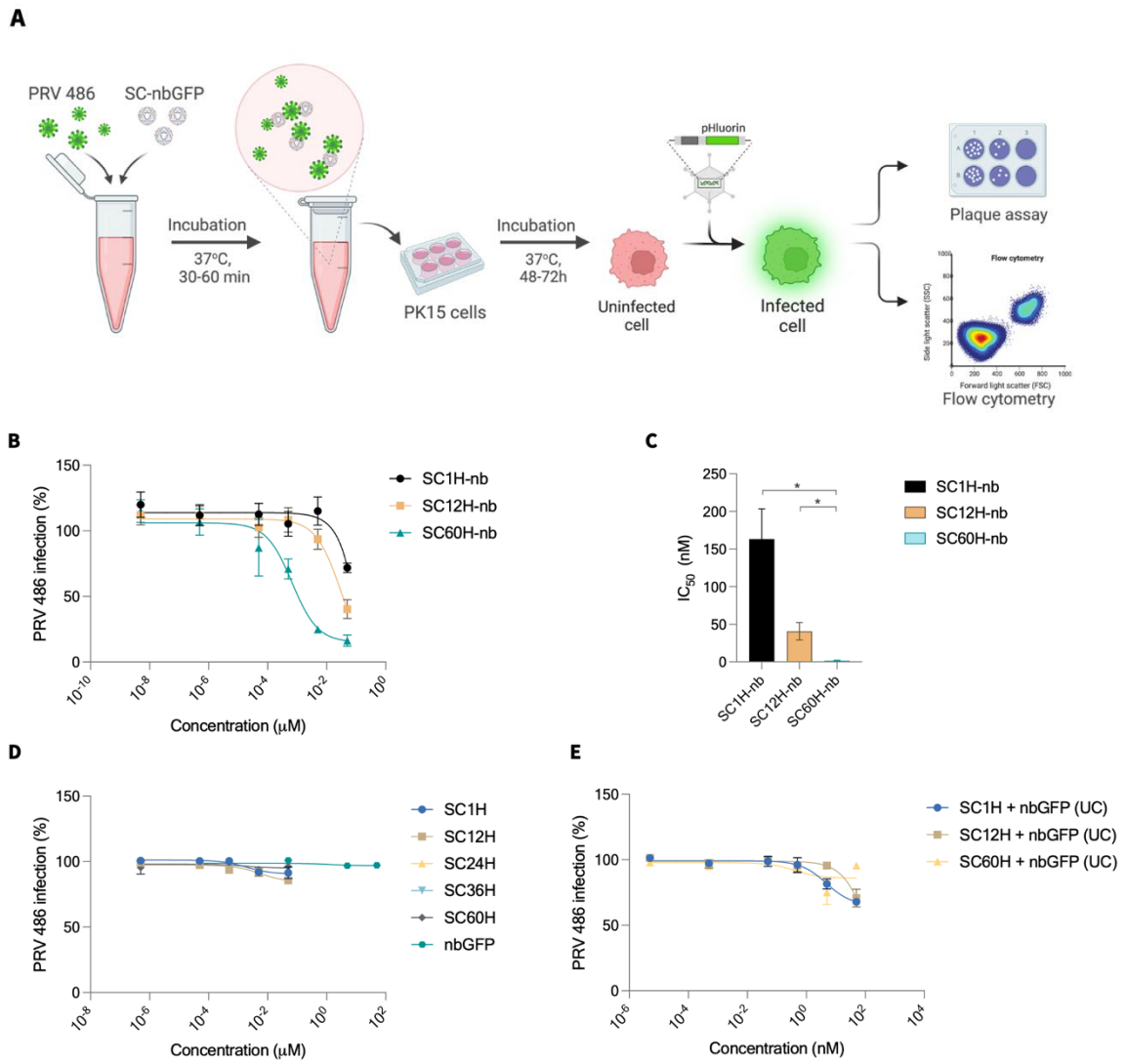

Fig. 4| Modulating valency in Phase I showed enhancement of PRV 486 inhibition with increasing valency of SC-nbGFP. **A**, Schematic illustrating the experimental design to assess PRV 486 infectivity after treatment with SC-nbGFP nanostructures. **B**, Dose-dependent, plaque-reduction inhibition curves for PRV 486 incubated with SC-nbGFP nanostructures of valency, n = 1, 12, and 60. Inhibitor concentration was standardized through DNA concentration. Data are presented as mean ± S.E.M., N = 3 biologically independent experiments. **C**, A comparison of half-maximal inhibitory concentration dosage (IC_{50}) calculated using non-linear regression analysis. **D**, Dose-dependent plaque-reduction inhibition curves for PRV 486 incubated with only SC scaffolds. **E**, Dose-dependent plaque-reduction inhibition curves for PRV 486 incubated with unconjugated (UC) SC and nbGFP. Data are presented as mean ± S.E.M., N = 3 biologically independent experiments.

3.2.3. Phase II: Effect of higher valencies on virus inhibition

In the second phase, we compared two valencies in the higher range with SC60H-nbGFP, including SC24H-nbGFP and SC36H-nbGFP. We incubated PRV 486 with increasing concentrations of SC24H-nbGFP, SC36H-nbGFP, and SC60H-nbGFP. We analyzed the residual infectivity using plaque reduction assays on PK15 cells. As controls, we tested the inhibition of the virus by their corresponding scaffolds without nbGFP and with just nbGFP alone.

SC-nbGFP constructs of all three valencies showed dose-dependent inhibition of the virus with exceptional half-maximal inhibitory concentration (IC_{50}) values, where a lower IC_{50} demonstrates a more potent inhibition (Fig. 5A). Non-linear regression analyses on the dose-response inhibition curves revealed the IC_{50} values for SC24H-nbGFP, SC36H-nbGFP, and SC60H-nbGFP to be approximately 49 nM, 47 nM, and 65 nM, respectively (Fig. 5B). 60H and 36H are 2.5-fold and 1.5-fold higher than 24H, respectively. The change in valency was not drastic between the three valencies we tested in this phase, and we found their corresponding IC_{50} values to be comparatively similar. Interestingly, the data suggested a plateauing effect on IC_{50} upon increasing the valency of SC-nbGFP from 24 to 36 or 60, which can be advantageous for the pharmacological profile of the multivalent inhibitor. Thus, all three SC-nbGFP nanostructures showed exceptional PRV 486 inhibition efficacies.

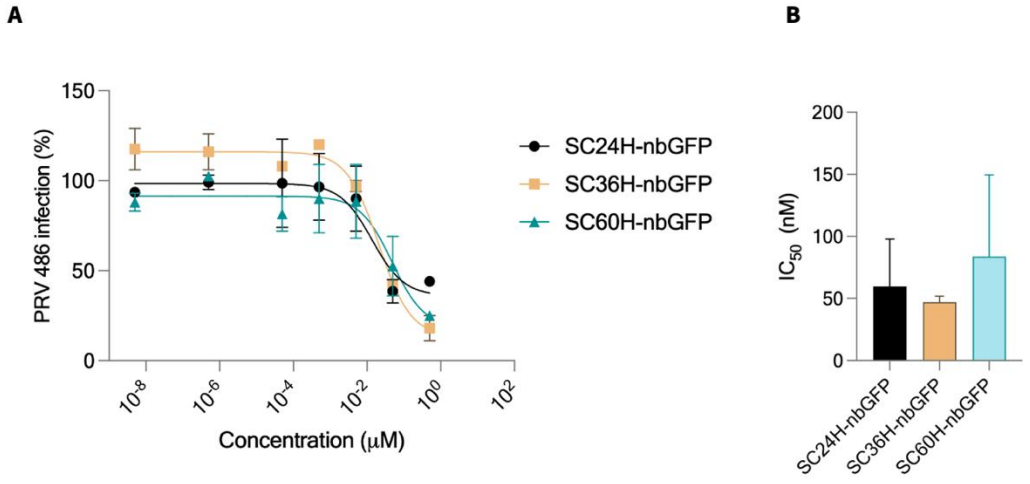

Fig. 5| Modulating SC-nbGFP valency in Phase II showed a plateauing effect of increasing valency to n > 24. **A**, Dose-dependent, plaque-reduction inhibition curves for the SC-nbGFP of valency, n =

24, 36, and 60. Inhibitor concentration was standardized through DNA concentration. Data are presented as mean ± S.E.M., N = 2 biologically independent experiments. **B**, A comparison of half-maximal inhibitory concentration dosage (IC_{50}). Data are presented as mean ± S.E.M., N = 2 biologically independent experiments.

3.2.4. Mechanism of inhibition

The biology of PRV shows that it initiates infection by adhering to target cells and then internalizing into the cytoplasm via membrane fusion. Since we are targeting pHluorin domains located outside PRV 486 envelope using SC-nbGFP and SP-aptGFP nanostructures, we anticipated that the multivalent interactions would obstruct the entry events of PRV particles resulting in their reduced attachment and internalization. For spherically inclined scaffolds, antiviral studies based on multivalent interactions have primarily identified two different mechanisms depending on the size and the spatial distribution of binders (Fig 8A). First, multivalent nanostructures similar to the virus size or slightly smaller than the virus can aggregate virus particles by forming virus and inhibitor clusters (13). This will depend on the size of the contact area of binding/interactions between the virus and the multivalent inhibitor. Aggregating viruses can reduce their Brownian motion and may also trigger other pathways of immune clearance in the physiological environment (24). Second, suppose virus particles are much larger than the inhibitor. In that case, the inhibitors will likely decorate the virus surface, sterically shielding them from adhering onto cells and interacting with cell surface receptors. The virus concentration also influences these mechanisms since the collision rate between virus-virus and virus-inhibitor particles largely depends on their local concentration. As such, the interplay of different factors governs if either or both mechanisms are likely to interfere with the virus infection cycle.

To investigate if SC-nbGFP nanostructures are aggregating PRV 486 particles, we analyzed the particle size distribution of viruses incubated with the multivalent nanostructures using nanosight (Fig 6A). As controls, we incubated viruses with SC (scaffold without the binders) and with nbGFP alone (binders without scaffold). For reference, PRV has a diameter of ~200 nm. The nanosight data we collected confirmed the size of PRV. In comparison, all the other groups also showed a uniform size distribution of ~200 nm, indicating the absence of formation of higher-order structures (Fig. 6B). Our studies of valency found that only one nbGFP per SC was sufficient to

produce antiviral effects. This suggests that a) not all binding sites on the virus are saturated since the size of SC would likely sterically block access from other SC-nbGFP and b) crosslinking interactions between two or more viral particles mediated by the SC are not a critical feature of the inhibition mechanism. These pieces of data provide strong evidence that SC-nbGFP does not function through the aggregation of PRV. It also provides supporting evidence that SC-nbGFP does not function by blocking all targeted PRV surface epitopes.

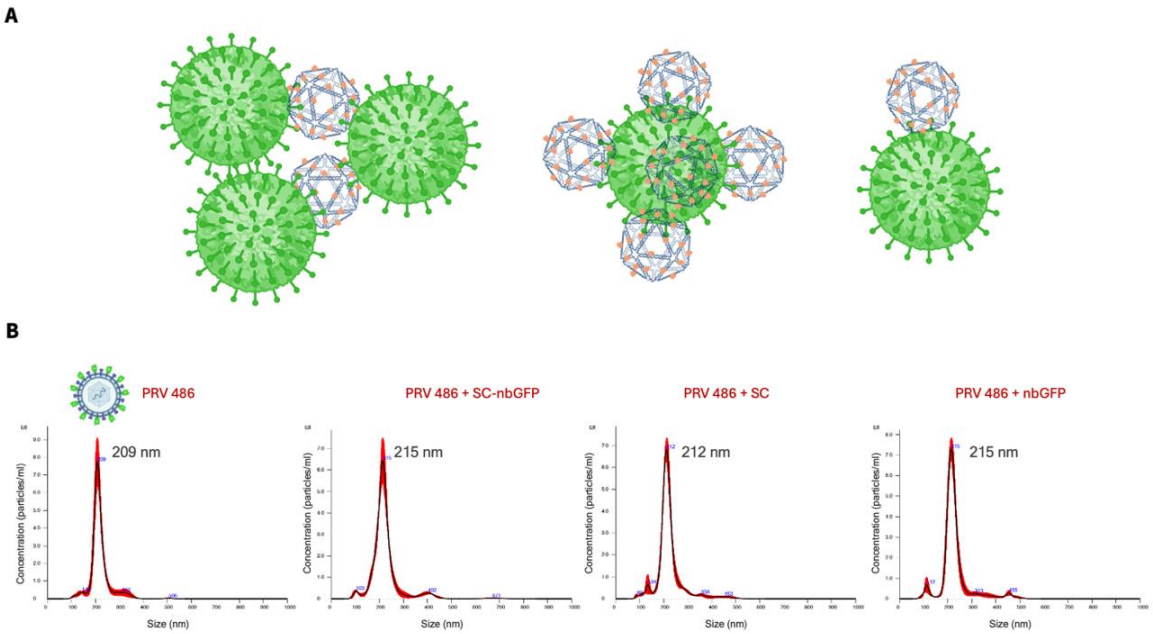

Fig 6| Characterization of different binding modes SC-nbGFP and PRV 486 interactions**. A**, Schematic illustrating different binding modes of PRV 486 with multivalent inhibitors like SC-nbGFP. Left: Inhibitors can aggregate virus particles by forming a network of viruses and inhibitors, slowing down their mobility. Middle: Inhibitors can decorate virus surface, effectively blocking them from interacting with cell surface attachment factors or receptors. Right: A one-to-one stoichiometry of binding that can increase the molecular weight of the viruses and slow down their mobility. **B**, Nanoparticle tracking analyses showing the particle size distributions of PRV 486 particles incubated with SC-nbGFP and components. The uniform size distributions indicate the absence of virus aggregation. PRV 486 is ~200 nm, and SC-nbGFP is ~60 nm.

To further assess whether SC-nbGFP exhibits antiviral activity by blocking all PRV surface epitopes, we performed time-lapsed live-cell imaging to track the early events of virus infection in real-time. To this end, we used PRV 483, a different recombinant strain expressing pHluorin on the virus envelope, and RFP on the virus capsid (Fig. 7A). Infectious PRV 483 particles can be seen

as colocalized green and red puncta at neutral pH using fluorescence microscopy. Using this strain, we could track the virus particles during their attachment phase by following the colocalized green and red puncta and after their internalization by following the red capsids (Fig. 7B). If SC-nbGFP blocks all viral epitopes, we anticipate that PRV will not attach to cells. If SC-nbGFP disrupts the internalization step, we anticipate seeing PRV attach to cells, but the green and red puncta arrested on the plasma membrane. We analyzed the RFP to GFP ratio at different time points to measure the proportion of virus internalized into the cells. If virus internalization is undisturbed, a high RFP to GFP ratio would indicate the increasing accumulation of virus capsids inside the cells. In contrast, under conditions that obstruct the virus internalization, a low RFP to GFP ratio would mean a smaller number of virus capsids inside the cells. Our analyses showed a lower RFP to GFP ratio for virus particles incubated with SC-nbGFP nanostructures compared to the control group with untreated virus particles (Fig. 7C). This indicates that the binding interactions between SC-nbGFP and PRV 483 particles do not block viral attachment but does appear to prevent the release of RFP-tagged virus capsids into the cells, effectively lowering the infectivity of the virus.

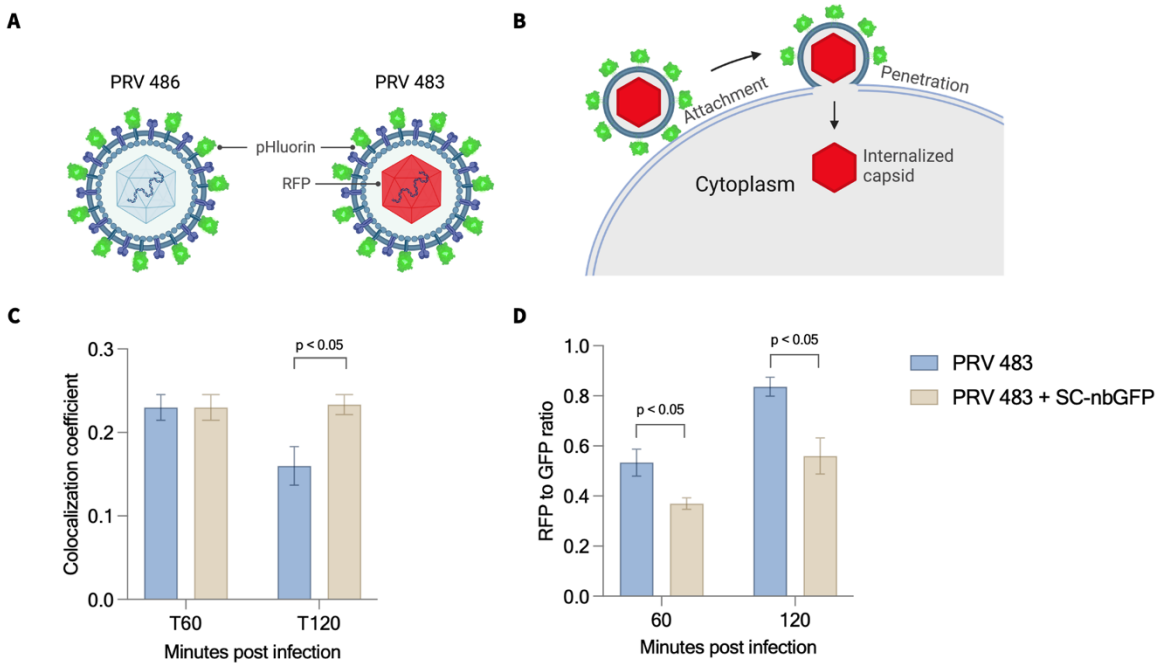

Fig. 7| Mechanism of inhibition. **A**, Schematic illustrating the pHluorin-tagged virus envelopes of PRV 486 and PRV 483 and RFP-tagged capsid of PRV 483. **B**, Schematic showing the early entry events of PRV comprising attachment followed by membrane fusion and internalization of virus capsids inside the cytoplasm. **C**, Colocalization coefficient showing the proportion of infectious virus with colocalized RFP and GFP puncta on the cell membrane. **D**, Ratio of intracellular RFP puncta to cell membrane-bound pHluorin puncta in cells infected with PRV 483 treated with SC-nbGFP. Cells infected with untreated viruses are used as the control group. Data were analyzed from ~60 cells from three fields of view. Data are presented as mean ± S.E.M.

3.2.5. Adapting SC scaffold to incorporate GFP aptamer binders

The unique property of DNA to be conjugated with different biomolecules (protein, peptides, nucleic acids), fluorophores, and inorganic particles enriches the functional diversity of DNA-based nano-enabled platforms. Previously, we demonstrated the exceptional ability of SC-nbGFP to inhibit PRV 486 by functionalizing SC with multiple copies of nbGFP-binders. Here, we used SC to incorporate aptamer binders to probe the PRV 486 pathosystem to illustrate the adaptability of DNA-based scaffolds.

A. Design, synthesis, and characterization of GFP aptamers to target PRV 486

Since EGFP and pHluorin share a ~96% amino acid sequence similarity, we anticipated that GFP-binding aptamers would also bind to pHluorin domains. We derived the GFP aptamer (aptGFP) sequence from a previously published study (25) and modified it to get two different designs. We added a 5' extension of 20-nucleotides to the aptamer sequences to enable the conjugation to the SC DNA origami nanostructures. The extension was complementary to the ss overhangs of SC edges. Furthermore, to independently assess the impact of binder flexibility on virus inhibition, we modified the second design to include a flexible 20-nucleotide ssRNA spacer between the SC docking region and the aptamer region (Fig 8A). We termed the first design without the flexible spacer as aptGFP and the second design with the flexible spacer as flex-aptGFP. The RNA aptamers were produced by T7 transcription *in vitro* from their corresponding DNA templates and further characterized using an 8% non-denaturing polyacrylamide gel electrophoresis (PAGE) (Fig

8B). Both aptGFP and flex-aptGFP bands aligned with their corresponding molecular weights of 116 and 136 bases, respectively.

B. Characterization of binding interactions between GFP aptamers and PRV 486

Before conjugating the aptamer sequences to SC, we used a semi-quantitative ELISA assay to confirm that the aptamers could bind to PRV 486 specifically (Fig 8C). For this assay, we hybridized a biotin-tagged 20-nucleotide ssDNA with the aptamers. The biotin linker was complementary to the SC docking region of the aptamer sequences. Next, we coated 96-well ELISA plates with PRV 486 and incubated biotin-tagged aptGFP and flex-aptGFP individually at concentrations ranging from 10 pM to 1 μM. The virus-bound aptamers were detected with an anti-streptavidin horseradish peroxidase that catalyzed a colorimetric reaction upon adding TMB substrate. The data from the ELISA binding assay are normalized to reflect specific binding values (Fig. 5D). Both aptamers demonstrated dose-dependent binding with the virus and similar binding curves, confirming their specificity for pHluorin domains.

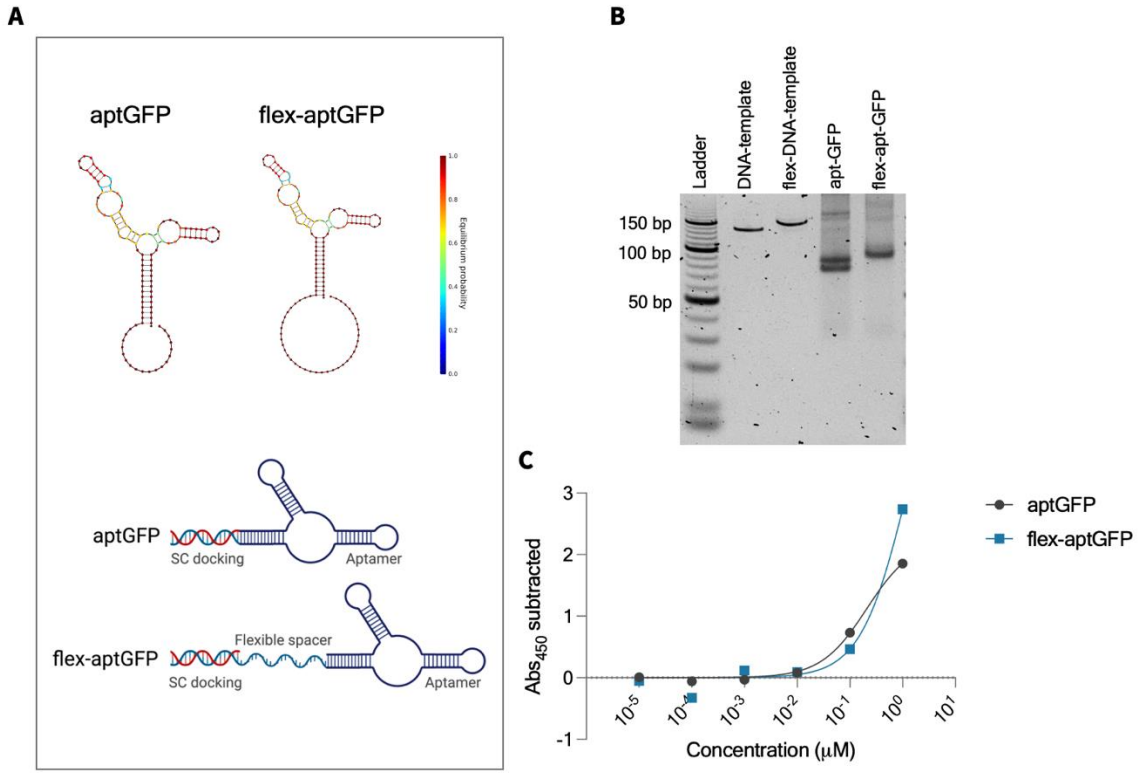

Fig. 8| Characterization of GFP aptamers. **A**, Top panel: Nupack simulation of aptGFP and flex-aptGFP at 25 °C. Bottom panel: Schematic illustrating the SC docking region, flexible spacer region, and the virus-binding aptamer region of aptGFP and flex-aptGFP. **B**, Characterization of aptGFP and flex-aptGFP and their corresponding DNA templates using non-denaturing PAGE. **C**, Representative ELISA binding curves of PRV 486 to aptGFP and flex-aptGFP. Absorbance values resulting from non-specific interactions without the virus were subtracted. Data are presented as the average of two technical replicates.

C. Design, assembly, and characterization of SC-aptGFP and SC-flex-aptGFP platforms

To investigate the effect of valency and binder flexibility on PRV 486 inhibition, we designed two groups (one with the flexible spacer and the other without the flexible spacer), each with three different valencies (n = 24, 36, and 60). We modified the strands making up the SC edges to include ssDNA overhangs that can be conjugated with complementary ssRNA attached to the GFP aptamer with or without the flexible spacer. The modifications to SC design to incorporate 24, 36, and 60 handles have been described previously.

The assembly of SC-aptGFP and SC-flex-aptGFP with different valencies was performed in two steps: i) synthesis of SC scaffolds with different valencies (n = 24, 36, and 60), ii) hybridization of GFP aptamers to the ssDNA overhangs of SC. The SC synthesis was carried out in individual one-pot reactions with M13mp18 ssDNA and a ten-fold molar excess of staple strands corresponding to the different valencies and in the presence of Mg_{2+} salt. We maintained a 12.5 mM Mg^{2+} concentration throughout all preparation and purification steps to retain the structural integrity of the 3D DNA nanostructures. We characterized the formation of SC, SC-aptGFP, and SC-flex-aptGFP of different valencies using 1% agarose gel electrophoresis (AGE) (Fig. 5E). We quantified the yield of the assembled nanostructures by measuring their DNA concentrations.

The gel shift assay showed distinct bands, validating the formation of DO nanostructures. In addition, the reduced electrophoretic mobility of the bands aligned with their relatively increasing molecular weights after each synthesis step, confirming the correct formation of nanostructures after each synthesis step. As expected, within each valency group of the nanostructure assembly, the final SC-aptGFP or SC-flex-aptGFP were the heaviest nanostructures showing the least mobility in AGE, followed by the SC constructs with the number of handle strands corresponding to their specific valency. Similarly, comparing different valency groups, the electrophoretic mobility

decreased with increasing valency of SC, SC-aptGFP, and SC-flex-aptGFP nanostructures, further confirming the formation of nanostructures with their corresponding valencies.

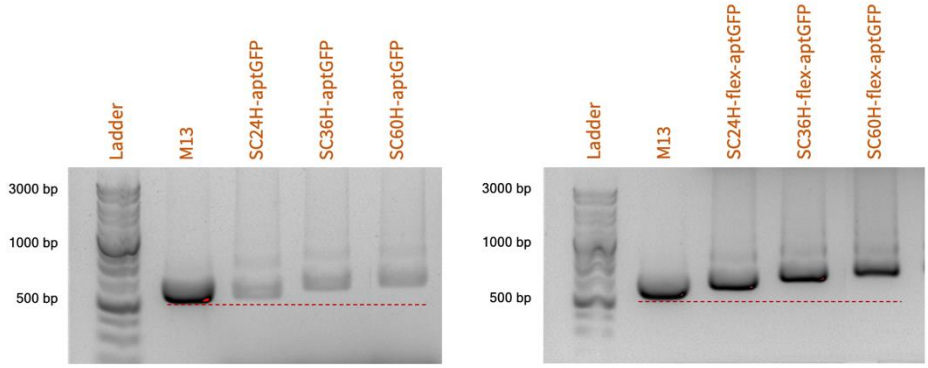

Fig. 9| Characterization of SC-aptGFP and SC-flex-aptGFP of different valencies. The gel shift assay with 1% AGE shows the successive formation of the respective nanostructures labeled in orange on top of each lane. The red dotted lines are shown as references to compare the electrophoretic mobility of different nanostructures.

3.2.6. Virus inhibition by SC-aptGFP and the effect of binder flexibility

Previously, we demonstrated the dose-dependent inhibition of PRV 486 by SC-nbGFP multivalent nanostructures and the plateauing effect of IC50 with increasing valency > n = 24. Here to illustrate the modularity of SC scaffolds and the impact of binder flexibility, we investigated the inhibition of PRV 486 by SC conjugated to GFP aptamers with and without flexible spacers. We performed dose-response analyses by incubating PRV 486 with increasing concentrations of three different valencies of SC-aptGFP and SC-flex-aptGFP nanostructures. The virus and inhibitor cocktails were used to infect PK15 cells, and the residual infectivity was determined using flow cytometry. Since PRV 486 is tagged with pHluorin, the virus-infected cells become pHluorin positive as well; therefore, PRV 486 infectivity can be quantified as the percentage of pHluorin-positive cells within a given cell population. The group infected with PRV 486 alone was used to normalize the data of virus infectivity for all other groups treated with the multivalent nanostructures or their components. SC-aptGFP and SC-flex-aptGFP demonstrated poor inhibition of PRV 486 in comparison to SC-nbGFP, with IC_{50} values ranging from 180 nM to 220 nM for SC-aptGFP and from 300 nM to 570 nM for SC-flex-aptGFP (Fig 6). SC-aptGFP without the flexible spacer provided better inhibition at all three valencies. Unlike nbGFP, which showed no inhibition at molar equivalent concentrations of SC-nbGFP nanostructures, monomeric aptGFP and flex-aptGFP showed comparable PRV 486

inhibitions at molar equivalent concentrations. Despite the poor therapeutic potential of SC-aptGFP and SC-flex-aptGFP nanostructures, these data demonstrate the modularity of SC to be conjugated with different binders for rapid screening, identification, and modulation of binders for multivalent antiviral platforms.

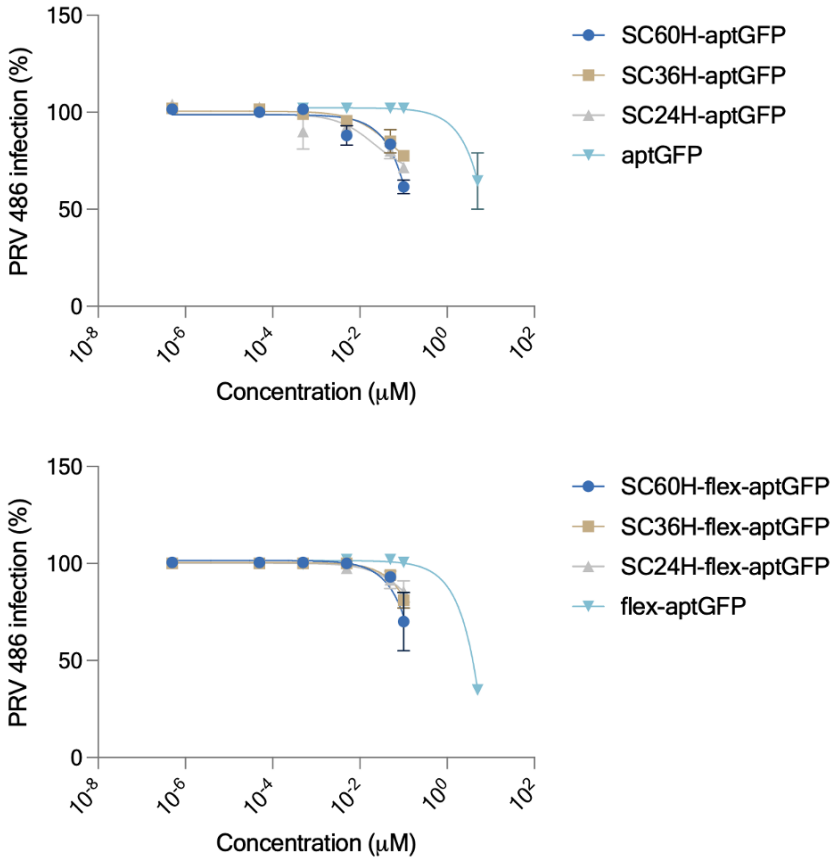

Fig. 10| Conjugation of aptamers to SC enhances PRV inhibition across all valencies. Dose-dependent, plaque-reduction inhibition curves for SC-aptGFP (top) and SC-flex-aptGFP (bottom). Inhibitor concentration was standardized through DNA concentration. Data are presented as mean ± S.E.M., N = 2 biologically independent experiments.

3.2.7. Serum stability of SC nanostructures

The structural integrity of 3D DNA origami nanostructures relies on a minimum concentration (~5 - 20 mM) of cations like Mg^{2+} to stabilize the negative charge-repulsive forces imparted by their nucleic acid phosphodiester backbone (26). We maintained a 12.5 mM concentration of Mg^{2+} throughout the synthesis and purification of SC and SC-associated nanostructures. This concentration is one order of magnitude higher than the physiological concentration found in the

human body, which is ~0.7 - 1 mM (27, 28). Previous studies have reported the loss of structural integrity of DNA nanostructures in cation-depleted-cell culture media, which could affect their functional efficacies (29). Furthermore, serum in physiological conditions can degrade DONs by the nuclease activity of DNA-degrading enzymes and proteins.

To characterize the physiological compatibility of SC-nbGFP and SC-aptGFP nanostructures, we evaluated their stability in cell culture media with different FBS concentrations. We incubated SC-nbGFP, SC-aptGFP and SC-flex-aptGFP nanostructures of different valencies in 0%, 2% and 10% FBS media for up to 8 h and assessed them on 1% AGE. The M13mp18 DNA was used as a control group. For SC-nbGFP, the presence of distinct bands revealed maintenance of structural integrity before and after 1 h, 2 h, and 8 h incubation in 0%, 2%, and 10% FBS. However, the reduced intensity of bands with increasing incubation time, particularly with 10% FBS media, indicated some degradation (Fig 11).

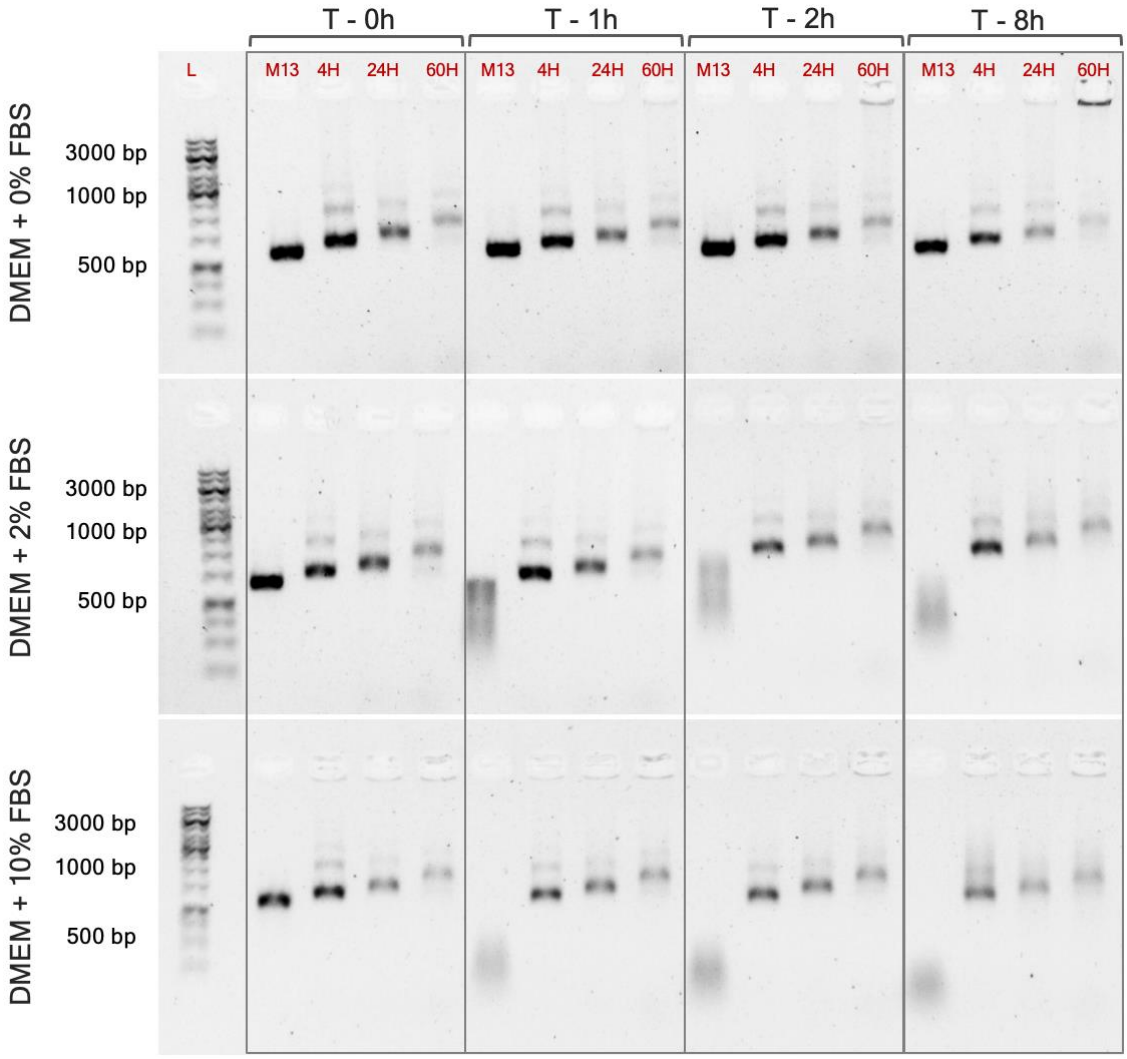

Fig. 11| Serum stability of SC-nbGFP nanostructures. 1% AGE analysis of SC-nbGFP nanostructures incubated in DMEM supplemented with FBS (0%, 2%, and 10%) for up to 8 h. L stands for 1 kb molecular weight ladder. The valency of SC-nbGFP is highlighted in red on top of each lane. M13mp18 is used as a positive control, which shows progressive degradation with increasing FBS strength and incubation time. Compared to the control group, other SC-nbGFP nanostructures are more stable. However, the reduced intensity of SC-nbGFP bands over time and with increasing FBS strength indicate some degree of degradation.

3.3. Discussion

One of the biggest challenges with multivalent inhibitors is developing scaffolds that allow precise spatiotemporal control of ligands. Structural DNA nanotechnology offers unprecedented addressability with sub-nanometer precision and accuracy to develop highly programmable 2D and

3D nanostructures that can be conjugated with diverse functional domains to probe viral pathosystems for diagnostic and therapeutic purposes. Previously, we developed SC60H-nbGFP, a 3D wireframe DNA origami-based multivalent platform presenting 60 copies of anti-GFP nanobody (nbGFP) binders on the snub cube (SC) scaffold to inhibit Pseudorabies virus (PRV) 486 infection. This chapter delved into mechanistic studies to manipulate and understand how the nanoscale spatial organization of virus binders modulates virus inhibition. To this end, we analyzed the particle size distributions of virus particles treated with SC-nbGFP nanostructures to get an insight into the binding modes between them. To understand the impact of valency, we varied the number of SC conjugation sites to display distinct nbGFP copy numbers that can interact with PRV 486. And finally, to understand any potential interferences that SC-nbGFP might have in the virus entry processes, we tracked the early events of virus attachment and internalization. Our findings suggest that while multivalency enhances the collective binding affinity (avidity) of the SC-nbGFP nanostructures, which also correlates with the enhancement of their inhibition efficacies, it may not be the only factor driving the switch of nbGFP from a non-inhibitor to a more potent one upon conjugation to the SC scaffold. Rather, the tagging of virus particles with the SC scaffold via nbGFP interferes with the initiation of viral infection by likely obstructing the internalization of the virus particles into target cells.

Previously, we reported a medium binding affinity of the monomeric nbGFP to PRV 486 (K_D ~24 nM). Based on our ELISA data, upon increasing the valency of SC-nbGFP, the relative K_D dropped to 24 pM for SC12H-nbGFP and 12 pM for SC60H-nbGFP. With SC1H-nbGFP, since the range of concentrations we tested fell below the saturation point on the ELISA binding curve, we could not compare its binding affinity with the other groups. However, the avidities of other groups showed an enhancement in virus binding by an approximate factor of 1000 and 2000 with SC12H-nbGFP and SC60H-nbGFP, respectively, compared to the monomeric nbGFP (Fig. 3). This enhancement of binding affinity upon increasing the valency of SC-nbGFP is consistent with previous studies using multivalent frameworks for virus binding (5, 6, 30, 31). Despite the limited knowledge of the gM spatial distribution on the PRV envelope, our data suggest an oligomeric (and potentially uniform) distribution, characteristic of many glycoproteins on the surface of bacterial and

viral pathogens (32, 33). The interactions of individual gM and nbGFP domains resulted in multiple simultaneous complexation events leading to high functional avidities of the multivalent assemblies.

To further understand the effect of multivalency on virus inhibition, we performed end-point infectivity assays using the standard plaque reduction assays and the orthogonal flow cytometry-based assays to measure the residual infectivity of viruses treated with the multivalent nanostructures. Since PRV 486 expresses pHluorin, the virus-infected cells become pHluorin positive as well; therefore, PRV 486 infectivity can be quantified as the percentage of pHluorin-positive cells within a given cell population (Fig. 4A). Virus inhibition was negligible with monomeric nbGFP and with SC scaffolds, for all the valencies we tested. On the other hand, all the SC-nbGFP conjugates, including the monovalent SC1H-nbGFP and the multivalent SC12H-nbGFP and SC60H-nbGFP nanostructures, inhibited PRV 486 infection, with IC_{50} corresponding to 150 nM, 38 nM, and 1.4 nM, respectively. The IC_{50} of SC60H-nbGFP obtained using flow cytometry in this work is similar to the previously obtained using plaque assay (~3 nM). Our findings indicate a positive correlation between K_D and IC_{50} of the SC-nbGFP nanostructures, such that increasing valency enhances the binding avidity that effectively translates into a more potent virus inhibition. Our study complements numerous other works with multivalent inhibitors in this aspect (5, 6, 16). Interestingly, unlike the monomeric nbGFP that failed to inhibit the virus at concentrations as high as 50 μM, the monovalent SC1H-nbGFP inhibited PRV 486 at 150 nM, the highest DNA concentration of SC-nbGFP we tested. This observation indicates that although avidity is a key to enhancing the inhibition efficacies of SC-nbGFP nanostructures, it is not (solely) responsible for the switch of nbGFP from a non-inhibitor to a potential one. Instead, the inhibitory effects are indirectly triggered upon conjugation of nbGFP to the SC scaffold. Furthermore, we identified a valency of 24 or more to achieve maximal inhibition efficiency with an almost plateauing effect on IC_{50} with $n > 24$. This could probably be related to ligand redundancy on SC scaffolds such that a higher number of nbGFP binders than the gM-pHluorin receptor domains are present in the multivalent contact area between the virus and the inhibitor. Also, since nbGFP are separated from the SC scaffold using a rigid ds-DNA handle, factors such as ligand clustering/congestion on the SC scaffold are less likely.

To orthogonally test the hypothesis that indirect attachment of the SC to the viral particle through a binder, we swapped out nbGFP binders with GFP aptamers targeting gM-pHluorin and repeated the dose-response analyses using plaque reduction infectivity assays. Furthermore, to assess the impact of binder flexibility, we introduced an ssDNA spacer between the virus binder and the dsDNA SC docking region. Consistent with our previous findings, we observed PRV 486 inhibition for all three valencies we tested with SC-aptGFP and SC-flex-aptGFP and a plateauing effect on IC_{50} with a valency of 24 or more.

Next, to understand the binding modes between SC-nbGFP and PRV 486, we evaluated the particle size distributions of virus pre-incubated with SC60H-nbGFP using nanoparticle tracking analysis. We anticipated three plausible binding modes (Fig. 8A):

1. One to many, in which the one multivalent inhibitor functions as an interconnector between multiple virus particles essentially aggregating them,
2. Many to one, in which multiple multivalent inhibitors partially or fully cover the surface of individual virus particles, sterically shielding the envelope glycoproteins and,
3. One to one, in which one multivalent inhibitor binds to one virus particle

The nanosight assays revealed that the size distribution of PRV particles pre-incubated with SC-nbGFP was comparable to that of control groups with untreated viruses or viruses pretreated with only SC scaffold or with only nbGFP binders. Therefore, no evidence of aggregation was observed for any of these groups under the imaging conditions employed. Our findings align with studies suggesting aggregation-mediated virus inhibition only when inhibitors are roughly the same size as the virus (13, 15). PRV particles are ~200 nm in size, whereas SC-nbGFP nanostructures are ~60 nm in size. In our case, the size of the virus particles is three times that of the inhibitors. Based on our findings, aggregation is not likely the primary mechanism underlying PRV 486 inhibition with SC-nbGFP nanostructures. Additionally, the virus inhibition we observed with the monovalent SC1H-nbGFP in our infectivity assays further supports this hypothesis. According to the nanosight data, the second and the third binding modes, many to one and one to one, respectively, also appear unlikely. Assuming a spherical shape, based on the size differences between PRV and SC-nbGFP, at least 11 units of SC-nbGFP are needed to cover the virus surface

completely, which should significantly increase the hydrodynamic radius of the PRV particles. However, nanosight failed to detect particles in control groups with only scaffolds (SC-nbGFP or SC), most likely owing to their wireframe structures as opposed to the solid structure of the virus particles. Although we cannot completely rule out these binding modes based on the nanosight data, our imaging data using confocal microscopy has provided further insight into these processes.

Finally, to test how SC-nbGFP obstructs the early events of PRV infection, we performed time-lapsed live-cell imaging of PRV particles on PK15 cells using confocal microscopy. PRV enters cells predominantly by the membrane fusion route, but it can also do so through low-pH-mediated endocytic pathways (34, 35). In either case, the capsids get internalized into the cells for transport into the periplasmic space. We used the recombinant PRV 483 which has a pHluorin-tagged envelope and RFP-tagged capsids, such that the virus particles can be tracked after their internalization into the target cells by monitoring the RFP puncta inside cells. Fluorescence microscopy can detect infectious PRV 483 particles as colocalized green and red puncta at neutral pH. Therefore, using this strain, we were able to track and differentiate the virus attachment by monitoring the colocalized red and green puncta on the cell surface and the virus internalization by monitoring the intracellular red puncta (Fig 9B). We monitored the RFP and GFP puncta at two different time points: the first-time point right after 1 h incubation at 4 ^{o}C to arrest the virus particles adsorbed on the cell surface and the second-time point after additional 1 h incubation at 37 ^{o}C to allow the natural progression of the infection cycle. Next, by analyzing the ratio of intracellular RFP to cell surface colocalized RFP/GFP, we determined the percentage of internalized viruses. We compared the progression of virus infection in two different cell groups: first, infected with viruses pre-incubated with SC-nbGFP, and second, infected with untreated viruses. Image analysis of cells after the 1 h time point showed similar colocalization of green and red puncta indicative of infectious viruses adsorbed on the cell surface. These findings suggest that SC-nbGFP nanostructures are less likely to interfere with the attachment of the virus particles on the cell surface. we observed a higher number of internalized viruses after the 2 h time point than the 1 h time point for untreated viruses, corresponding to the continuation of entry processes upon raising the incubation temperature to 37 ^{o}C. Interestingly, we observed a lower RFP to GFP ratio in the cell group infected

with treated viruses. This suggests less number of virus particles internalized when treated with SC-nbGFP as opposed to untreated viruses. These data suggest the binding interactions between SC-nbGFP and PRV 483 particles prevent the release of RFP-tagged virus capsids into the cells. These two observations, 1) surface attachment of the virus to cells is unaffected by SC and 2) capsid internalization is lower in presence of SC, support a hypothesis in which the SC's mechanism of action lies in disrupting the internalization process of PRV.

Taken together, our results indicate that indirect conjugation of the SC structure to the viral particle mediated through a binder is the critical component of inhibition of PRV. The presence of the SC 'payload' appears to block the internalization of PRV into the host cell critically and not the attachment step of PRV on the host cell. Furthermore, the binder element that links the SC to PRV does not appear to be specific to the nanobody and in fact, is reproducible when the nanobody is swapped with an aptamer. Another factor is that the binder does not even need exceptionally high-affinity interactions for the viral epitope because the SC allows for the presentation of multiple binders, which collectively can have an avidity effect to lower the effective Kd; in this case, a 3-order of magnitude improvement. Taken together, our findings suggest that tagging viral binders, including mAbs, or aptamers, with a DNA origami scaffold may be a strategy in which inhibitory properties can be imparted or enhanced and warrants further consideration.

3.4. Conclusion

In conclusion, our study provided preliminary insights into the mechanism of SC-nbGFP-mediated inhibition of PRV 486. Our findings suggest a more nuanced and active role of the scaffold than being a mere inert backbone for the spatial presentation of virus binders in modulating viral infectivity. In our study, the scaffold modulated virus infectivity by directly targeting the virus through binders but also indirectly by interfering with cellular mechanisms independent of viral factors responsible for them. The fact that we observed reduced viral infectivity even with a valency, n = 1, and no inhibition with monomeric binders attests to the predominant role of the scaffold in triggering the inhibitory effects of the nanostructures. It also suggests that this strategy will likely work with low-affinity binders by leveraging multivalency to offset weak binding, given that the binders are

highly selective for their target viral epitopes. In addition, the avidity resulting from multivalency can be instrumental in further enhancing the platform's inhibition potency.

Since our strategy of targeting non-essential virus domains is novel, it becomes even more important to investigate the inhibition mechanisms of multivalent systems. It would be interesting to know how the inhibition potential of SC1H-binder and the dynamics of multivalent SC-binders change with low-affinity binders as opposed to medium affinity binders we tested in this work. More importantly, it will be helpful to know how the inhibitory effects change with different scaffold geometries and architectures and if such platforms will work on viral systems employing different routes for internalization into cells, such as endocytic vs non-endocytic routes. By the virtue of the high programmability of DNA nanostructures and high-throughput technologies to rapidly screen and identify virus-specific binders independent of structural characterization, this strategy could be potentially implemented in a wide array of viral pathogens.

REFERENCES

1. Imberty A, Varrot A. Microbial recognition of human cell surface glycoconjugates. Current opinion in structural biology. 2008;18(5):567-76.

2. Karlsson K-A. Pathogen-host protein-carbohydrate interactions as the basis of important infections. The Molecular Immunology of Complex Carbohydrates—2. 2001:431-43.

3. Reuter JD, Myc A, Hayes MM, Gan Z, Roy R, Qin D, et al. Inhibition of viral adhesion and infection by sialic-acid-conjugated dendritic polymers. Bioconjugate chemistry. 1999;10(2):271-8.

4. Kwon S-J, Na DH, Kwak JH, Douaisi M, Zhang F, Park EJ, et al. Nanostructured glycan architecture is important in the inhibition of influenza A virus infection. Nature nanotechnology. 2017;12(1):48-54.

5. Lauster D, Glanz M, Bardua M, Ludwig K, Hellmund M, Hoffmann U, et al. Multivalent peptide–Nanoparticle conjugates for influenza-virus inhibition. Angewandte Chemie International Edition. 2017;56(21):5931-6.

6. Waldmann M, Jirmann R, Hoelscher K, Wienke M, Niemeyer FC, Rehders D, et al. A nanomolar multivalent ligand as entry inhibitor of the hemagglutinin of avian influenza. Journal of the American Chemical Society. 2014;136(2):783-8.

7. Bandlow V, Liese S, Lauster D, Ludwig K, Netz RR, Herrmann A, et al. Spatial screening of hemagglutinin on influenza A virus particles: sialyl-LacNAc displays on DNA and PEG scaffolds reveal the requirements for bivalency enhanced interactions with weak monovalent binders. Journal of the American Chemical Society. 2017;139(45):16389-97.

8. Gambaryan A, Tuzikov A, Chinarev A, Juneja L, Bovin N, Matrosovich M. Polymeric inhibitor of influenza virus attachment protects mice from experimental influenza infection. Antiviral research. 2002;55(1):201-5.

9. Albertazzi L, Gherardini L, Brondi M, Sulis Sato S, Bifone A, Pizzorusso T, et al. In vivo distribution and toxicity of PAMAM dendrimers in the central nervous system depend on their surface chemistry. Molecular pharmaceutics. 2013;10(1):249-60.

10. Haag R. Multivalency as a chemical organization and action principle. Beilstein-Institut; 2015. p. 848-9.

11. Bhatia S, Camacho LC, Haag R. Pathogen inhibition by multivalent ligand architectures. Journal of the American Chemical Society. 2016;138(28):8654-66.

12. Gestwicki JE, Cairo CW, Strong LE, Oetjen KA, Kiessling LL. Influencing receptor− ligand binding mechanisms with multivalent ligand architecture. Journal of the American Chemical Society. 2002;124(50):14922-33.

13. Vonnemann J, Sieben C, Wolff C, Ludwig K, Böttcher C, Herrmann A, et al. Virus inhibition induced by polyvalent nanoparticles of different sizes. Nanoscale. 2014;6(4):2353-60.

14. Papp I, Sieben C, Sisson AL, Kostka J, Böttcher C, Ludwig K, et al. Inhibition of influenza virus activity by multivalent glycoarchitectures with matched sizes. ChemBioChem. 2011;12(6):887-95.

15. Vonnemann J, Liese S, Kuehne C, Ludwig K, Dernedde J, Böttcher C, et al. Size dependence of steric shielding and multivalency effects for globular binding inhibitors. Journal of the American Chemical Society. 2015;137(7):2572-9.

16. Illescas BM, Rojo J, Delgado R, Martín N. Multivalent glycosylated nanostructures to inhibit Ebola virus infection. Journal of the American Chemical Society. 2017;139(17):6018-25.

17. Kwon PS, Ren S, Kwon S-J, Kizer ME, Kuo L, Xie M, et al. Designer DNA architecture offers precise and multivalent spatial pattern-recognition for viral sensing and inhibition. Nature chemistry. 2020;12(1):26-35.

18. Lauster D, Klenk S, Ludwig K, Nojoumi S, Behren S, Adam L, et al. Phage capsid nanoparticles with defined ligand arrangement block influenza virus entry. Nature nanotechnology. 2020;15(5):373-9.

19. Branson TR, McAllister TE, Garcia-Hartjes J, Fascione MA, Ross JF, Warriner SL, et al. A protein-based pentavalent inhibitor of the cholera toxin B-subunit. Angewandte Chemie. 2014;126(32):8463-7.

20. Zhang Z, Merritt EA, Ahn M, Roach C, Hou Z, Verlinde CL, et al. Solution and crystallographic studies of branched multivalent ligands that inhibit the receptor-binding of cholera toxin. Journal of the American Chemical Society. 2002;124(44):12991-8.

21. Branson TR, Turnbull WB. Bacterial toxin inhibitors based on multivalent scaffolds. Chemical Society Reviews. 2013;42(11):4613-22.

22. Kitov PI, Bundle DR. On the nature of the multivalency effect: a thermodynamic model. Journal of the American Chemical Society. 2003;125(52):16271-84.

23. Zhang F, Jiang S, Wu S, Li Y, Mao C, Liu Y, et al. Complex wireframe DNA origami nanostructures with multi-arm junction vertices. Nature nanotechnology. 2015;10(9):779-84.

24. Pradhan S, Varsani A, Leff C, Swanson CJ, Hariadi RF. Viral Aggregation: The Knowns and Unknowns. Viruses. 2022;14(2):438.

25. Shui B, Ozer A, Zipfel W, Sahu N, Singh A, Lis JT, et al. RNA aptamers that functionally interact with green fluorescent protein and its derivatives. Nucleic acids research. 2012;40(5):e39-e.

26. Dietz H, Douglas SM, Shih WM. Folding DNA into twisted and curved nanoscale shapes. Science. 2009;325(5941):725-30.

27. Barbagallo M, Dominguez LJ. Magnesium metabolism in type 2 diabetes mellitus, metabolic syndrome and insulin resistance. Archives of biochemistry and biophysics. 2007;458(1):40-7.

28. Yang SJ, Hwang SY, Baik SH, Lee KW, Nam MS, Park YS, et al. Serum magnesium level is associated with type 2 diabetes in women with a history of gestational diabetes mellitus: the Korea National Diabetes Program study. Journal of Korean medical science. 2014;29(1):84-9.

29. Hahn J, Wickham SF, Shih WM, Perrault SD. Addressing the instability of DNA nanostructures in tissue culture. ACS nano. 2014;8(9):8765-75.

30. Mammen M, Choi SK, Whitesides GM. Polyvalent interactions in biological systems: implications for design and use of multivalent ligands and inhibitors. Angewandte Chemie International Edition. 1998;37(20):2754-94.

31. Tang S, Puryear WB, Seifried BM, Dong X, Runstadler JA, Ribbeck K, et al. Antiviral agents from multivalent presentation of sialyl oligosaccharides on brush polymers. ACS Macro Letters. 2016;5(3):413-8.

32. Bertozzi CR, Kiessling aLL. Chemical glycobiology. Science. 2001;291(5512):2357-64.

33. Bhatia S, Dimde M, Haag R. Multivalent glycoconjugates as vaccines and potential drug candidates. MedChemComm. 2014;5(7):862-78.

34. Miller JL, Weed DJ, Lee BH, Pritchard SM, Nicola AV. Low-pH endocytic entry of the porcine alphaherpesvirus pseudorabies virus. Journal of virology. 2019;93(2):e01849-18.

35. Pomeranz LE, Reynolds AE, Hengartner CJ. Molecular biology of pseudorabies virus: impact on neurovirology and veterinary medicine. Microbiology and molecular biology reviews. 2005;69(3):462-500.

REFERENCES

1. Rohrmann, G.F. Baculovirus structural proteins. *J. Gen. Virol.* **1992**, *73 Pt 4*, 749-761.

2. Federici, B.A.; Vlak, J.M.; Hamm, J.J. Comparative study of virion structure, protein composition and genomic DNA of three ascovirus isolates. *J. Gen. Virol.* **1990**, *71 Pt 8*, 1661-1668.

3. Hirst, G.K.; Pons, M.W. Mechanism of influenza recombination: II. Virus aggregation and its effect on plaque formation by so-called noninfective virus. *Virol. J.* **1973**, *56*, 620-631.

4. Galasso, G.J.; Sharp, J.; Sharp, D.G. The influence of degree of aggregation and virus quality on the plaque titer of aggregated vaccinia virus. *J. Immunol.* **1964**, *92*, 870-878.

5. Floyd, R.; Sharp, D.G. Aggregation of poliovirus and reovirus by dilution in water. *Appl. Environ. Microbiol.* **1977**, *33*, 159-167.

6. Narang, H.K.; Codd, A.A. Frequency of preclumped virus in routine fecal specimens from patients with acute nonbacterial gastroenteritis. *J. Clin. Microbiol.* **1981**, *13*, 982-988.

7. Williams, F.P. Membrane-associated viral complexes observed in stools and cell culture. *Appl. Environ. Microbiol.* **1985**, *50*, 523-526.

8. Chen, Y.H.; Du, W.; Hagemeijer, M.C.; Takvorian, P.M.; Pau, C.; Cali, A.; Brantner, C.A.; Stempinski, E.S.; Connelly, P.S.; Ma, H.C. Phosphatidylserine vesicles enable efficient en bloc transmission of enteroviruses. *Cell* **2015**, *160*, 619-630.

9. Santiana, M.; Ghosh, S.; Ho, B.A.; Rajasekaran, V.; Du, W.L.; Mutsafi, Y.; De Jésus-Diaz, D.A.; Sosnovtsev, S.V.; Levenson, E.A.; Parra, G.I. Vesicle-cloaked virus clusters are optimal units for inter-organismal viral transmission. *Cell Host Microbe* **2018**, *24*, 208-220.e8.

10. Perez-Caballero, D.; Zang, T.; Ebrahimi, A.; McNatt, M.W.; Gregory, D.A.; Johnson, M.C.; Bieniasz, P.D. Tetherin inhibits HIV-1 release by directly tethering virions to cells. *Cell* **2009**, *139*, 499-511.

11. Arnaud, F.; Black, S.G.; Murphy, L.; Griffiths, D.J.; Neil, S.J.; Spencer, T.E.; Palmarini, M. Interplay between ovine bone marrow stromal cell antigen 2/tetherin and endogenous retroviruses. *J. Virol.* **2010**, *84*, 4415-4425.

12. Kaletsky, R.L.; Francica, J.R.; Agrawal-Gamse, C.; Bates, P. Tetherin-mediated restriction of filovirus budding is antagonized by the Ebola glycoprotein. *Proc. Natl. Acad. Sci. USA* **2009**, *106*, 2886-2891.

13. Ilinskaya, A.; Derse, D.; Hill, S.; Princler, G.; Heidecker, G. Cell-cell transmission allows human T-lymphotropic virus 1 to circumvent tetherin restriction. *Virology* **2013**, *436*, 201-209.

14. Sanjuán, R. Collective infectious units in viruses. *Trends Microbiol.* **2017**, *25*, 402-412.

15. Bald, J.G.; Briggs, G.E. Aggregation of Virus Particles. *Nature* **1937**, *140*, 111.

16. Hirst, G.K. Studies of antigenic differences among strains of influenza A by means of red cell agglutination. *J. Exp. Med.* **1983**, *78*, 407-423.

17. Hilleman, M.R. System for measuring and designating antigenic components of influenza viruses with analyses of recently isolated strains. *Proc. Soc. Exp. Biol. Med.* **1951**, *78*, 208-215.

18. Floyd, R. Viral aggregation: Mixed suspensions of poliovirus and reovirus. *Appl. Environ. Microbiol.* **1979**, *38*, 980-986.

19. Sharp, D.G.; Floyd, R.; Johnson, J.D. Nature of the surviving plaque-forming unit of reovirus in water containing bromine. *Appl. Environ. Microbiol.* **1975**, *29*, 94-101.

20. Galdiero, F. Adenovirus aggregation and preservation in extracellular environment. *Arch. Virol.* **1979**, *59*, 99-105.

21. Fiszman, M.; Bucchini, D.; Girard, M. Purification of the Sabin strain of poliovirus type I through treatment with sarkozyl. *J. Virol.* **1971**, *7*, 687-689.

22. Young, D.C.; Sharp, D.G. Poliovirus aggregates and their survival in water. *Appl. Environ. Microbiol.* **1977**, *33*, 168-177.

23. Floyd, R.; Sharp, D.G. Viral aggregation: Effects of salts on the aggregation of poliovirus and reovirus at low pH. *Appl. Environ. Microbiol.* **1978**, *35*, 1084-1094.

24. Totsuka, A.; Ohtaki, K.; Tagaya, I. Aggregation of enterovirus small plaque variants and polioviruses under low ionic strength conditions. *J. Gen. Virol.* **1978**, *38*, 519-533.

25. Floyd, R.; Sharp, D.G. Viral aggregation: Quantitation and kinetics of the aggregation of poliovirus and reovirus. *Appl. Environ. Microbiol.* **1978**, *35*, 1079-1083.

26. Von Zeipel, G. Neutralization of Aggregated Strains of Enterovirus 71 and Echovirus Type 4 in RD and Vero or GMK-AH1 Cells. *Acta Pathol. Microbiol. Scand. B* **1979**, *87*, 71-73.

27. Katouzian-safadi, M.; Favre, A.; Haenni, A. Effect of freezing and thawing on the structure of turnip yellow mosaic virus. *Eur. J. Biochem.* **1980**, *112*, 479-486.

28. Galasso, G.J.; Sharp, D.G. Effect of particle aggregation on the survival of irradiated vaccinia virus. *J. Bacteriol.* **1965**, *90*, 1138-1142.

29. Kahler, A.M.; Cromeans, T.L.; Metcalfe, M.G.; Humphrey, C.D.; Hill, V.R. Aggregation of adenovirus 2 in source water and impacts on disinfection by chlorine. *Food Environ. Virol.* **2016**, *8*, 148-155.

30. Tucker, S.P.; Thornton, C.L.; Wimmer, E.; Compans, R.W. Vectorial release of poliovirus from polarized human intestinal epithelial cells. *J. Virol.* **1993**, *67*, 4274-4282.

31. Gollins, S.W.; Porterfield, J.S. Flavivirus infection enhancement in macrophages: An electron microscopic study of viral cellular entry. *J. Gen. Virol.* **1985**, *66*, 1969-1982.

32. Gassilloud, B.; Gantzer, C. Adhesion-aggregation and inactivation of poliovirus 1 in groundwater stored in a hydrophobic container. *Appl. Environ. Microbiol.* **2005**, *71*, 912-920.

33. Michen, B.; Graule, T. Isoelectric points of viruses. *J. Appl. Microbiol.* **2010**, *109*, 388-397.

34. Wong, K.; Mukherjee, B.; Kahler, A.M.; Zepp, R.; Molina, M. Influence of Inorganic Ions on Aggregation and Adsorption Behaviors of Human Adenovirus. *Environ. Sci. Technol.* **2012**, *46*, 11145-11153.

35. da Silva, A.K.; Kavanagh, O.V.; Estes, M.K.; Elimelech, M. Adsorption and aggregation properties of norovirus GI and GII virus-like particles demonstrate differing responses to solution chemistry. *Environ. Sci. Technol.* **2011**, *45*, 520-526.

36. Langlet, J.; Gaboriaud, F.; Gantzer, C. Effects of pH on plaque forming unit counts and aggregation of MS2 bacteriophage. *J. Appl. Microbiol.* **2007**, *103*, 1632-1638.

37. Zoueva, O.P.; Bailly, J.E.; Nicholls, R.; Brown, E.G. Aggregation of influenza virus ribonucleocapsids at low pH. *Virus Res.* **2002**, *85*, 141-149.

38. Libersou, S.; Albertini, A.A.V.; Ouldali, M.; Maury, V.; Maheu, C.; Raux, H.; de Haas, F.; Roche, S.; Gaudin, Y.; Lepault, J. Distinct structural rearrangements of the VSV glycoprotein drive membrane fusion. *J. Cell Biol.* **2010**, *191*, 199-210.

39. Davis, H.E.; Rosinski, M.; Morgan, J.R.; Yarmush, M.L. Charged Polymers Modulate Retrovirus Transduction via Membrane Charge Neutralization and Virus Aggregation. *Biophys. J.* **2004**, *86*, 1234-1242.

40. Gutierrez, L.; Mylon, S.E.; Nash, B.; Nguyen, T.H. Deposition and aggregation kinetics of rotavirus in divalent cation solutions. *Environ. Sci. Technol.* **2010**, *44*, 4552-4557.

41. Langlet, J.; Gaboriaud, F.; Jérôme, F.; Gantzer, C. Aggregation and surface properties of F-specific RNA phages: implication for membrane filtration processes. *Water Res.* **2008**, *42*, 2769-2777.

42. Gerba, C.P.; Betancourt, W.Q. Viral Aggregation: Impact of virus behavior in the environment. *Environ. Sci. Technol.* **2017**, *51*, 7318-7325.

43. Cuevas, J.M.; Moreno, M.D.; Sanjuán, R. Multi-virion infectious units arise from free viral particles in an enveloped virus. *Nat. Microbiol.* **2017**, *2*, 1-7.

44. Anschau, V.; Sanjuán, R. Fibrinogen Gamma Chain Promotes Aggregation of Vesicular Stomatitis Virus in Saliva. *Viruses* **2020**, *12*, 282.

45. Corno, G.; Coci, M.; Giardina, M.; Plechuk, S.; Campanile, F.; Stefani, S. Antibiotics promote aggregation within aquatic bacterial communities. *Front. Microbiol.* **2014**, *5*, 297.

46. Blom, J.F.; Zimmermann, Y.S.; Ammann, T.; Pernthaler, J. Scent of danger: floc formation by a freshwater bacterium is induced by supernatants from a predator-prey coculture. *Appl. Environ. Microbiol.* **2010**, *76*, 6156-6163.

47. Hahn, M.W.; Moore, E.R.B.; Höfle, M.G. Role of Microcolony Formation in the Protistan Grazing Defense of the Aquatic Bacterium Pseudomonas sp. MWH1. *Microb. Ecol.* **2000**, *39*, 175-185.

48. Sherlock, O.; Schembri, M.A.; Reisner, A.; Klemm, P. Novel roles for the AIDA adhesin from diarrheagenic Escherichia coli: cell aggregation and biofilm formation. *J. Bacteriol.* **2004**, *186*, 8058-8065.

49. O'Toole, G.A.; Kolter, R. Flagellar and twitching motility are necessary for Pseudomonas aeruginosa biofilm development. *Mol. Microbiol.* **1998**, *30*, 295-304.

50. Abdel-Nour, M.; Duncan, C.; Prashar, A.; Rao, C.; Ginevra, C.; Jarraud, S.; Low, D.E.; Ensminger, A.W.; Terebiznik, M.R.; Guyard, C. The Legionella pneumophila collagen-like

protein mediates sedimentation, autoaggregation, and pathogen-phagocyte interactions. *Appl. Environ. Microbiol.* **2014**, *80*, 1441–1454.

51. Kuroda, M.; Ito, R.; Tanaka, Y.; Yao, M.; Matoba, K.; Saito, S.; Tanaka, I.; Ohta, T. Staphylococcus aureus surface protein SasG contributes to intercellular autoaggregation of Staphylococcus aureus. *Biochem. Biophys. Res. Commun.* **2008**, *377*, 1102–1106.

52. Arenas, J.; Cano, S.; Nijland, R.; van Dongen, V.; Rutten, L.; van der Ende, A.; Tommassen, J. The meningococcal autotransporter AutA is implicated in autoaggregation and biofilm formation. *Environ. Microbiol.* **2015**, *17*, 1321–1337.

53. Trunk, T.; Khalil, H.S.; Leo, J.C. Bacterial autoaggregation. *AIMS Microbiol.* **2018**, *4*, 140.

54. Jung, A.; Maier, R.; Vartanian, J.P.; Bocharov, G.; Jung, V.; Fischer, U.; Meese, E.; Hobsor, S.W.; Meyerhans, A. Multiply infected spleen cells in HIV patients. *Nature* **2002**, *418*, 144–144.

55. Sanjuán, R.; Cuevas, J.M.; Furió, V.; Holmes, E.C.; Moya, A. Selection for Robustness in Mutagenized RNA Viruses. *PLoS Genet.* **2007**, *3*, e93.

56. Novella, I.S.; Reissig, D.D.; Wilke, C.O. Density-dependent selection in vesicular stomatitis virus. *J. Virol.* **2004**, *78*, 5799–5804.

57. Kim, K.S.; Sharp, D.G. Electron microscopic observations on the nature of vaccinia virus particle aggregation. *J. Immunol.* **1966**, *97*, 197–202.

58. Flint, S.J.; Enquist, L.W.; Racaniello, V.R.; Skalka, A.M. *Principles of Virology*, 3rd ed.; John Wiley & Sons, Inc.: Hoboken, NJ, USA, 2009.

59. Snijder, B.; Sacher, R.; Rämö, P.; Damm, E.M.; Liberali, P.; Pelkmans, L. Population context determines cell-to-cell variability in endocytosis and virus infection. *Nature* **2009**, *461*, 520–523.

60. Heldt, F.S.; Kupke, S.Y.; Dorl, S.; Reichl, U.; Frensing, T. Single-cell analysis and stochastic modelling unveil large cell-to-cell variability in influenza A virus infection. *Nat. Commun.* **2015**, *6*, 1–12.

61. Pearson, J.E.; Krapivsky, P.; Perelson, A.S. Stochastic theory of early viral infection: continuous versus burst production of virions. *PLoS Comput. Biol.* **2011**, *7*, e1001058.

62. Patton, J.T.; Spencer, E. Genome replication and packaging of segmented double-stranded RNA viruses. *J. Virol.* **2000**, *277*, 217–225.

63. Reijnders, L. The origin of multicomponent small ribonucleoprotein viruses. In *Advances in Virus Research*; Elsevier: Amsterdam, The Netherlands, 1978; Volume 23, pp. 79–102.

64. Jaspars, E.M.J. Plant viruses with a multipartite genome. In *Advances in Virus Research*; Elsevier: Amsterdam, The Netherlands, 1974; Volume 19, pp. 37–149.

65. Palese, P.; Schulman, J.L. Mapping of the influenza virus genome: Identification of the hemagglutinin and the neuraminidase genes. *Proc. Natl. Acad. Sci. USA* **1976**, *73*, 2142–2146.

66. Palese, P.; Ritchey, M.B.; Schulman, J.L. Mapping of the influenza virus genome II. Identification of the P1, P2, and P3 genes. *J. Virol.* **1977**, *76*, 114–121.

67. Ritchey, M.B.; Palese, P.; Schulman, J.L. Mapping of the influenza virus genome. III. Identification of genes coding for nucleoprotein, membrane protein, and nonstructural protein. *J. Virol.* **1976**, *20*, 307-313.

68. Brooke, C.B.; Ince, W.L.; Wrammert, J.; Ahmed, R.; Wilson, P.C.; Bennink, J.R.; Yewdell, J.W. Most influenza a virions fail to express at least one essential viral protein. *J. Virol.* **2013**, *87*, 3155-3162.

69. Jacobs, N.T.; Onuoha, N.O.; Antia, A.; Steel, J.; Antia, R.; Lowen, A.C. Incomplete influenza A virus genomes occur frequently but are readily complemented during localized viral spread. *Nat. Commun.* **2019**, *10*, 1-17.

70. Varsani, A.; Lefeuvre, P.; Roumagnac, P.; Martin, D. Notes on recombination and reassortment in multipartite/segmented viruses. *Curr. Opin. Virol.* **2018**, *33*, 156-166.

71. Ladner, J.T.; Wiley, M.R.; Beitzel, B.; Auguste, A.J.; Dupuis, A.P., II; Lindquist, M.E.; Sibley, S.D.; Kota, K.P.; Fetterer, D.; Eastwood, G. A multicomponent animal virus isolated from mosquitoes. *Cell Host Microbe* **2016**, *20*, 357-367.

72. Sanjuán, R. Collective properties of viral infectivity. *Curr. Opin. Virol.* **2018**, *33*, 1-6.

73. Andreu-Moreno, I.; Sanjuán, R. Collective infection of cells by viral aggregates promotes early viral proliferation and reveals a cellular-level Allee effect. *Curr. Biol.* **2018**, *28*, 3212-3219.e4.

74. Feng, Z.; Hensley, L.; McKnight, K.L.; Hu, F.; Madden, V.; Ping, L.; Jeong, S.H.; Walker, C.; Lanford, R.E.; Lemon, S.M. A pathogenic picornavirus acquires an envelope by hijacking cellular membranes. *Nature* **2013**, *496*, 367-371.

75. Casartelli, N.; Sourisseau, M.; Feldmann, J.; Guivel-Benhassine, F.; Mallet, A.; Marcelin, A.G.; Guatelli, J.; Schwartz, O. Tetherin restricts productive HIV-1 cell-to-cell transmission. *PLoS Pathog.* **2010**, *6*, e1000955.

76. Jones, J.C.; Settles, E.W.; Brandt, C.R.; Schultz-Cherry, S. Virus aggregating peptide enhances the cell mediated response to influenza virus vaccine. *Vaccine* **2011**, *29*, 7696-7703.

77. Sturman, L.S.; Ricard, C.S.; Holmes, K.V. Conformational change of the coronavirus peplomer glycoprotein at pH 8.0 and 37 degrees C correlates with virus aggregation and virus-induced cell fusion. *J. Virol.* **1990**, *64*, 3042-3050.

78. Clavijo, G.; Williams, T.; Mun, D.; Caballero, P.; Lopez-Ferber, M. Mixed genotype transmission bodies and virions contribute to the maintenance of diversity in an insect virus. *Proc. Biol. Sci.* **2010**, *277*, 943-951.

79. Sajjan, D.B.; Hinchigeri, S.B. Structural Organization of Baculovirus Occlusion Bodies and Protective Role of multilayered polyhedron envelope protein. *Food Environ. Virol.* **2016**, *8*, 86-100.

80. Jolly, C.; Booth, N.J.; Neil, S.J.D. Cell-cell spread of human immunodeficiency virus type 1 overcomes tetherin/BST-2-mediated restriction in T cells. *J. Virol.* **2010**, *84*, 12185-12199.

81. Correia, A.M.P. Biofilm-Like Extracellular Viral Assemblies Mediate HTLV-1 (Human T Cell Leukemia Virus Type-1) Cell-to-Cell Transmission at Virological Synapses. *Nat. Med.* **2010**, *16*, 83-89.

82. Tecle, T.; White, M.R.; Gantz, D.; Crouch, E.C.; Hartshorn, K.L. Human neutrophil defensins increase neutrophil uptake of influenza A virus and bacteria and modify virus-induced respiratory burst responses. *J. Immunol.* **2007**, *178*, 8046–8052.

83. Doss, M.; White, M.R.; Tecle, T.; Gantz, D.; Crouch, E.C.; Jung, G.; Ruchala, P.; Waring, A.J.; Lehrer, R.I.; Hartshorn, K.L. Interactions of α-, β-, and θ-defensins with influenza A virus and surfactant protein D. *J. Immunol.* **2009**, *182*, 7878–7887.

84. Hoeksema, M.; Tripathi, S.; White, M.; Qi, L.; Taubenberger, J.; van Eijk, M.; Haagsman, H.; Hartshorn, K.L. Arginine-rich histones have strong antiviral activity for influenza A viruses. *Innate Immun.* **2015**, *21*, 736–745.

85. Aguilera, E.R.; Erickson, A.K.; Jesudhasan, P.R.; Robinson, C.M.; Pfeiffer, J.K. Plaques Formed by Mutagenized Viral Populations Have Elevated Coinfection Frequencies. *mBio* **2017**, *8*, e02020-16.

86. Bird, S.W.; Maynard, N.D.; Covert, M.W.; Kirkegaard, K. Nonlytic viral spread enhanced by autophagy components. *Proc. Natl. Acad. Sci. USA* **2014**, *111*, 13081–13086.

87. Andreadis, S.; Lavery, T.; Davis, H.E.; Le Doux, J.M.; Yarmush, M.L.; Morgan, J.R. Toward a more accurate quantification of the activity of recombinant retroviruses: Alternatives to titer and multiplicity of infection. *J. Virol.* **2000**, *74*, 3431–3439.

88. Vahey, M.D.; Fletcher, D.A. Influenza A virus surface proteins are organized to help penetrate host mucus. *Elife* **2019**, *8*, e43764.

89. Baccam, P.; Beauchemin, C.; Macken, C.A.; Hayden, F.G.; Perelson, A.S. Kinetics of influenza A virus infection in humans. *J. Virol.* **2006**, *80*, 7590–7599.

90. Chuck, A.S.; Clarke, M.F.; Palsson, B.O. Retroviral infection is limited by Brownian motion. *Hum. Gene Ther.* **1996**, *7*, 1527–1534.

91. Marsh, M.; Helenius, A. Virus entry: Open sesame. *Cell* **2006**, *124*, 729–740.

92. Cohen, S.; Au, S.; Pante, N. How viruses access the nucleus. *Biochim. Biophys. Acta Mol. Cell Res.* **2011**, *1813*, 1634–1645.

93. Altan-Bonnet, N.; Perales, C.; Domingo, E. Extracellular vesicles: Vehicles of en bloc viral transmission. *Virus Res.* **2019**, *265*, 143–149.

94. Brandenburg, B.; Zhuang, X. Virus trafficking-learning from single-virus tracking. *Nat. Rev. Microbiol.* **2007**, *5*, 197–208.

95. Robinson, S.M.; Tsueng, G.; Sin, J.; Mangale, V.; Rahawi, S.; McIntyre, L.L.; Williams, W.; Kha, N.; Cruz, C.; Hancock, B.M. Coxsackievirus B exits the host cell in shed microvesicles displaying autophagosomal markers. *PLoS Pathog.* **2014**, *10*, e1004045.

96. Kerviel, A.; Zhang, M.; Bonnet, N.A. A new infectious unit: extracellular vesicles carrying virus populations. *Annu. Rev. Cell Dev. Biol.* **2021**, *37*, 171–197.

97. Jackson, W.T.; Giddings, T.H., Jr.; Taylor, M.P.; Mulinyawe, S.; Rabinovitch, M.; Kopito, R.R. Subversion of Cellular Autophagosomal Machinery by RNA Viruses. *PLoS Biol.* **2005**, *3*, e156.

98. Jouvenet, N.; Neil, S.J.D.; Zhadina, M.; Zang, T.; Kratovac, Z.; Lee, Y.; McNatt, M.; Hatziioannou, T.; Bieniasz, P.D. Broad-spectrum inhibition of retroviral and filoviral particle release by tetherin. *J. Virol.* **2009**, *83*, 1837–1844.

99. Pardieu, C.; Vigan, R.; Wilson, S.J.; Calvi, A.; Zang, T.; Bieniasz, P.; Kellam, P.; Towers, G.J.; Neil, S.J.D. The RING-CH Ligase K5 Antagonizes Restriction of KSHV and HIV-1 Particle Release by Mediating Ubiquitin-Dependent Endosomal Degradation of Tetherin. *PLoS Pathog.* **2010**, *6*, e1000843.

100. Weidner, J.M.; Jiang, D.; Pan, X.B.; Chang, J.; Block, T.M.; Guo, J.T. Interferon-Induced Cell Membrane Proteins, IFITM3 and Tetherin, Inhibit Vesicular Stomatitis Virus Infection via Distinct Mechanisms. *J. Virol.* **2010**, *84*, 12646–12657.

101. Miyagi, E.; Andrew, A.J.; Kao, S.; Strebel, K. Vpu enhances HIV-1 virus release in the absence of Bst-2 cell surface down-modulation and intracellular depletion. *Proc. Natl. Acad. Sci. USA* **2009**, *106*, 2868–2873.

102. Kuhl, B.D.; Sloan, R.D.; Donahue, D.A.; Bar-Magen, T.; Liang, C.; Wainberg, M.A. Tetherin restricts direct cell-to-cell infection of HIV-1. *Retrovirology* **2010**, *7*, 115.

103. Rudnicka, D.; Feldmann, J.; Porrot, F.; Wietgrefe, S.;Guadagnini, S.; Prévost, M.C.; Estaquier, J.; Haase, A.T.; Sol-Foulon, N.; Schwartz, O. Simultaneous cell-to-cell transmission of human immunodeficiency virus to multiple targets through polysynapses. *J. Virol.* **2009**, *83*, 6234–6246.

104. Sherer, N.M.; Lehmann, M.J.; Jimenez-Soto, L.F.; Horensavitz, C.; Pypaert, M.; Mothes, W. Retroviruses can establish fiopodial bridges for efficient cell-to-cell transmission. *Nat. Cell Biol.* **2007**, *9*, 310–315.

105. Sowinski, S.; Jolly, C.; Berninghausen, O.; Purbhoo, M.A.; Chauveau, A.; Köhler, K.; Oddos, S.; Eissmann, P.; Brodsky, F.M.; Hopkins, C. Membrane nanotubes physically connect T cells over long distances presenting a novel route for HIV-1 transmission. *Nat. Cell Biol.* **2008**, *10*, 211–219.

106. Braciale, T.J.; Hahn, Y.S. Immunity to viruses. *Immunol. Rev.* **2013**, *255*, 5–12.

107. Mueller, S.N.; Rouse, B.T. Immune responses to viruses. *Clin. Immunol.* **2008**, *2008*, 421.

108. Rouse, B.T.; Sehrawat, S. Immunity and immunopathology to viruses: what decides the outcome? *Nat. Rev. Immunol.* **2010**, *10*, 514–526.

109. Wallis, C.; Melnick, J.L. Virus aggregation as the cause of the non-neutralizable persistent fraction. *J. Virol.* **1967**, *1*, 478–488.

110. Jayasekera, J.P.; Moseman, E.A.; Carroll, M.C. Natural antibody and complement mediate neutralization of influenza virus in the absence of prior immunity. *J. Virol.* **2007**, *81*, 3487–3494.

111. Qi,L.; Kash, J.C.; Dugan, V.G.; Jagger, B.W.; Lau, Y.F.; Sheng, Z.M.; Crouch, E.C.; Hartshorn, K.L.; Taubenberger, J.K. The ability of pandemic influenza virus hemagglutinins to induce lower respiratory pathology is associated with decreased surfactant protein D binding. *Virology* **2011**, *412*, 426–434.

112. Doss, M.; Ruchala, P.; Tecle, T.; Gantz, D.; Verma, A.; Hartshorn, A.; Crouch, E.C.; Luong, H.; Micewicz, E.D.; Lehrer, R.I.; et al. Hapivirins and diprovirins: novel *θ*-defensin analogs with potent activity against influenza A virus. *J. Immunol.* **2012**, *188*, 2759–2768.

113. Hartshorn, K.L.; White, M.R.; Crouch, E.C. Contributions of the N-andC-terminal domains of surfactant protein d to the binding, aggregation, and phagocytic uptake of bacteria. *Infect. Immun.* **2002**, *70*, 6129–6139.

114. Hartshorn, K.L.; White, M.R.; Tecle, T.; Holmskov, U.; Crouch, E.C. Innate defense against influenza A virus: activity of human neutrophil defensins and interactions of defensins with surfactant protein D. *J. Immunol.* **2006**, *176*, 6962–6972.

115. Hartshorn, K.L.; Webby, R.; White, M.R.; Tecle, T.; Pan, C.; Boucher, S.; Moreland, R.J.; Crouch, E.C.; Scheule, R.K. Role of viral hemagglutinin glycosylation in anti-influenza activities of recombinant surfactant protein D. *Respir. Res.* **2008**, *9*, 65.

116. Williams, J.A.; Gui, L.; Hom, N.; Mileant, A.; Lee, K.K. Dissection of epitope-specific mechanisms of neutralization of influenza virus by intact IgG and Fab fragments. *J. Virol.* **2017**, *92*, e02006-17.

117. Jones, J.C.; Settles, E.W.; Brandt, C.R.; Schultz-Cherry, S. Identification of the Minimal Active Sequence of an Anti-Influenza Virus Peptide. *Antimicrob. Agents Chemother.* **2011**, *55*, 1810–1813.

118. White, M.R.; Kandel, R.; Hsieh, I.N.; De Luna, X.; Hartshorn, K.L. Critical role of C-terminal residues of the Alzheimer's associated *β*-amyloid protein in mediating antiviral activity and modulating viral and bacterial interactions with neutrophils. *PLoS ONE* **2018**, *13*, e0194001.

119. Outlaw, M.C.; Dimmock, N.J. Mechanisms of neutralization of influenza virus on mouse tracheal epithelial cells by mouse monoclonal polymeric IgA and polyclonal IgM directed against the viral haemagglutinin. *J. Gen. Virol.* **1990**, *71*, 69–76.

120. Jones, J.C.; Turpin, E.A.; Bultmann, H.; Brandt, C.R.; Schultz-Cherry, S. Inhibition of influenza virus infection by a novel antiviral peptide that targets viral attachment to cells. *J. Virol.* **2006**, *80*, 11960–11967.

121. Kwon, P.S.; Ren, S.; Kwon, S.J.; Kizer, M.E.; Kuo, L.; Xie, M.; Zhu, D.; Zhou, F.; Zhang, F.; Kim, D. Designer DNA architecture offers precise and multivalent spatial pattern-recognition for viral sensing and inhibition. *Nat. Chem.* **2020**, *12*, 26–35.

122. Gao, G.; Vandenberghe, L.H.; Alvira, M.R.; Lu, Y.; Calcedo, R.; Zhou, X.; Wilson, J.M. Clades of Adeno-associated viruses are widely disseminated in human tissues. *J. Virol.* **2004**, *78*, 6381–6388.

123. Boutin, S.; Monteilhet, V.; Veron, P.; Leborgne, C.; Benveniste, O.; Montus, M.F.; Masurier, C. Prevalence of serum IgG and neutralizing factors against adeno-associated virus (AAV) types 1, 2, 5, 6, 8, and 9 in the healthy population: implications for gene therapy using AAV vectors. *Hum. Gene Ther.* **2010**, *21*, 704–712.

124. Zincarelli, C.; Soltys, S.; Rengo, G.; Rabinowitz, J.E. Analysis of AAV serotypes 1-9 mediated gene expression and tropism in mice after systemic injection. *Mol. Ther.* **2008**, *16*, 1073–1080.

125. Halbert, C.L.; Allen, J.M.; Miller, A.D. Efficient mouse airway transduction following recombination between AAV vectors carrying parts of a larger gene. *Nat. Biotechnol.* **2002**, *20*, 697-701.

126. Lai, Y.; Yue, Y.; Liu, M.; Ghosh, A.; Engelhardt, J.F.; Chamberlain, J.S.; Duan, D. Efficient in vivo gene expression by trans-splicing adeno-associated viral vectors. *Nat. Biotechnol.* **2005**, *23*, 1435-1439.

127. Cuevas JM, Geller R, Garijo R, López-Aldeguer J, Sanjuán R. Extremely high mutation rate of HIV-1 in vivo. PLoS biology. 2015;13(9):e1002251.

128. Ribeiro RM, Li H, Wang S, Stoddard MB, Learn GH, Korber BT, et al. Quantifying the diversification of hepatitis C virus (HCV) during primary infection: estimates of the in vivo mutation rate. 2012.

129. Cuevas JM, González-Candelas F, Moya A, Sanjuán R. Effect of ribavirin on the mutation rate and spectrum of hepatitis C virus in vivo. Journal of virology. 2009;83(11):5760-4.

130. Dropulic LK, Cohen JI. The challenge of developing a herpes simplex virus 2 vaccine. Expert review of vaccines. 2012;11(12):1429-40.

131. **Moderna's Work on a Potential Vaccine Against COVID-19**. Available from: https://www.sec.gov/Archives/edgar/data/1682852/000119312520074867/d884510dex991.htm#:~:text=On%20January%2013%2C%202020%2C%20the,vaccine%20against%20the%20novel%20coronavirus.

132. Walsh EE, Frenck Jr RW, Falsey AR, Kitchin N, Absalon J, Gurtman A, et al. Safety and immunogenicity of two RNA-based Covid-19 vaccine candidates. New England Journal of Medicine. 2020;383(25):2439-50.

133. Jackson LA, Anderson EJ, Rouphael NG, Roberts PC, Makhene M, Coler RN, et al. An mRNA vaccine against SARS-CoV-2—preliminary report. New England journal of medicine. 2020.

134. The COVID-19 vaccine race. Available from: https://www.gavi.org/vaccineswork/covid-19-vaccine-race.

135. Ball P. The lightning-fast quest for COVID vaccines - and what it means for other diseases. 2020.

136. WHO Coronavirus (COVID-19) Dashboard [Available from: https://covid19.who.int/.

137. Bauer D, St Vincent L. Prophylactic Treatment of Smallpox Contacts with N-Methylisatin (β-Thiosemicarbazone (Compound 33T57, Marboran). Lancet. 1963:494-6.

138. Hoy-Ellis C, Fredriksen-Goldsen K. Is AIDS chronic or terminal? The perceptions of persons living with AIDS and their informal support partners. AIDS care. 2007;19(7):835-43.

139. De Clercq E, Li G. Approved antiviral drugs over the past 50 years. Clinical microbiology reviews. 2016;29(3):695-747.

140. Antiviral Drugs That Are Approved, Authorized, or Under Evaluation for the Treatment of COVID-192022. Available from: https://www.covid19treatmentguidelines.nih.gov/therapies/antiviral-therapy/summary-recommendations/.

141. Tompa DR, Immanuel A, Srikanth S, Kadhirvel S. Trends and strategies to combat viral infections: A review on FDA approved antiviral drugs. International journal of biological macromolecules. 2021;172:524-41.

142. Li Q, Kang C. Mechanisms of action for small molecules revealed by structural biology in drug discovery. International Journal of Molecular Sciences. 2020;21(15):5262.

143. Declerck PJ. Biologicals and biosimilars: a review of the science and its implications. GaBI J. 2012;1(1):13-6.

144. Kumar M, Kuroda K, Dhangar K, Mazumder P, Sonne C, Rinklebe J, et al. Potential emergence of antiviral-resistant pandemic viruses via environmental drug exposure of animal reservoirs. Environmental science & technology. 2020;54(14):8503-5.

145. Bright RA, Medina M-j, Xu X, Perez-Oronoz G, Wallis TR, Davis XM, et al. Incidence of adamantane resistance among influenza A (H3N2) viruses isolated worldwide from 1994 to 2005: a cause for concern. The Lancet. 2005;366(9492):1175-81.

146. Deyde VM, Xu X, Bright RA, Shaw M, Smith CB, Zhang Y, et al. Surveillance of resistance to adamantanes among influenza A (H3N2) and A (H1N1) viruses isolated worldwide. The Journal of infectious diseases. 2007;196(2):249-57.

147. Crumpacker CS, Schnipper LE, Marlowe SI, Kowalsky PN, Hershey BJ, Levin MJ. Resistance to antiviral drugs of herpes simplex virus isolated from a patient treated with acyclovir. New England Journal of Medicine. 1982;306(6):343-6.

148. McCallum M, Bassi J, De Marco A, Chen A, Walls AC, Di Iulio J, et al. SARS-CoV-2 immune evasion by the B. 1.427/B. 1.429 variant of concern. Science. 2021;373(6555):648-54.

149. Dejnirattisai W, Zhou D, Supasa P, Liu C, Mentzer AJ, Ginn HM, et al. Antibody evasion by the P. 1 strain of SARS-CoV-2. Cell. 2021;184(11):2939-54. e9.

150. Chen RE, Zhang X, Case JB, Winkler ES, Liu Y, VanBlargan LA, et al. Resistance of SARS-CoV-2 variants to neutralization by monoclonal and serum-derived polyclonal antibodies. Nature medicine. 2021;27(4):717-26.

151. Diamond M, Chen R, Winkler E, Case J, Aziati I, Bricker T, et al. In vivo monoclonal antibody efficacy against SARS-CoV-2 variant strains. Research square. 2021.

152. McCallum M, Walls A, Sprouse K, Bowen J, Rosen L, Dang H, et al. Molecular basis of immune evasion by the delta and kappa SARS-CoV-2 variants. bioRxiv [Preprint]. 2021 Aug 12: 2021.08. 11.455956. doi: 10.1101/2021.08. 11.455956. PMID.

153. Cameroni E, Bowen JE, Rosen LE, Saliba C, Zepeda SK, Culap K, et al. Broadly neutralizing antibodies overcome SARS-CoV-2 Omicron antigenic shift. Nature. 2022;602(7898):664-70.

154. VanBlargan LA, Errico JM, Halfmann PJ, Zost SJ, Crowe JE, Purcell LA, et al. An infectious SARS-CoV-2 B. 1.1. 529 Omicron virus escapes neutralization by therapeutic monoclonal antibodies. Nature medicine. 2022;28(3):490-5.

155. Case JB, Mackin S, Errico JM, Chong Z, Madden EA, Whitener B, et al. Resilience of S309 and AZD7442 monoclonal antibody treatments against infection by SARS-CoV-2 Omicron lineage strains. Nature communications. 2022;13(1):1-11.

156. Mercorelli B, Palù G, Loregian A. Drug repurposing for viral infectious diseases: how far are we? Trends in microbiology. 2018;26(10):865-76.

157. Sissoko D, Laouenan C, Folkesson E, M'lebing A-B, Beavogui A-H, Baize S, et al. Experimental treatment with favipiravir for Ebola virus disease (the JIKI Trial): a historically controlled, single-arm proof-of-concept trial in Guinea. PLoS medicine. 2016;13(3):e1001967.

158. Haffizulla J, Hartman A, Hoppers M, Resnick H, Samudrala S, Ginocchio C, et al. Effect of nitazoxanide in adults and adolescents with acute uncomplicated influenza: a double-blind, randomised, placebo-controlled, phase 2b/3 trial. The Lancet Infectious diseases. 2014;14(7):609-18.

159. Arabi YM, Alothman A, Balkhy HH, Al-Dawood A, AlJohani S, Al Harbi S, et al. Treatment of Middle East respiratory syndrome with a combination of lopinavir-ritonavir and interferon-β1b (MIRACLE trial): study protocol for a randomized controlled trial. Trials. 2018;19(1):1-13.

160. Mammen M, Choi SK, Whitesides GM. Polyvalent interactions in biological systems: implications for design and use of multivalent ligands and inhibitors. Angewandte Chemie International Edition. 1998;37(20):2754-94.

161. Imberty A, Varrot A. Microbial recognition of human cell surface glycoconjugates. Current opinion in structural biology. 2008;18(5):567-76.

162. Karlsson K-A. Pathogen-host protein-carbohydrate interactions as the basis of important infections. The Molecular Immunology of Complex Carbohydrates—2. 2001:431-43.

163. TAKEMOTO DK, SKEHEL JJ, WILEY DC. A surface plasmon resonance assay for the binding of influenza virus hemagglutinin to its sialic acid receptor. Virology. 1996;217(2):452-8.

164. Sauter NK, Bednarski MD, Wurzburg BA, Hanson JE, Whitesides GM, Skehel JJ, et al. Hemagglutinins from two influenza virus variants bind to sialic acid derivatives with millimolar dissociation constants: a 500-MHz proton nuclear magnetic resonance study. Biochemistry. 1989;28(21):8388-96.

165. Moscona A. Medical management of influenza infection. Annu Rev Med. 2008;59:397-413.

166. Schirmer P, Holodniy M. Oseltamivir for treatment and prophylaxis of influenza infection. Expert opinion on drug safety. 2009;8(3):357-71.

167. Bhatia S, Camacho LC, Haag R. Pathogen inhibition by multivalent ligand architectures. Journal of the American Chemical Society. 2016;138(28):8654-66.

168. Dinleyici EC, Yargic ZA. Pneumococcal conjugated vaccines: impact of PCV-7 and new achievements in the postvaccine era. Expert review of vaccines. 2008;7(9):1367-94.

169. Lauer KB, Borrow R, Blanchard TJ. Multivalent and multipathogen viral vector vaccines. Clinical and Vaccine Immunology. 2017;24(1):e00298-16.

170. Lauster D, Klenk S, Ludwig K, Nojoumi S, Behren S, Adam L, et al. Phage capsid nanoparticles with defined ligand arrangement block influenza virus entry. Nature nanotechnology. 2020;15(5):373-9.

171. Kwon S-J, Na DH, Kwak JH, Douaisi M, Zhang F, Park EJ, et al. Nanostructured glycan architecture is important in the inhibition of influenza A virus infection. Nature nanotechnology. 2017;12(1):48-54.

172. Varga N, Sutkeviciute I, Ribeiro-Viana R, Berzi A, Ramdasi R, Daghetti A, et al. A multivalent inhibitor of the DC-SIGN dependent uptake of HIV-1 and Dengue virus. Biomaterials. 2014;35(13):4175-84.

173. Bastian AR, Nangarlia A, Bailey LD, Holmes A, Sundaram RVK, Ang C, et al. Mechanism of multivalent nanoparticle encounter with HIV-1 for potency enhancement of peptide triazole virus inactivation. Journal of Biological Chemistry. 2015;290(1):529-43.

174. Hunt AC, Case JB, Park Y-J, Cao L, Wu K, Walls AC, et al. Multivalent designed proteins neutralize SARS-CoV-2 variants of concern and confer protection against infection in mice. Science translational medicine. 2022;14(646):eabn1252.

175. Haag R. Multivalency as a chemical organization and action principle. Beilstein-Institut; 2015. p. 848-9.

176. Rothemund PW. Folding DNA to create nanoscale shapes and patterns. Nature. 2006;440(7082):297-302.

177. Zhang Y, Pan V, Li X, Yang X, Li H, Wang P, et al. Dynamic DNA structures. Small. 2019;15(26):1900228.

178. Zhao Y-X, Shaw A, Zeng X, Benson E, Nystrom AM, Högberg Br. DNA origami delivery system for cancer therapy with tunable release properties. ACS nano. 2012;6(10):8684-91.

179. Wiraja C, Zhu Y, Lio DCS, Yeo DC, Xie M, Fang W, et al. Framework nucleic acids as programmable carrier for transdermal drug delivery. Nature communications. 2019;10(1):1-12.

180. Song L, Jiang Q, Liu J, Li N, Liu Q, Dai L, et al. DNA origami/gold nanorod hybrid nanostructures for the circumvention of drug resistance. Nanoscale. 2017;9(23):7750-4.

181. Liu J, Song L, Liu S, Zhao S, Jiang Q, Ding B. A tailored DNA nanoplatform for synergistic RNAi-/chemotherapy of multidrug-resistant tumors. Angewandte Chemie International Edition. 2018;57(47):15486-90.

182. Douglas SM, Bachelet I, Church GM. A logic-gated nanorobot for targeted transport of molecular payloads. Science. 2012;335(6070):831-4.

183. Keller A, Linko V. Challenges and perspectives of DNA nanostructures in biomedicine. Angewandte Chemie International Edition. 2020;59(37):15818-33.

184. Kwon PS, Ren S, Kwon S-J, Kizer ME, Kuo L, Xie M, et al. Designer DNA architecture offers precise and multivalent spatial pattern-recognition for viral sensing and inhibition. Nature chemistry. 2020;12(1):26-35.

185. Sigl C, Willner EM, Engelen W, Kretzmann JA, Sachenbacher K, Liedl A, et al. Programmable icosahedral shell system for virus trapping. Nature Materials. 2021:1-9.

186. Veneziano R, Moyer TJ, Stone MB, Wamhoff E-C, Read BJ, Mukherjee S, et al. Role of nanoscale antigen organization on B-cell activation probed using DNA origami. Nature nanotechnology. 2020;15(8):716-23.

187. Chauhan N, Xiong Y, Ren S, Dwivedy A, Magazine N, Zhou L, et al. Net-shaped DNA nanostructure designed for rapid/sensitive detection and potential inhibition of SARS-CoV-2 virus (preprint). 2022.

188. Dijkstra JM, Visser N, Mettenleiter TC, Klupp BG. Identification and characterization of pseudorabies virus glycoprotein gM as a nonessential virion component. Journal of Virology. 1996;70(8):5684-8.

189. Brack AR, Dijkstra JM, Granzow H, Klupp BG, Mettenleiter TC. Inhibition of virion maturation by simultaneous deletion of glycoproteins E, I, and M of pseudorabies virus. Journal of virology. 1999;73(7):5364-72.

190. Browne H, Bell S, Minson T. Analysis of the requirement for glycoprotein m in herpes simplex virus type 1 morphogenesis. Journal of virology. 2004;78(2):1039-41.

191. Jöns A, Dijkstra JM, Mettenleiter TC. Glycoproteins M and N of pseudorabies virus form a disulfide-linked complex. Journal of virology. 1998;72(1):550-7.

192. Hogue IB, Bosse JB, Hu J-R, Thiberge SY, Enquist LW. Cellular mechanisms of alpha herpesvirus egress: live cell fluorescence microscopy of pseudorabies virus exocytosis. PLoS pathogens. 2014;10(12):e1004535.

193. Crump CM, Bruun B, Bell S, Pomeranz LE, Minson T, Browne HM. Alphaherpesvirus glycoprotein M causes the relocalization of plasma membrane proteins. Journal of General Virology. 2004;85(12):3517-27.

194. Dijkstra JM, Gerdts V, Klupp BG, Mettenleiter TC. Deletion of glycoprotein gM of pseudorabies virus results in attenuation for the natural host. Journal of General Virology. 1997;78(9):2147-51.

195. Nixdorf R, Klupp BG, Mettenleiter TC. Role of the cytoplasmic tails of pseudorabies virus glycoproteins B, E and M in intracellular localization and virion incorporation. Journal of General Virology. 2001;82(1):215-26.

196. Sommese R, Hariadi R, Kim K, Liu M, Tyska M, Sivaramakrishnan S. Patterning protein complexes on DNA nanostructures using a GFP nanobody. Protein Science. 2016;25(11):2089-94.

197. Kubala MH, Kovtun O, Alexandrov K, Collins BM. Structural and thermodynamic analysis of the GFP: GFP-nanobody complex. Protein Science. 2010;19(12):2389-401.

198. Kirchhofer A, Helma J, Schmidthals K, Frauer C, Cui S, Karcher A, et al. Modulation of protein properties in living cells using nanobodies. Nature structural & molecular biology. 2010;17(1):133-8.

199. Rothbauer U, Zolghadr K, Tillib S, Nowak D, Schermelleh L, Gahl A, et al. Targeting and tracing antigens in live cells with fluorescent nanobodies. Nature methods. 2006;3(11):887-9.

200. Seitz KJ, Rizzoli SO. GFP nanobodies reveal recently-exocytosed pHluorin molecules. Scientific reports. 2019;9(1):1-10.

201. Sehnal D, Bittrich S, Deshpande M, Svobodová R, Berka K, Bazgier V, et al. Mol* Viewer: modern web app for 3D visualization and analysis of large biomolecular structures. Nucleic Acids Research. 2021;49(W1):W431-W7.

202. Seeman NC. Nanomaterials based on DNA. Annual review of biochemistry. 2010;79:65.

203. Hahn J, Wickham SF, Shih WM, Perrault SD. Addressing the instability of DNA nanostructures in tissue culture. ACS nano. 2014;8(9):8765-75.

204. Ahmadi Y, De Llano E, Barišić I. (Poly) cation-induced protection of conventional and wireframe DNA origami nanostructures. Nanoscale. 2018;10(16):7494-504.

205. Mei Q, Wei X, Su F, Liu Y, Youngbull C, Johnson R, et al. Stability of DNA origami nanoarrays in cell lysate. Nano letters. 2011;11(4):1477-82.

206. Wang P, Rahman MA, Zhao Z, Weiss K, Zhang C, Chen Z, et al. Visualization of the cellular uptake and trafficking of DNA origami nanostructures in cancer cells. Journal of the American Chemical Society. 2018;140(7):2478-84.

207. Liang L, Li J, Li Q, Huang Q, Shi J, Yan H, et al. Single-particle tracking and modulation of cell entry pathways of a tetrahedral DNA nanostructure in live cells. Angewandte Chemie International Edition. 2014;53(30):7745-50.

208. Lee H, Lytton-Jean AK, Chen Y, Love KT, Park AI, Karagiannis ED, et al. Molecularly self-assembled nucleic acid nanoparticles for targeted in vivo siRNA delivery. Nature nanotechnology. 2012;7(6):389-93.

209. Perrault SD, Shih WM. Virus-inspired membrane encapsulation of DNA nanostructures to achieve in vivo stability. ACS nano. 2014;8(5):5132-40.

210. Bhatia D, Surana S, Chakraborty S, Koushika S, Krishnan Y. A Synthetic Icosahedral DNA-Based Host-Cargo Complex for Functional. Vivo; 2011.

211. Vonnemann J, Sieben C, Wolff C, Ludwig K, Böttcher C, Herrmann A, et al. Virus inhibition induced by polyvalent nanoparticles of different sizes. Nanoscale. 2014;6(4):2353-60.

212. Papp I, Sieben C, Sisson AL, Kostka J, Böttcher C, Ludwig K, et al. Inhibition of influenza virus activity by multivalent glycoarchitectures with matched sizes. ChemBioChem. 2011;12(6):887-95.

213. Zhang F, Jiang S, Wu S, Li Y, Mao C, Liu Y, et al. Complex wireframe DNA origami nanostructures with multi-arm junction vertices. Nature nanotechnology. 2015;10(9):779-84.

214. Katzung B, Masters S, Trevor A. Basic and clinical pharmacology. 12. New York: Companies. Inc; 2012.

215. Zeng Y, Liu J, Yang S, Liu W, Xu L, Wang R. Time-lapse live cell imaging to monitor doxorubicin release from DNA origami nanostructures. Journal of Materials Chemistry B. 2018;6(11):1605-12.

216. Li X, Yang F, Hu X, Tan F, Qi J, Peng R, et al. Two classes of protective antibodies against Pseudorabies virus variant glycoprotein B: Implications for vaccine design. PLoS pathogens. 2017;13(12):e1006777.

217. Pattnaik P, Babu JP, Verma SK, Tak V, Rao PL. Bacterially expressed and refolded envelope protein (domain III) of dengue virus type-4 binds heparan sulfate. Journal of Chromatography B. 2007;846(1-2):184-94.

218. Kaufmann B, Rossmann MG. Molecular mechanisms involved in the early steps of flavivirus cell entry. Microbes and infection. 2011;13(1):1-9.

219. Lauster D, Glanz M, Bardua M, Ludwig K, Hellmund M, Hoffmann U, et al. Multivalent Peptide-Nanoparticle Conjugates for Influenza-Virus Inhibition. Angewandte Chemie International Edition. 2017;56(21):5931-6.

220. Papp I, Sieben C, Ludwig K, Roskamp M, Böttcher C, Schlecht S, et al. Inhibition of influenza virus infection by multivalent sialic-acid-functionalized gold nanoparticles. Small. 2010;6(24):2900-6.

221. Ogata M, Umemura S, Sugiyama N, Kuwano N, Koizumi A, Sawada T, et al. Synthesis of multivalent sialyllactosamine-carrying glyco-nanoparticles with high affinity to the human influenza virus hemagglutinin. Carbohydrate polymers. 2016;153:96-104.

222. Pomeranz LE, Reynolds AE, Hengartner CJ. Molecular biology of pseudorabies virus: impact on neurovirology and veterinary medicine. Microbiology and molecular biology reviews. 2005;69(3):462-500.

223. Beilstein F, Cohen GH, Eisenberg RJ, Nicolas V, Esclatine A, Pasdeloup D. Dynamic organization of Herpesvirus glycoproteins on the viral envelope revealed by super-resolution microscopy. PLoS pathogens. 2019;15(12):e1008209.

224. Raniolo S, Croce S, Thomsen RP, Okholm AH, Unida V, Iacovelli F, et al. Cellular uptake of covalent and non-covalent DNA nanostructures with different sizes and geometries. Nanoscale. 2019;11(22):10808-18.

225. Bastings MM, Anastassacos FM, Ponnuswamy N, Leifer FG, Cuneo G, Lin C, et al. Modulation of the cellular uptake of DNA origami through control over mass and shape. Nano letters. 2018;18(6):3557-64.

226. Zhang J, Xu Y, Huang Y, Sun M, Liu S, Wan S, et al. Spatially patterned neutralizing icosahedral DNA nanocage for efficient SARS-CoV-2 blocking. Journal of the American Chemical Society. 2022.

227. Lacroix AI, Vengut-Climent E, de Rochambeau D, Sleiman HF. Uptake and fate of fluorescently labeled DNA nanostructures in cellular environments: a cautionary tale. ACS central science. 2019;5(5):882-91.

228. Imberty A, Varrot A. Microbial recognition of human cell surface glycoconjugates. Current opinion in structural biology. 2008;18(5):567-76.

229. Karlsson K-A. Pathogen-host protein-carbohydrate interactions as the basis of important infections. The Molecular Immunology of Complex Carbohydrates—2. 2001:431-43.

230. Reuter JD, Myc A, Hayes MM, Gan Z, Roy R, Qin D, et al. Inhibition of viral adhesion and infection by sialic-acid-conjugated dendritic polymers. Bioconjugate chemistry. 1999;10(2):271-8.

231. Kwon S-J, Na DH, Kwak JH, Douaisi M, Zhang F, Park EJ, et al. Nanostructured glycan architecture is important in the inhibition of influenza A virus infection. Nature nanotechnology. 2017;12(1):48-54.

232. Lauster D, Glanz M, Bardua M, Ludwig K, Hellmund M, Hoffmann U, et al. Multivalent peptide-Nanoparticle conjugates for influenza-virus inhibition. Angewandte Chemie International Edition. 2017;56(21):5931-6.

233. Waldmann M, Jirmann R, Hoelscher K, Wienke M, Niemeyer FC, Rehders D, et al. A nanomolar multivalent ligand as entry inhibitor of the hemagglutinin of avian influenza. Journal of the American Chemical Society. 2014;136(2):783-8.

234. Bandlow V, Liese S, Lauster D, Ludwig K, Netz RR, Herrmann A, et al. Spatial screening of hemagglutinin on influenza A virus particles: sialyl-LacNAc displays on DNA and PEG scaffolds reveal the requirements for bivalency enhanced interactions with weak monovalent binders. Journal of the American Chemical Society. 2017;139(45):16389-97.

235. Gambaryan A, Tuzikov A, Chinarev A, Juneja L, Bovin N, Matrosovich M. Polymeric inhibitor of influenza virus attachment protects mice from experimental influenza infection. Antiviral research. 2002;55(1):201-5.

236. Albertazzi L, Gherardini L, Brondi M, Sulis Sato S, Bifone A, Pizzorusso T, et al. In vivo distribution and toxicity of PAMAM dendrimers in the central nervous system depend on their surface chemistry. Molecular pharmaceutics. 2013;10(1):249-60.

237. Haag R. Multivalency as a chemical organization and action principle. Beilstein-Institut; 2015. p. 848-9.

238. Bhatia S, Camacho LC, Haag R. Pathogen inhibition by multivalent ligand architectures. Journal of the American Chemical Society. 2016;138(28):8654-66.

239. Gestwicki JE, Cairo CW, Strong LE, Oetjen KA, Kiessling LL. Influencing receptor− ligand binding mechanisms with multivalent ligand architecture. Journal of the American Chemical Society. 2002;124(50):14922-33.

240. Vonnemann J, Sieben C, Wolff C, Ludwig K, Böttcher C, Herrmann A, et al. Virus inhibition induced by polyvalent nanoparticles of different sizes. Nanoscale. 2014;6(4):2353-60.

241. Papp I, Sieben C, Sisson AL, Kostka J, Böttcher C, Ludwig K, et al. Inhibition of influenza virus activity by multivalent glycoarchitectures with matched sizes. ChemBioChem. 2011;12(6):887-95.

242. Vonnemann J, Liese S, Kuehne C, Ludwig K, Dernedde J, Böttcher C, et al. Size dependence of steric shielding and multivalency effects for globular binding inhibitors. Journal of the American Chemical Society. 2015;137(7):2572-9.

243. Illescas BM, Rojo J, Delgado R, Martín N. Multivalent glycosylated nanostructures to inhibit Ebola virus infection. Journal of the American Chemical Society. 2017;139(17):6018-25.

244. Kwon PS, Ren S, Kwon S-J, Kizer ME, Kuo L, Xie M, et al. Designer DNA architecture offers precise and multivalent spatial pattern-recognition for viral sensing and inhibition. Nature chemistry. 2020;12(1):26-35.

245. Lauster D, Klenk S, Ludwig K, Nojoumi S, Behren S, Adam L, et al. Phage capsid nanoparticles with defined ligand arrangement block influenza virus entry. Nature nanotechnology. 2020;15(5):373-9.

246. Branson TR, McAllister TE, Garcia-Hartjes J, Fascione MA, Ross JF, Warriner SL, et al. A protein-based pentavalent inhibitor of the cholera toxin B-subunit. Angewandte Chemie. 2014;126(32):8463-7.

247. Zhang Z, Merritt EA, Ahn M, Roach C, Hou Z, Verlinde CL, et al. Solution and crystallographic studies of branched multivalent ligands that inhibit the receptor-binding of cholera toxin. Journal of the American Chemical Society. 2002;124(44):12991-8.

248. Branson TR, Turnbull WB. Bacterial toxin inhibitors based on multivalent scaffolds. Chemical Society Reviews. 2013;42(11):4613-22.

249. Kitov PI, Bundle DR. On the nature of the multivalency effect: a thermodynamic model. Journal of the American Chemical Society. 2003;125(52):16271-84.

250. Zhang F, Jiang S, Wu S, Li Y, Mao C, Liu Y, et al. Complex wireframe DNA origami nanostructures with multi-arm junction vertices. Nature nanotechnology. 2015;10(9):779-84.

251. Pradhan S, Varsani A, Leff C, Swanson CJ, Hariadi RF. Viral Aggregation: The Knowns and Unknowns. Viruses. 2022;14(2):438.

252. Shui B, Ozer A, Zipfel W, Sahu N, Singh A, Lis JT, et al. RNA aptamers that functionally interact with green fluorescent protein and its derivatives. Nucleic acids research. 2012;40(5):e39-e.

253. Dietz H, Douglas SM, Shih WM. Folding DNA into twisted and curved nanoscale shapes. Science. 2009;325(5941):725-30.

254. Barbagallo M, Dominguez LJ. Magnesium metabolism in type 2 diabetes mellitus, metabolic syndrome and insulin resistance. Archives of biochemistry and biophysics. 2007;458(1):40-7.

255. Yang SJ, Hwang SY, Baik SH, Lee KW, Nam MS, Park YS, et al. Serum magnesium level is associated with type 2 diabetes in women with a history of gestational diabetes mellitus: the Korea National Diabetes Program study. Journal of Korean medical science. 2014;29(1):84-9.

256. Hahn J, Wickham SF, Shih WM, Perrault SD. Addressing the instability of DNA nanostructures in tissue culture. ACS nano. 2014;8(9):8765-75.

257. Mammen M, Choi SK, Whitesides GM. Polyvalent interactions in biological systems: implications for design and use of multivalent ligands and inhibitors. Angewandte Chemie International Edition. 1998;37(20):2754-94.

258. Tang S, Puryear WB, Seifried BM, Dong X, Runstadler JA, Ribbeck K, et al. Antiviral agents from multivalent presentation of sialyl oligosaccharides on brush polymers. ACS Macro Letters. 2016;5(3):413-8.

259. Bertozzi CR, Kiessling aLL. Chemical glycobiology. Science. 2001;291(5512):2357-64.

260. Bhatia S, Dimde M, Haag R. Multivalent glycoconjugates as vaccines and potential drug candidates. MedChemComm. 2014;5(7):862-78.

261. Miller JL, Weed DJ, Lee BH, Pritchard SM, Nicola AV. Low-pH endocytic entry of the porcine alphaherpesvirus pseudorabies virus. Journal of virology. 2019;93(2):e01849-18.

262. Pomeranz LE, Reynolds AE, Hengartner CJ. Molecular biology of pseudorabies virus: impact on neurovirology and veterinary medicine. Microbiology and molecular biology reviews. 2005;69(3):462-500.

APPENDIX A

MATERIALS AND METHODS FOR CHAPTERS 2 AND 3

1. Chemicals and kits

Tris-acetate EDTA (TAE) buffer, magnesium chloride hexahydrate ($MgCl_2.6H_2O$), methylene blue, pluronic-F127, casein, dimethyl formamide (DMF), agarose and polyethylene glycol 8000 (PEG8000), triethylammonium acetate (TEAA) were purchased from Sigma Aldrich, Inc. Cell culture consumables were purchased from Corning, Inc. µ-slide 8-well plates for confocal imaging were purchased from Ibidi, Inc. DNA ladders, SYBR gold dye, anti-His HRP, streptavidin-HRP, and TMB substrate was purchased from Thermo Fisher Scientific, Inc. All ELISA reagents (except for TMB) were purchased from Bethyl Laboratories, Inc. The BG-GLA-NHS (#S9151S), Monarch PCR and DNA Cleanup kit (#T1030S), and HiScribe T7 Quick High Yield RNA Synthesis kit (#E2050S) were purchased from New England Biolabs, Inc. The CytoTox 96 non-radioactive cytotoxicity assay kit (#G1780) was purchased from Promega, Inc.

2. Oligonucleotides and DNA templates

A total of 16 DNA origami nanostructures (9 conjugated with nbGFP, 6 conjugated with GFP aptamers, and 1 without handles) were designed using Tiamat. All DNA staple strands used for assembling scaffolded snub cube (SC) DNA origami nanostructures and modified DNA oligonucleotides for docking virus binders onto the SC scaffold were purchased in 96-well plates from Integrated DNA Technologies (www.IDTDNA.com) at 100 nmol synthesis scale with concentrations normalized to 500 µM. The M13mp18 single-stranded DNA scaffold was produced in-house using a previously published protocol(Douglas et al. 2007; Bellot et al. 2013).

3. Cell culture and virus propagation

Pig kidney (PK15) cells and the recombinant viruses, PRV 486 and PRV 483, were a kind gift from Dr. Ian Hogue's lab at the Biodesign Center for Immunotherapy, Vaccines and Vaccination (CIVV), Arizona State University.

Cells were maintained in full medium comprising Dulbecco's modified Eagle's medium (DMEM) supplemented with 10% fetal bovine serum (FBS), 4 mM L-glutamine, 100 U/mL penicillin, and 100 µg/mL streptomycin in a humidified 37 °C, 5% CO_2 incubator.

The viruses were propagated in PK15 cells based on the detailed protocol in this work (Card and Enquist 2014). In brief, PK15 cells were grown in full medium to 90% confluency in a sterile 10 cm cell culture dish. After removing the media and washing the cells once with 1X PBS, they were infected with PRV at a multiplicity of infection (MOI) of 0.01 in a final volume of 1 mL. The cells were incubated to allow virus adsorption for 1 h in a humidified 37 °C, 5% CO_2 incubator. After 1 h, the infection inoculum was removed and replaced with 10 mL of fresh virus medium (DMEM supplemented with 2% FBS, 4 mM L-glutamine, 100 U/mL penicillin, and 100 µg/mL streptomycin). The cells were incubated further until 80-90% cytopathic effects were observed, at which point the cells and supernatant were harvested. The mixture was centrifuged at 2000xg for 5 min to remove the cell debris, and the virus supernatant was divided into 100-200 uL aliquots and stored at -80 °C until further use.

4. Plaque assay

PK15 cells were seeded a day before in 6-well plates at a density of 4 x 10^5 cells per well. The cells reached 90-95% confluency at this seeding density the next day.

For determining the infectious virus concentration, serial dilution plaque assays were performed based on the descriptive protocol in this work (Card and Enquist 2014). Virus stock stored at -80 °C was thawed in a 37 °C water bath and sonicated in a cup sonicator (10 pulses, one second on and one second off for a total of 20 sec at an amplitude of 80%). A series of 10-fold serial dilutions of the virus stock was made. Cells were washed once with 1X PBS before infecting individual wells with 10^{-5}, $10^{-6,}$ and 10^{-7} dilutions in a final 200 µL volume. After infection, the cells were incubated to allow virus adsorption for 1 h in a humidified 37 °C, 5% CO_2 incubator. The unbound virus was removed and replaced with 3 mL of methocel overlay medium (virus medium supplemented with 2% methylcellulose). After 3 days of incubation, the plaques were stained with a 70% methylene blue solution and incubated at room temperature (RT) for up to 24 h. The staining solution was removed, and plaques were counted at each dilution. To determine the infectious virus titer (PFU/mL), the total plaque count was divided by the total volume plated, based on the lowest

dilution giving a countable number of plaques, and multiplied by the reciprocal of the corresponding dilution factor.

For the plaque reduction assay, approximately 100-200 plaque-forming units (PFU) of the PRV 486 were mixed with different concentrations of SCnbGFP in a final 200 µL. For dilution of the virus and SCnbGFP, fresh DMEM (without supplements) was used. The mixtures were incubated at 37 °C for 1 h. Before infection, the spent media from 6-well plates was removed, and the cells were washed once with 1X PBS. The virus mixtures were added to the individual wells, and the cells were incubated to allow virus adsorption for 1 h in a humidified 37 °C, 5% CO_2 incubator. After 1 hr, the inoculated mixtures were removed and replaced with a 3 mL methocel overlay medium. After 3 days of incubation, plaque staining and counting were performed as described above. The residual infectivity (%) was calculated using the control group with just the virus as the reference. Nonlinear regression for dose-response: inhibition was used to curve fit the data and analyze the half-maximal inhibitory concentration dosage (IC_{50}).

5. ONI-based detection of interactions between viruses and nbGFP

Corning glass coverslips of two different sizes were used to make flow cells for this experiment. The coverslips were cleaned in multiple steps. First, they were sonicated in 100% ethanol for 10 min, then extensively washed with MiliQ water and sonicated in acetone for 30 min. Next, the coverslips were incubated in 100% ethanol for 10 min at room temperature (RT), rinsed with MiliQ water, and then incubated in 2% Hellmanex III solution for 2 h at RT. Finally, the coverslips were washed with MiliQ water, dried with nitrogen gas, and filtered airflow and plasma cleaned for 10 min (Harrick Plasma; PDC-32G). Immediately after plasma cleaning, flow cells were made by sandwiching double-sided Kapton tape between a larger and a smaller coverslip. The Kapton tape was cut to include two channels for replicate testing.

For binding experiments, all the wash steps were performed with 200 µL of PBS. 10 µL of 5 µM nbGFP was flowed into the flow cells and incubated for 10 min in a humidity chamber. After washing excess nbGFP, 1 mg/mL casein was flowed into the flow cells to block unspecific binding and incubated for 10 min. Excess casein was washed, and 10 µL of 100 pM PRV 486 was added

to the flow cells. As a positive control for the virus, 100 nM EGFP was used. The virus was incubated for 10 minutes before washing the unbound viruses with PBS. The flow cells were sealed with a coverslip sealant and incubated in a humidity chamber before and in between imaging. The bound viruses were imaged using the Oxford Nanoimager microscope (ONI) with a 473 nm laser at 2% intensity, or < 20 mW, a TIRF angle of 55°, and an exposure of 100 ms.

6. GFP aptamer synthesis

DNA templates for the aptamer transcription were purchased from IDT and hybridized after mixing the sense and anti-sense strands in a 1:1 ratio in 100 mM Potassium Acetate, 30 mM HEPES, pH 7.5 at a final duplex concentration of 100 mM. The double-stranded template was prepared by heating the mixture to 94 °C for 2 min followed by cooling to 5 °C at a rate of 1 °C/min. The DNA was amplified using standard PCR and purified using the Monarch PCR & DNA Cleanup Kit. The transcription reactions were prepared using the Hiscribe T7 Quick High Yield RNA Synthesis kit (NEB) using the protocol for short transcripts. The duplex template was included at a final concentration of 2 mM, and the reaction mix was incubated for 16 h at 37 °C. After incubation, the mixture was treated with DNase I and incubated at 37°C for 30 min. 3.5 volumes of 100% ethanol and ⅛ volume of 3 M sodium acetate were added per volume of unpurified aptamer before incubation for 2 h at -80°C. The mix was centrifuged at 13000 x g for 20 min at 4°C before two wash steps with 70% ethanol. After each wash step, the mix was centrifuged at 13000 xg for 10 min at 4°C. The pellet was then resuspended in water resulting in purified GFP aptamers for future experimentation.

7. Assembly of snub cube with virus binders

   a. Assembly of snub cube-nanobody GFP nanostructures (SC-nbGFP_

The DNA SC used for conjugation to nbGFP were self-assembled in a one-pot reaction in which a 100 nM M13 scaffold was mixed with a 10-fold molar excess of common staple strands, a 10-fold molar excess of the handles corresponding to the valency of the SC, a 10-fold molar excess of the handles which block the remaining spots corresponding to the valency of the SC, and 1 mM

TAE + 12.5 mM $MgCl_2$. A final reaction volume of 100 µL was annealed in a thermocycler with the following program: 95 ºC for 5 mins; 90 ºC to 86 ºC at a rate of 4 ºC per 5 minutes; 85 ºC to 70 ºC at a rate of 1 ºC per 5 minutes; 70 ºC to 40 ºC at a rate of 1 ºC per 15 minutes; 40 ºC to 25 ºC at 1 ºC per 10 minutes; and hold at 4 ºC at the end of the cycle.

Following annealing, the SC nanostructures were purified from excess staple strands using 100 kDa Amicon spin-column filtration. Columns were passivated for 2 mins with 500 µL of 10% Pluronic-F127 in 1x TAE + 12.5 mM $MgCl_2$ and centrifuged at 16000 xg for 10 mins. The columns were washed with 500 µL of 1x TAE + 12.5 mM $MgCl_2$ prior to addition of the samples and additional 1x TAE + 12.5 mM $MgCl_2$ up to 500 µL. The columns were spun at 1000 x g for 15 minutes before replenishing the 1x TAE + 12.5 mM $MgCl_2$ to 500 µL.

The purified SC scaffolds were mixed with a 10-fold molar excess of BG-conjugated complementary DNA strands and incubated for 90 mins at 37°C. Following annealing, another 2 rounds of 100 kDa Amicon spin-column filtration with passivation were performed following the same procedure described above. Finally, the SC-BG-DNA was mixed with nbGFP at a 5x molar excess of the SC valency in a solution of 1X PBS + 12.5 mM $MgCl_2$ + 1 mM DTT and incubated overnight at 4°C with gentle rotation. A final set of 5 rounds of 100 kDa Amicon spin-column filtration with passivation was performed with 1X PBS + 12.5 mM $MgCl_2$ used as the wash buffer in place of 1X TAE + 12.5 mM $MgCl_2$ and all steps were performed at 4°C to preserve the stability of the assembled SC-nbGFP. Gel electrophoresis was performed following each purification step to confirm the assembly of the DNA origami nanostructures.

b. Assembly of snub cube-GFP aptamers with and without flexible spacer (SC-aptGFP and SC-flex-aptGFP)

The assembly of SC-aptGFP and SC-flex-aptGFP was accomplished in a one-step reaction using the one-pot reaction mix for SC synthesis (described above) complemented with aptamer strands at a 10-fold molar excess of the SC valency. The purification protocol was the same as described above for SC purification.

8. Agarose gel electrophoresis

DNA nanostructures were analyzed by agarose gel electrophoresis to assure purity and confirm conjugation. Samples were loaded into a 1% agarose gel according to the following mixture: 1 µL sample, 3 µL MilliQ H_2O, 1 µL 6X loading dye, and 1 µL 6X SYBR GOLD dye. Along with a 1kb plus DNA ladder, the samples were run in a buffer of 1X TAE + 12.5 mM $MgCl_2$ for 1 hr at 100 V. Gels were imaged with a Bio-Rad Molecular Imager Gel Doc XR System transilluminator at the SYBR GOLD excitation wavelength (495 nm).

9. Synthesis of benzylguanine conjugated DNA oligonucleotides

3'-amine modified (3AmMO) single-stranded DNA oligonucleotides complementary to the SC overhang handles were ordered from IDT and diluted in 0.1 M HEPES pH 8.5 to a final concentration of 1 mM. N-hydroxysuccinimide ester-functionalized benzyl guanine (BG-GLA-NHS) from NEB was freshly reconstituted in DMF to a 50 mM final concentration. For conjugation, the two solutions were mixed in a molar ratio of oligonucleotide-amine: BG-GLA-NHS = 1:10. The final concentration of HEPES was maintained between 50 mM and 100 mM. The reaction was incubated at 4 °C for 16 h with continuous rotation. After incubation, the reaction was desalted using the Biorad micro spin columns and further purified using reverse-phase HPLC to remove unconjugated DNA-amine. 100 mM TEAA and 100% methanol were used as the HPLC buffers. The HPLC purified fractions were lyophilized and reconstituted in water. The concentration of BG-conjugated DNA was determined using a NanoDrop spectrophotometer.

10. Purification of BG-conjugated DNA using reverse phase HPLC

BG-conjugated DNA strands were purified from unreacted DNA using a C-18 column on an Agilent 1220 Infinity LC-HPLC system. Sample DNA mixtures were injected into the column in 50-100 ul volume. The purification was performed using a linear gradient method, with Buffer-A (100 mM TEAA) and Buffer-B (100% methanol). The gradient was run from 10% to 100% of Buffer-B over 40 mins. Migration of the DNA and DNA conjugates were monitored using absorbance at 260 nm. Purified volumes of DNA conjugates were collected and further confirmed for their purity

and identity using MALDI-TOF mass spectrometry. The purified DNA conjugates were lyophilized and stored at -20 °C until further use.

11. Mass characterization of BG-DNA conjugates using MALDI-TOF mass spectrometry

All purified products were characterized on an AB SCIEX 4800 MALDI TOF/TOF in the positive ion mode, with 3-Hydropicolinic acid (HPA) as the matrix. Samples were spotted onto a MALDI plate using a sandwich technique (sample-matrix-sample).

12. nbGFP synthesis

The nbGFP protein was expressed from the recombinant plasmid, pBiEX1-nbGFP, which was a kind gift from Dr. Sivaraj Sivaramakrishnan (University of Minnesota, Twin Cities, USA). The SNAP-tagged protein construct contained, from the N- to C-terminus: the GFP nanobody (nbGFP), the SNAP-tag for oligo labeling, and both FLAG and 6xHis tags for purification.

The plasmid was transformed into BL21 (DE3) competent *E. coli* (New England Biolabs), and a single colony of transformed cells was picked from LB-agar plates and used to inoculate a 50 mL culture in LB broth containing carbenicillin (100 µg/mL) antibiotics. This culture was grown for 16 h at 37 °C, and 250 rpm, at which point it was used to inoculate a 500 mL culture in LB supplemented with carbenicillin at the above concentration. The optical density of the culture was monitored until an OD_{600} of 0.6-0.8 was reached. It was followed by gene induction using 0.5 mM IPTG for 16 h at 220 rpm and 18 °C. Cells were harvested via centrifugation at 3000 xg for 15 min at 4 °C. The supernatant was discarded, and the pellet was resuspended in 50 mL of lysis buffer (100 mM NaCl, 25 mM Tris at pH 8.0, 5 mM EDTA, 1% Triton-X, 1 mM DTT, and 1X cOmplete protease inhibitor (Roche)) for 1 h at -80 °C. After thawing the lysate in RT, it was treated with hen egg white lysozyme (HEWL; Sigma-Aldrich) and DNase I (Sigma-Aldrich), each at a concentration of 1 mg/mL, for 30 min at 37 °C. The mixture was transferred to an ice bath and sonicated for 10 min (1 s on, 2 s off, 50% amplitude). The lysate was centrifuged at 20000 xg for 30 min at RT to separate cell debris from the periplasmic fraction.

The supernatant containing the nbGFP was loaded directly onto the HisTrap FF (Cytiva) 5 mL column equilibrated with Nickel Wash Buffer containing 25 mM Tris at pH 7.6, 500 mM NaCl, and 10 mM imidazole. To remove nonspecifically bound proteins, the resin was washed with 15 CV of the wash buffer, and the bound proteins were subsequently eluted with an elution buffer containing 25 mM Tris at pH 7.6, 150 mM NaCl, and 500 mM imidazole. The eluted fractions were run on a 15% SDS-PAGE gel to confirm protein expression. The fractions mainly containing pure proteins with 35 kDa bands were pooled together and buffer exchanged using a 3.5 kDa MWCO centrifugal filter unit (Amicon) into an anion exchange buffer containing 20 mM Tris at pH 8.0, 10 mM NaCl. The protein solution was then injected into a HiTrap Q FF anion exchange 5 mL column (Cytiva), equilibrated with the anion exchange buffer, and finally eluted using a buffer containing 20 mM Tris at pH 8.0 and 500 mM NaCl. Nanobody constructs were buffer exchanged into PBS using a 3.5k MWCO centrifugal filter unit and divided into aliquots that were flash frozen in liquid nitrogen and kept at -80 °C until further use.

13. ELISA assay

96-well Nunc maxisorp flat bottom ELISA plates were coated with 100 µL of PRV 486 at $1x10^9$ particles/mL, diluted in ELISA coating buffer, and incubated overnight at 4 °C. All the wash steps were performed thrice with 200 µL of 1X Tris Buffered Saline + 0.05% Tween20 (TBST), each wash lasting 5 min. Wells without virus coating and with EGFP coating were used as negative controls and positive controls, respectively. After incubation, the plates were washed and blocked with 200 µL of 1mg/mL casein in TBST for 2 h at room temperature (RT). Plates were washed, after which 100 µL of nbGFP or nbGFP conjugates or GFP aptamers were added in different concentrations after dilution in TBST + 0.1% BSA and incubated for 1 h at RT. Rabbit anti-pHluorin antibodies were used as positive controls for nbGFP and GFP aptamers. Plates were washed, and 100 µL of 1:10000 dilution of anti-His Horseradish peroxidase (HRP) for nbGFP, 100 µL of 1:10000 dilution of anti-rabbit HRP for anti-GFP antibodies, and 100 µL of 1:10000 dilution of streptavidin-HRP for GFP aptamers were added and incubated for 1 h at RT. Plates were washed, and 100 µL of 3,3',5,5'-tetramethylbenzidine (TMB) substrate was added and incubated in the dark for 2-3

minutes at RT. The reaction was quenched with 100 µL of 0.15 M H_2SO_4, and absorbance was read immediately at 450 nm using a microplate reader (Spectra MAX 190, Molecular Devices, Inc.).

14. Flow cytometry-based neutralization assay

PK15 cells were seeded a day before in 24-well cell culture plates at a density of 75000 cells per well. The cells reached 70-80% confluency at this seeding density the next day. Approximately 15000 PFU of PRV 486 were incubated with different concentrations of SCnbGFP in a final volume of 100 µL for 1 h at 37 °C. Fresh DMEM was used to dilute stocks of SCnbGFP constructs and to make up the final reaction volume. Before infection, the media from 24-well plates was removed, and the cells were washed once with 1X PBS. The virus mixtures were added to the individual wells, and the cells were incubated to allow virus adsorption for 1 hr in a humidified 37 °C, 5% CO_2 incubator. After 1 hr, 400 µL of virus medium was added to the wells to make up the final volume of 500 µL per well. After 48 h, cells were harvested for flow cytometry.

After 48 h, cell supernatant was removed from the wells, and the cells were washed once with PBS. Then the cells were fixed with 100 µL of 4% paraformaldehyde (PFA) for 20 min at RT with gentle shaking. Cells were washed and dissociated with 100 µL of 0.15% trypsin for 5 min at RT with gentle shaking. The trypsin was inactivated by adding 200 µL of PBS + 2% FBS. Plates were centrifuged at 300 g for 5 min. The supernatant was discarded, and the cell pellets were reconstituted in 200 µL of PBS + 2% FBS and transferred to individual wells in 96-well flow cytometry round bottom plates. Samples were acquired and analyzed using an Attune NxT Flow Cytometer and software (Thermo Fisher), respectively. In total, 30,000 single cell events, gated on side scatter area versus height, were recorded for analysis. EGFP was excited with a 488-nm laser, and emission was measured with a 530/30-nm bandpass filter. Untreated cells were used as negative controls, and cells treated only with PRV 486 were used as positive controls. The residual infectivity (%) was calculated using the control group with just the virus as the reference. Nonlinear regression for dose-response: inhibition was used to curve fit the data and analyze the half-maximal inhibitory concentration dosage (IC_{50}).

15. Cytotoxicity assay

Cytotoxicity resulting from treatment with SCnbGFP constructs or individual components was analyzed using the Promega LDH kit. In brief, PK15 cells were seeded in a 96-well cell culture plate a day before at a density of 50000 cells per well. To remove residual LDH activity from the cells, the overnight media was replaced with 100 µL of fresh media. SC60H-nbGFP, SC60H, nbGFP, and M13mp18 constructs were diluted to different concentrations in DMEM and added to the wells at 50 µL per well, for a total of 150 µL per well. Cells were incubated for 24 h in a humidified incubator at 37 °C and 5% CO_2. Untreated cells were used as negative controls. Cells treated with the lysis buffer were used as positive controls and as a reference to calculate the cell viability of other groups. After incubation, the cell supernatant was removed and carefully transferred into individual wells of an optically clear 96-well flat bottom microplate. A 50 µL LDH reaction mixture was added to the wells, and the plate was incubated in the dark for 30 min at RT. To stop the reaction, 50 µL of the stop solution was added to each well, and the absorbance was read within one hour using a microplate reader (Spectra MAX 190, Molecular Devices, Inc.). Cytotoxicity was calculated according to the manufacturer's protocol, and cell viability was calculated as 1 - cytotoxicity.

16. Serum stability assay

The stability of the conjugated snub cube nanostructures was evaluated *in vitro* by incubation at 37°C for periods of 0, 1, 2, and 8 h. 20 µL reactions containing 5 nM of the conjugated snub cube and DMEM supplemented with 0, 2, or 10% FBS were incubated for the respective duration before analysis with agarose gel electrophoresis. 2 µL of the sample were combined with 3 µL of water and 1 µL of 6X loading dye and loaded into a 1% agarose gel prestained with 1X SYBR GOLD. The samples were run for 1 h in a running buffer of 1X TAE + 12.5 mM $MgCl_2$ at 100V for 1 h before visualization with a Bio-Rad Molecular Imager Gel Doc XR System transilluminator at the SYBR GOLD excitation wavelength (495 nm).

17. Particle size distribution analyses

NanoSight assays were performed to characterize the particle size distributions of complexes formed by the interactions between PRV 486 and SC60H-nbGFP. Nanoparticle tracking analysis (NTA) measurements were performed using a NanoSight NS300 instrument (Malvern Panalytical Ltd.), following the manufacturer's instructions. The virus samples with or without SC60H-nbGFP were serially diluted with PBS to reach a particle concentration of 10^7-10^9 particles/mL, suitable for NTA. The samples were injected into the sample unit with 1 mL Luer-Slip sterile syringes (VWR). The capture settings (shutter and gain) and analysis settings were manually set. Each group was run in at least two different sample dilutions, and each sample was analyzed thrice. The video was recorded for 60 s at 30 fps for each measurement and analyzed using Nanoparticle Tracking Analysis (NTA) 2.0 Analytical software.

To roughly estimate the size of SC60H-nbGFP, we performed a dynamic light scattering (DLS) analysis. DLS measurements were acquired on a Zetasizer instrument (Malvern Panalytical Ltd.). The SC60H-nbGFP samples were diluted in buffer containing TAE + 12.5 mM $MgCl_2$ to final concentrations of 50 pM, 500 pM and 5 nM. 1 mL sample volume was loaded into a glass cuvette. Each sample was analyzed twice, and the size distributions of samples with an acceptable polydispersity index (PDI) were considered.

18. Confocal microscopy

For confocal microscopy experiments, PK15 cells were seeded a day before in a μ-slide 8-well plate (Ibidi) at a density of 10000 cells per well. Approximately 1E + 8 PFU of PRV 483 were mixed with 50 nM of SC60H-nbGFP in a final 100 μL volume and incubated at 37 ^{o}C for 1 h. 30 mins before imaging, cells were washed and incubated with Hoechst solution at 1 μM final concentration. The Hoechst solution was removed, and the virus and inhibitor cocktails were added to the cells. Cells were imaged on a Zeiss LSM 880 confocal microscope using three fluorescent wavelengths, 405 (nucleus blue), 488 (virus envelope, green), and 555 (virus capsid, red). Z-stacks consisted of ~10 images per stack, spaced by 0.2 μm, and ~5 fields of view (~20 cells per field of

view) were acquired for each sample. Image analyses were performed using Mathematica and ImageJ software.

19. Statistical analysis

Analyses were performed with GraphPad Prism 9 with measurements taken from distinct samples.

APPENDIX B

SUPPLEMENTARY INFORMATION FOR CHAPTER 2

1. 3D snub cube scaffolded DNA origami

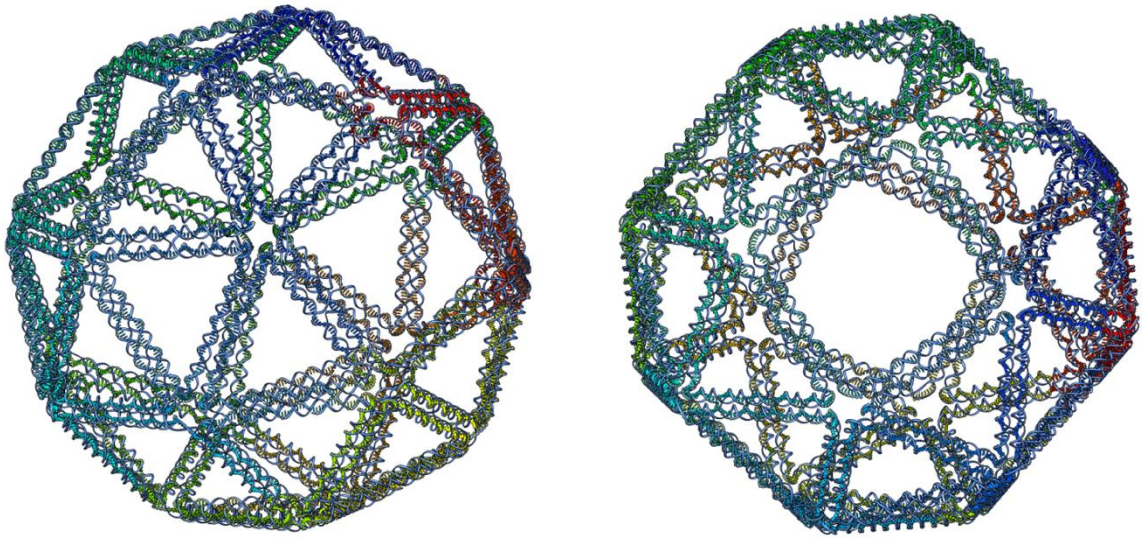

Supplementary Fig. 1| All-atom model of the 3D snub cube scaffolded DNA origami. The all-atom model was generated using DAEDALUS.

2. ONI-based detection of binding between PRV 486 and nbGFP

We first performed a quick imaging-based assay to assess the binding interactions between them visually. In brief, we added PRV 486 to flow cells coated with nbGFP and removed unbound particles after a short incubation. We used casein as the blocking agent to minimize non-specific interactions. We used an anti-GFP antibody (AbGFP) as a positive control for nbGFP and EGFP as a positive control for PRV 486. In the presence of binding between nbGFP and PRV 486, the virus particles would immobilize on the glass slide, which can be visualized under a 473nm laser owing to the pHluorin tags on the viral envelope. We used super-resolution fluorescence microscopy to visualize bound virus particles. The results of the imaging-based binding assay have been summarized in Fig. 1A. The white puncta represent the virus particles bound to nbGFP. We observed the immobilization of virus particles on the glass slide coated with nbGFP, as demonstrated by the distinct white puncta (first square, top row). Similar results were observed with glass slides coated with AbGFP (second square, top row). Without nbGFP and AbGFP, virus binding was negligible (third square, top row).

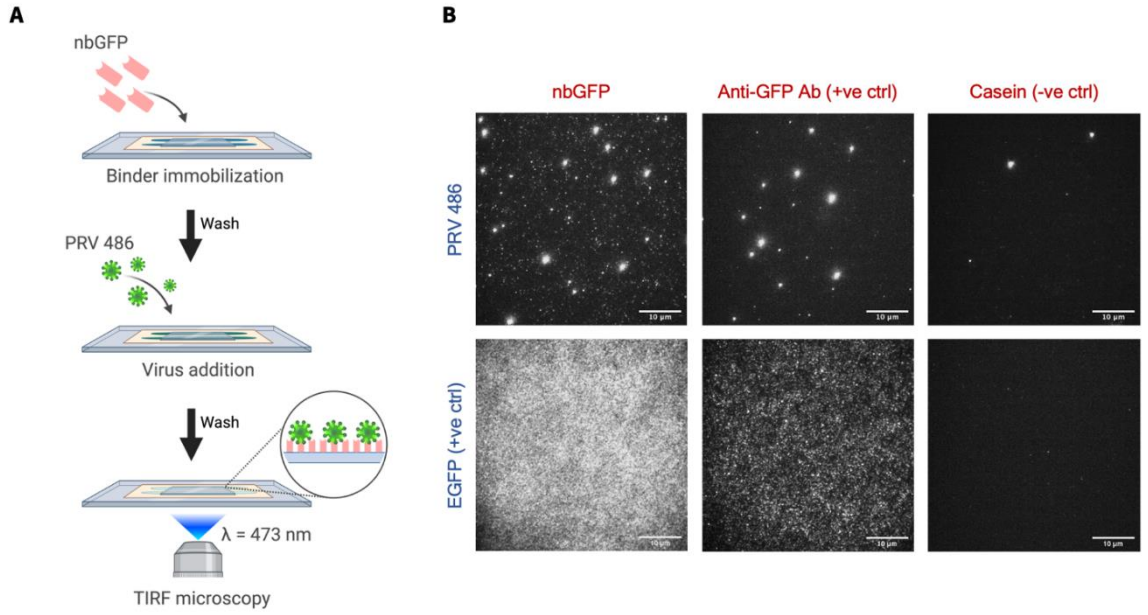

Supplementary Fig. 2| **ONI microscopy showing binding interactions between PRV 486 and nbGFP**. **A,** Schematic workflow of the assay. **B,** Representative ONI microscopy images showing binding between nbGFP and PRV 486. Anti-GFP antibody (AbGFP) used as the positive controls for nbGFP and EGFP is used as positive control for PRV 486. Casein (blocking agent) is used as negative control for nbGFP. Scale bar is 10um.

3. Sequences of the SC60H

Number	**Sequence (5'to 3')**
1--snub--	AGA CTT TTT TTC AAA TAT CGC GGA AGC AAA CTT TTT TCC AAC
2--snub--	AGG TCG AAC CAT CAC CTT TTC AAA TCA AGT TCG GA
3--snub--	ACG TCA TTT TAA GGG CGA AAT GAT AAG AGG TTT TTT CAT TTT TGC GCT GTA

4--(sh)snub_V3--	TTT TTT TTT TTT TTT TTT TTT TCA CTA CGT AGG ATT AGA GAG TAC CTT TAA CAG GGC GAT GGC C
5--snub--	TTG CTC CTT TAA CCG TCT AT
6--snub--	TGA TTC CAT TAG ATA CTT TTT ATT TCG CAA ACT CCA
7--snub--	AGT GTT TTT TGT TCC AGT TTA GTG CCA AGC TTT TTT TGC AT

8--(sh)snub_V3--	TTT TTT TTT TTT TTT TTT TTT TAA CGT GGA TGG TCA ATA ACG ACG TTG TAA TCC ACT ATT AAA G
9--snub--	AAC GAC GGC CGG AAC AAG AG
10--snub--	AAT TCC TTT TTA CAC AAC ATA TGC CTA ATG AGT TTT TTG AGC TAA CTG GTT G
11--snub--	CGA AAT TTT TCG GCA AAA TCT TCC AGT CGG GTT TTT AAA CC
12--(sh)snub_V3--	TTT TTT TTT TTT TTT TTT TTT TCG AGA TAG CAC ATT AAT TGC GTT GCG CTC CAA AAG AAT AGC C
13--snub--	ACT GCC CGC TCC TTA TAA AT
14--snub--	ACC CTA TTT TTA AGG GAG CCC GAC TAT TAT AGT TTT TTC AGA AGC AAC CGA A
15--snub_V3--	GGC GAA AGC CGT AAA GCA CTA AAT TTT TGG GGT CG
16--snub--	GGG CAA TTT TTC AGC TGA TTG CAA GCG GTC CAT TTT TCG CTG GTT TGG GTT C
17--(sh)snub_V3--	TTT TTT TTT TTT TTT TTT TTT TAG GTA TCC TGT TTG ATG GTC CCC AGC A
18--snub--	TGG ATT TTT TTA TTT ACA TTG AAA GGG ACA TTT TTT TCT GGC CAA CAA GAA T
19--snub--	ACG TGG TTT TTC ACA GAC AAT TTA CCT TTT TTT TTT TAA TGG
20--(th)snub_V3--	TTT TTT TTT TTT TTT TTT TTT TAC GTG ACC TGA AAG CGT AGA GAT AGA
21--snub_V3--	ACC CTT CAG TAG ATT TAG TTT GAC CCA ATT CTG CGA
22--snub_V3--	GCT CAA TTT TTC ATG TTT TAA CAT TCC ATA TAT TTT TAC AGT
23--(th)snub_V3--	TTT TTT TTT TTT TTT TTT TTT TTA CCG GTG TCT GGA AGT TTA TAT GCA A
24--snub_V3--	CTA AAG TAC GAA CGA ACC ACC AGC GCC ATT AAA AA

25--snub_V3--	AAA CAT TTT TTC AAG AAA ACA GAA CTG ATA GCT TTT TCC TAA AAC ATC AGA A
26--snub_V3--	GAT AAA TTT TTA CAG AGG TGA ATC GGG AGA AAT TTT TCA ATA
27--snub_V3--	AAT CTA AAT TGC TGA ATA TAA TGG ATG GCT TAG A
28--(th)snub_V3--	TTT TTT TTT TTT TTT TTT TTT TGC TTA AGC ATC ACC TTG CTG AAA TGA AA
29--snub--	GCT GAG TTT TTA GCC AGC AGC AAC CTC AAA TAT TTT TTC AAA
30--snub--	GCC TGG CTC GAA TTC GTT TTT TAA TCA TGG TCT CAC
31--snub_V3--	ACC AGT CGA TCC CCG GGT ACC GAC AGG TCG ACT C
32--(th)snub_V3--	TTT TTT TTT TTT TTT TTT TTT TTA GAG ACA CGA CCA GTA ATA GCA GAT TC
33--snub_V3--	GAA CAA TGT GAA ATT GTT ATC CGC ATA GCT GTT TC
34--snub--	CTA TAT TTT TTG TAA ATG CTG CAA ACT ATC GGT TTT TCC TTG CTG GTT GCA A
35--snub--	CAG GAA TTT TTA AAC GCT CAT ACA TAG CGA TAT TTT TGC TTA
36--(th)snub_V3--	TTT TTT TTT TTT TTT TTT TTT TCT GTA TTA CCG CCA GCC ATA ATA TCC A
37--snub_V3--	CCA TCA CAG TGT AAA GCC TGG GGC GAG CCG GAA GCA
38--snub--	AGG CCA TTT TTC CGA GTA AAA TAG CAA TAC TTT TTT TCT TTG
39--(th)snub_V3--	TTT TTT TTT TTT TTT TTT TTT TTA AGC AAA TTA ACC GTT GGA GTC TGT
40--snub--	GTC TTT ACC CTC CGA TTT AGA G
41--(th)snub_V3--	TTT TTT TTT TTT TTT TTT TTT TAA GCC GGC GGA CCA TAA ATC AAA AAT CAG CTT GAC GGG GA
42--snub--	TTC AGA TTT TTA AAC GAG AAT AAC GTG GCG AGT TTT TAA AGG
43--snub_V3--	TAC ATT TAA GAT TAA GAG GAA GCA GCG GAT TGC AT

44--snub--	ATA TAA TTT TTT CCT GAT TGT ACT AAT AGA TTT TTT TAG AGC CGT CAT TAG A
45--snub--	CTT TAC TTT TTA AAC AAT TCG TTA TTA ATT TTT TTT TAA AAG
46--(th)snub_V3--	TTT TTT TTT TTT TTT TTT TTT TCA AAG AGG ATT TAG AAG TAA TAG ATA A
47--(th)snub_V3--	TTT TTT TTT TTT TTT TTT TTT TTC CAA AGC GAA CCA GAC CGT TTT AAT
48--snub_V3--	TCG AGC TTA GTT GGC AAA TCA ACA ATC AAT ATC TGG
49--snub_V3--	CCC TCA GTT GAA AGG ATT TTT ATT GAG GAA GAG AAC
50--snub--	TGT CGG GGG AGA GGC GTT TTT GTT TGC GTA TGA GAC
51--(th)snub_V3--	TTT TTT TTT TTT TTT TTT TTT TGA GGA ATC GGC CAA CGC GCT GCC AGC T
52--snub_V3--	GCA TTA ATA AGT GTT TTT ATA ATC GCC AGA ATC CT
53--snub_V3--	TTG AAA TTT TTT ACC GAC CGT GGA TTT TAG ACT TTT TAG GAA CGG TAC AGT G
54--snub_V3--	TGC TTT GTT TTC TTT TCA CCA GTT GGG CGC CAG GG
55--snub--	TTT AAC TTT TTA ACG CCA ACA ATG CGC CGC TAT TTT TCA GGG CGC GTG TGC T
56--snub--	TTC CTC TTT TTG TTA GAA TCA ACC GGA ATC ATT TTT TAA TTA
57--(th)snub_V3--	TTT TTT TTT TTT TTT TTT TTT TTG GTA CGA GCA CGT ATA ACA CTA TGG T
58--snub_V3--	GAA AGG ACC TGA GAG AGT TGC AGC CCT TCA CCG CC
59--snub--	AAG GGC TGG CAA GTG TTT TTT AGC GGT CAC GTA ATA
60--(th)snub_V3--	TTT TTT TTT TTT TTT TTT TTT TTG GCG CGG GCG CTA GGG CGA AGA AAG C
61--snub--	TTC ATT TGA AAT TTT TGA AT

62--(th)snub_V3--	TTT TTT TTT TTT TTT TTT TTT TTT TAA CAA TGG CTA TTA GTC TTT AAT GCG CAA ATT AAT TAC A
63--snub--	AAA CAT TGC TTC TGT ATT TTT AAT CGT CGC TTG AAA
64--snub--	ATC CTT GAA AGG AAA TAC CT
65--(sh)snub_V3--	TTT TTT TTT TTT TTT TTT TTT TCC CTT AGA ACA TTT TGA CGC TCA ATC GTC ATT AAT TAA TTT T
66--snub--	AAA GAA CGC GTA ATA ACA TC
67--snub--	ATT AGA GAA AAC TTT TTT TTT TCA AAT ATA TAT GGT
68--(th)snub_V3--	TTT TTT TTT TTT TTT TTT TTT TTC GCA AGA CAC TTG CCT GAG TAG AAG AAC TAT GCA AAT CCA A
69--(sh)snub_V3--	TTT TTT TTT TTT TTT TTT TTT TCG TTA AAT TAA ACA GGA GGC CGA TTA AAG GTG ATA AAT AAG G
70--snub--	AAG AAT AAA CGA GCG GGA GC
71--snub--	TTC GAG CCA GCT GCG CGT AA
72--snub--	AGA GAA TTT TTT ATA AAG TAC CCA ATA CTG CGT TTT TGA ATC GTC ATA ACA G
73--(th)snub_V3--	TTT TTT TTT TTT TTT TTT TTT TGA GGC ATT CCA CCA CAC CCG CCG CGC TTA TGT AAT TTA GGC A
74--(sh)snub_V3--	TTT TTT TTT TTT TTT TTT TTT TAA TGC TTT AAA ATA TTC ATT GAA TCT CCT TTG C
75--snub_V3--	CCG AAC GAC AAC TCG TAT TAA ACC CCT CA
76--snub--	TGG AAG GGT TGT TAT CTA AA
77--snub--	CTA CCA TTT TTT ATC AAA ATT GTA GAT TTT CAT TTT TGG TTT AAC GTG CCA C
78--(th)snub_V3--	TTT TTT TTT TTT TTT TTT TTT TTC TGA ATA AAT ATC TTT AGG AGC ACT AAC ATT GGA TTA TAC T

79--(sh)snub_V3--	TTT TTT TTT TTT TTT TTT TTT TTG CAA CAG TCA GAT GAA TAT ACA GTA ACA GAT TAA CAC CGC C
80--snub--	TAC CTT TTA CGG CGG TCA GT
81--snub--	AAT TGA TTT TTG TTA AGC CCA ATA GCT ATC TTT TTT TAC CGA AGC CCA GTT A
82--snub--	CCA GAA TTT TTG GAA ACC GAG AAT AGG AAC CCT TTT TAT GTA
83--snub--	CCG TAA ACG CCT GTA GTT TTT CAT TCC ACA GAC AAG
84--snub--	TAA CAT TTT TTA AAA ACA GGG ACC CTG AAC AAT TTT TAG TCA
85--snub--	GAG GGG TTT TGT CGT CTT TTT TTT CCA GAC GGC TAA
86--snub--	ACA ACT TTT TTT TCA ACA GTT AGA AAC GAT TTT TTT TTT TGT TTA ACG AGA A
87--snub--	TTT TAT TTT TTC CTG AAT CTT TAA TTT GCC AGT TTT TTT ACA AAA TAA AGG A
88--snub--	ATT GCG TTT TTA ATA ATA ATT CTC CAA AAG GAT TTT TGC CTT
89--snub--	TAA TTA ATT TCT TAA ATT TTT CAG CTT GAT ATA CAA
90--snub--	AGG TTT TTT TTT GAA GCC TTA TCG CCC ACG CAT TTT TTA ACC GAT ATA GGC C
91--snub--	GCT TTT TTT TTG CGG GAT CGT CAT CGT AGG AAT TTT TTC ATT
92--snub--	AAA CCA TTT TTA TCA ATA ATC GTA TTA AAC CAT TTT TAG TAC CGC ACG AGG G
93--snub--	TAG CAA TTT TTC GGC TAC AGA GAA GTT TCC ATT TTT TTA AAC
94--snub--	GGG TAC CTA AAA CGA ATT TTT AGA GGC AAA ATG TAG
95--snub--	AAT AAA TTT TTC AAC ATG TTC AAT AGA TAA GTT TTT TCC TGA
96--snub--	ACA AGA GCG ATT ATA CTT TTT CAA GCG CGA ACT GAT
97--snub--	AAA TTG TTT TTT GTC GAA ATC AAA GAA GTT TTT TTT TGC CAG AGG GGA CGA C
98--snub--	CGT TTA TTT TTC CAG ACG ACG GAG GCG CAG ACT TTT TGG TCA

99--snub--	ATC ATG GAC AGA TGA ATT TTT CGG TGT ACA GAA GAG
100--snub--	TAA TCT TTT TTT GAC AAG AAC TAC ATA ACG CCT TTT TAA AAG GAA TTA CCC T
101--snub--	AAT AAT AGA AAG ATT CTT TTT ATC AGT TGA GAG CTG
102--snub--	CTC ATT TTT TTC AGT GAA TAA GTA GTA AAT TGT TTT TGG CTT GAG ATT ACC T
103--snub--	TAT GCG TTT TTA TTT TAA GAA AAG AAA AAT CTT TTT TAC GTT
104--(sh)snub_V3--	TTT TTT TTT TTT TTT TTT TTT TCT CAG TAC GCA GCA CCG TAA TCA GTA GCG TAG CGG GGT TTT G
105--snub--	AAT GAA TTT TTA CCA TCG ATA CAG GCG GAT AAT TTT GTG CC
106--snub--	GTC GAA CAA AAG GGC GTT TTT ACA TTC AAC CAT TAT
107--snub--	TCA TTA TTT TTA AGG TGA ATT TAG AGC CAG CAT TTT TAA ATC ACC AGT CAC C
109--(sh)snub_V3--	TTT TTT TTT TTT TTT TTT TTT TAG TAT AGC CCG GAA TAG GAG AAA ATT CAT ATG GTT TAC CAT A
108--snub--	AGC GCC AAA GGA GGG TTG AT
110--snub--	CAT AAA TTT TTG GTG GCA ACA GTT TAT TTT GTT TTT TCA CAA TCA ATT GTA T
111--snub--	CAC CGT TTT TAC TCA GGA GGC AGA ACC GCC ATT TTT CCC TC
112--snub--	AGA GCA CTG GCA TGA TTT TTT TAA GAC TCC TAC ATA
113--(sh)snub_V3--	TTT TTT TTT TTT TTT TTT TTT TGC CTC AGA ACC GCC ACC CTT TTA GTA C
114--snub_V3--	CGC CAC CCC GTA TAA ACA GTT AAT TGA GTA ACA GT
115--snub--	TAC CCA AAA GAC ACC ACC CTC A
116--(th)snub_V3--	TTT TTT TTT TTT TTT TTT TTT TTA ACG GAA TTT TCA GGG ATA GCA AGC CCG AAA CGC AAT AA

117--(th)snub_V3--	TTT TTT TTT TTT TTT TTT TTT TCA GAC CAG TAC AAA CTA CAC ACT GAG
118--snub_V3--	TTT CGT CGA GTG TAC TGG TAA TAG CTT TTG ATG ATA
119--snub--	GAG ATA ACC CAC AGC CCT CA
120--(th)snub_V3--	TTT TTT TTT TTT TTT TTT TTT TAA TAT CAG ATA GTT AGC GTA ACG ATC TAA ATA ATT GAG CGC T
121--snub_V3--	AAA GCG CAT CTG TAT GGG ATT TTT TAG TAA ATG AA
122--(th)snub_V3--	TTT TTT TTT TTT TTT TTT TTT TTT TGT CTC TGA ATT TAC CGC AGA ATG G
123--snub--	AAT CCA AAT ATC AGC GGA GT
124--(sh)snub_V3--	TTT TTT TTT TTT TTT TTT TTT TTT TAT CCC GAG AAT AGA AAG GAA CAA CTA AAC AGC CAT ATT A
125--(th)snub_V3--	TTT TTT TTT TTT TTT TTT TTT TTT GGT CTC CAA AAA AAA GGT TTT CAC G
126--snub_V3--	TTG AAA ACC TTG ATA TTC ACA AAC AGG TCA GAC GA
127--snub_V3--	CGC CAC CCC TTG CTT TCG AGG TGG TAT CGG TTT A
128--(th)snub_V3--	TTT TTT TTT TTT TTT TTT TTT TTC AGT CAG AAC CGC CAC CCT CTC AGA GC
129--snub--	TGC ACC CAG CCC GAT AGT TG
130--(th)snub_V3--	TTT TTT TTT TTT TTT TTT TTT TCC GAC AAT GAC AAC AAC CAA ATC AAG ATT AGT TGC TAT TTC G
131--snub_V3--	ATA ATC AAC TTG CAG GGA GTT AAA TTC GGT CGC TG
132--(th)snub_V3--	TTT TTT TTT TTT TTT TTT TTT TAG GAA TCA CCG GAA CCA GAA TCT TTT C
133--snub--	TTT TTA TTT TCA CCC TCA GC
134--(sh)snub_V3--	TTT TTT TTT TTT TTT TTT TTT TAT CGG AAC TCA TCG AGA ACA AGC AAG CCG AGC GAA AGA CAG C

135--snub_V3--	TTT TCA TCA GAC TTT TTC ATG AGG GCT TTG AGG AC
136--(th)snub_V3--	TTT TTT TTT TTT TTT TTT TTT TTA AGG CAT TTT CGG TCA TAG TAG CGC G
137--(th)snub_V3--	TTT TTT TTT TTT TTT TTT TTT TCA TTC TAC GAA GGC ACC AAA AAT ACG T
138--snub_V3--	AAT GCC AAG CAA GGC CGG AAA CGT AGC ACC ATT AC
139--snub--	TTT ACG AGC AGA ATA CAC TA
140--(th)snub_V3--	TTT TTT TTT TTT TTT TTT TTT TCC ATC CTA AAA ACA CTC ATC TTT GAC CCC CAA AAA TAA TAT C
141--(th)snub_V3--	TTT TTT TTT TTT TTT TTT TTT TGA CTG ATT TGT ATC ATC GCA CAA AGT A
142--snub_V3--	CAA CGG ATG AGC CAT TTG GGA ATA TCA CCG TCA CC
143--snub--	GGC TTT TGC ACG CGA CCT GC
144--(sh)snub_V3--	TTT TTT TTT TTT TTT TTT TTT TAT AGC GAG ATC CAT GTT ACT TAG CCG GAA CAT AAA AAC CAA A
145--snub_V3--	GAG GGA AGA CCA ACT TTG AAA GAA AGG GAA CCG AAC
146--(th)snub_V3--	TTT TTT TTT TTT TTT TTT TTT TTG GTA AAT ATT GAC GGA AGA TTG AGG
147--snub_V3--	AAA CGC AAT GGC TGA CCT TCA TCA CCA GGC GCA TA
148--(th)snub_V3--	TTT TTT TTT TTT TTT TTT TTT TGG CAG ACA CCA CGG AAT AAT ATA AAA G
149--snub--	CTA ATG CAG ACG GAT ATT CA
150--(th)snub_V3--	TTT TTT TTT TTT TTT TTT TTT TCG TAA CAA ATT TAG GAA TAC CAC ATT CAA TTA CCC AAA TCA A
151--(th)snub_V3--	TTT TTT TTT TTT TTT TTT TTT TTG TTG AAA CAC CAG AAC GAG GCT TGC C
152--snub_V3--	CTG ACG AAG CAA ACG TAG AAA ATT ATT ACG CAG TA

153--(sh)snub_V3--	TTT TTT TTT TTT TTT TTT TTT TTG TGA ATG GTT TAA TTT CAA CTG CAG ATA G
154--snub--	CCG AAC AAT TTT TAA GAA AAG TAA TTA ATC AT
155--snub--	ACA GAA TCA AGG ATT AGG AT
156--snub--	GAG AAG TTT GCC TTT ATT TTT GCG TCA GAC TGC CCC
157--snub--	CTT ATT TTT TTA GCG TTT GCC GCC ACC ACC GGT TTT TAA CCG CCT CCC AGA G
158--snub--	CCA CCA TTT TTC CCT CAG AGC GGC TGA GAC TCT TTT CTC AA
159--(sh)snub_V3--	TTT TTT TTT TTT TTT TTT TTT TTA TTA AGA CGC CAC CAG AAC CAC CAC CAG TGA AAC ATG AAA G
160--snub--	AGC CGC CGC CCC TAT TAT TC
161--snub--	GTG CCT GCC CCC TGC CTT TTT ATT TCG GAA AGC AT
162--snub--	TGA CAG TTT TTG AGG TTG AGG CAA ATA AAT CCT TTT TTC ATT AAA GCT TCC A
163--snub--	GTA AGC TTT TTG TCA TAC ATG AGT TTT AAC GGT TTT TGG TCA
164--(sh)snub_V3--	TTT TTT TTT TTT TTT TTT TTT TAC CGA AAT AAA GAA ATT GCA TTT GCA C
165--snub_V3--	GTA AAA CAA GTC AGG ACG TTG GGC TGG CTC ATT AT
166--snub--	GAT TAA AAA TCA TAG GTT TTT TCT GAG AGA CTA TAA
167--snub_V3--	GTT TTA GGG CTT AGG TTG GGT TAT ACC TTT TTA AC
168--snub--	ACC GCG CTT ATC CGG TTT TTT ATT CTA AGA AGC GGG
169--(th)snub_V3--	TTT TTT TTT TTT TTT TTT TTT TCT CCC GAA CCT CCC GAC TTC GCG AGG C
170--snub--	CTA GAA ATT CTT ACC ATT TTT GTA TAA AGC CCC ATA
171--(th)snub_V3--	TTT TTT TTT TTT TTT TTT TTT TAA CGG CTT AAT TGA GAA TCG AAC GCT CA
172--snub_V3--	ACA GTA GGC GCC TGT TTA TCA ACA GCT AAT GCA G

173--snub--	TTT GAA CCA GAA GGA GTT TTT CGG AAT TAT CCA TCA
174--snub_V3--	AAC GGA ATC AGA TGA TGG CAA TTA TCA TAT TCC TG
175--(th)snub_V3--	TTT TTT TTT TTT TTT TTT TTT TAT TAC AAC ATT ATT ACA GGA ACG AAC T
176--snub--	ACG GAA ATC GCG CAG ATT TTT GGC GAA TTA TGA AAC
177--snub_V3--	TAG ACG GAG CAA AAG AAG ATG ATT CAT TTC AAT TAC
178--(th)snub_V3--	TTT TTT TTT TTT TTT TTT TTT TCT GGA GAA TTA ACT GAA CAA GCG CAT
179--snub_V3--	ATC AAT ATA GCA GCC TTT ACA GAG TCA AAA ATG AA
180--(sh)snub_V3--	TTT TTT TTT TTT TTT TTT TTT TAA TAT GTG AGT GAA TAA CCG TAC ATA A
181--(sh)snub_V3--	TTT TTT TTT TTT TTT TTT TTT TCA TTC TGA CCT AAA TTT ATT TAG TTA
182--snub_V3--	ATTTCATCAATCAGATATAGAAGGCCCAATAGCAAG
183--snub--	TGG ATA GCG TCG ACA AAA GG
184--(sh)snub_V3--	TTT TTT TTT TTT TTT TTT TTT TTC CAG ACG GTA ATA GTA AAA TGT TTA GAC TAA AGT AAT TCT G
185--snub_V3--	ATCATTTTAGCAACACTATCATAACGAGGCATAG
186--(sh)snub_V3--	TTT TTT TTT TTT TTT TTT TTT TTA AGG CGG AAC AAA GAA ACC GTA ACA TT
187--snub_V3--	ATTGCTTTAACAATGAAATAGCAATAATAAGAGCA
188--(sh)snub_V3--	TTT TTT TTT TTT TTT TTT TTT TAG AGA ATA CCA AGT TAC AAT TCG CCT G
189--(sh)snub_V3--	TTT TTT TTT TTT TTT TTT TTT TGA GCA ATA GTG AAT TTA TCA GAC GCT G
190--snub_V3--	AGAAGAGTCGTCTTTCCAGAGCCACCAACGCTAAC

191--snub_V3--	TTCCTTATCATATGCGTTATACAAAAAGCCTGTTT
192--(sh)snub_V3---	TTT TTT TTT TTT TTT TTT TTT TAG TAT CAT TCC AAG AAC GGG GCT GTC T

APPENDIX C

SUPPLEMENTARY INFORMATION FOR CHAPTER 3

1. GFP aptamer sequences

Strand name	Type	Sequence (5'-3')
aptGFP-sense	Sense	TTC TAATACGACTCACTATAG GGAGGGAGGGAGGGAGGGA GGGAGA AGCTTCTGGACTGCGATGGGAGCACGAAACGTCGTGGCGCAATT GGGTGGGGAAAGTCCTTAAAAGAGGGCCACCACAGAAGCT TCTCCC
aptGFP-antisense	Anti-sense	GGGAGAAGCTTCTGTGGTGGCCCTCTTTTAAGGACTTTCCCCAC CCAATTGCGCCACGACGTTTCGTGCTCCCATCGCAGTCCAGAAG CT TCTCCC TCCCTCCCTCCCTCCCTCC CTATAGTGAGTCGTATTA GAA
flex-aptGFP-sense	Sense	TTC TAATACGACTCACTATAG GGAGGGAGGGAGGGAGGGA AAAAAAAAAAAAAAAAAAAA GGGAGA AGCTTCTGGACTGCGATGGGAGCACGAAACGTCGTGGCGCAATT GGGTGGGGAAAGTCCTTAAAAGAGGGCCACCACAGAAGCT TCTCCC
flex-aptGFP-antisense	Anti-sense	GGGAGAAGCTTCTGTGGTGGCCCTCTTTTAAGGACTTTCCCCAC CCAATTGCGCCACGACGTTTCGTGCTCCCATCGCAGTCCAGAAG CT TCTCCC TTTTTTTTTTTTTTTTTTTT CCCTCCCTCCCTCCCTCC CTATAGTGAGTCGTATTA GAA
aptGFP_Fwd	Primer (Tm = 59.44°C)	TTCTAATACGACTCACTATAGGGAGGGAGG
aptGFP_Rev	Primer (Tm = 56.71°C)	GGGAGAAGCTTCTGTGGTGG
aptGFP-Biotin-linker	Biotin-linker	TCCCTCCCTCCCTCCCTCCC TTTT-Biotin

2. DNA sequence annotation for aptGFP and flex-aptGFP

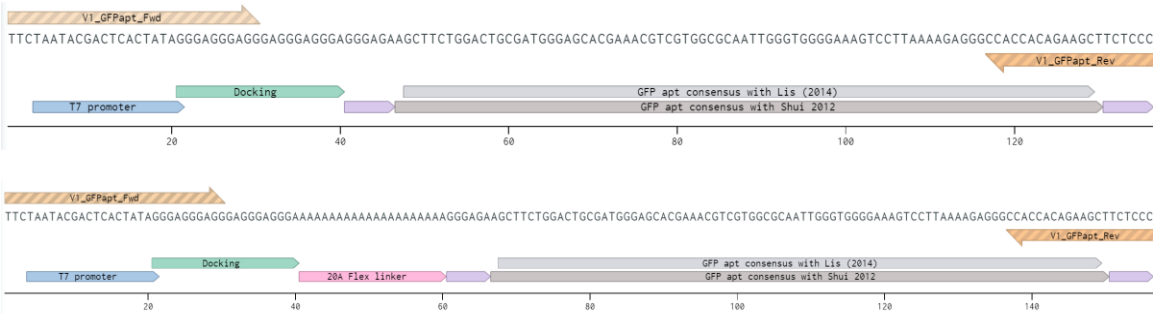

3. Handle sequences for SC36H

S.N.	Handle position	Sequence
1	20	TTTTTTTTTTTTTTTTTTTTACGTGACCTGAAAGCGTAGAGATAGA
2	23	TTTTTTTTTTTTTTTTTTTTACCGGTGTCTGGAAGTTTATATGCAA
3	28	TTTTTTTTTTTTTTTTTTTTGCTTAAGCATCACCTTGCTGAAATGAAA
4	32	TTTTTTTTTTTTTTTTTTTTAGAGACACGACCAGTAATAGCAGATTC
5	36	TTTTTTTTTTTTTTTTTTTTCTGTATTACCGCCAGCCATAATATCCA
6	39	TTTTTTTTTTTTTTTTTTTTAAGCAAATTAACCGTTGGAGTCTGT

7	41	TTTTTTTTTTTTTTTTTTTTTAAGCCGGCGGACCATAAATCAAAAATCAGCTTGACGGGGA
8	46	TTTTTTTTTTTTTTTTTTTTCAAAGAGGATTTAGAAGTAATAGATAA
9	47	TTTTTTTTTTTTTTTTTTTTTCCAAAGCGAACCAGACCGTTTTAAT
10	51	TTTTTTTTTTTTTTTTTTTTGAGGAATCGGCCAACGCGCTGCCAGCT
11	57	TTTTTTTTTTTTTTTTTTTTTGGTACGAGCACGTATAACACTATGGT
12	60	TTTTTTTTTTTTTTTTTTTTTGGCGCGGGCGCTAGGGCGAAGAAAGC
13	62	TTTTTTTTTTTTTTTTTTTTTTAACAATGGCTATTAGTCTTTAATGCGCAAATTAATTACA
14	68	TTTTTTTTTTTTTTTTTTTTTCGCAAGACACTTGCCTGAGTAGAAGAACTATGCAAATCCAA
15	73	TTTTTTTTTTTTTTTTTTTTGAGGCATTCCACCACACCCGCCGCGCTTATGTAATTTAGGCA
16	78	TTTTTTTTTTTTTTTTTTTTCTGAATAAATATCTTTAGGAGCACTAACATTGGATTATACT
17	116	TTTTTTTTTTTTTTTTTTTTAACGGAATTTTCAGGGATAGCAAGCCCGAAACGCAATAA
18	117	TTTTTTTTTTTTTTTTTTTTCAGACCAGTACAAACTACACACTGAG
19	120	TTTTTTTTTTTTTTTTTTTTAATATCAGATAGTTAGCGTAACGATCTAAATAATTGAGCGCT
20	122	TTTTTTTTTTTTTTTTTTTTTGTCTCTGAATTTACCGCAGAATGG
21	125	TTTTTTTTTTTTTTTTTTTTGGTCTCCAAAAAAAAGGTTTTCACG
22	128	TTTTTTTTTTTTTTTTTTTTCAGTCAGAACCGCCACCCTCTCAGAGC
23	130	TTTTTTTTTTTTTTTTTTTTCCGACAATGACAACAACCAAATCAAGATTAGTTGCTATTTCG
24	132	TTTTTTTTTTTTTTTTTTTTAGGAATCACCGGAACCAGAATCTTTTC
25	136	TTTTTTTTTTTTTTTTTTTTAAGGCATTTTCGGTCATAGTAGCGCG
26	137	TTTTTTTTTTTTTTTTTTTTCATTCTACGAAGGCACCAAAAATACGT
27	140	TTTTTTTTTTTTTTTTTTTTCCATCCTAAAAACACTCATCTTTGACCCCCAAAAATAATATC
28	141	TTTTTTTTTTTTTTTTTTTTGACTGATTTGTATCATCGCACAAAGTA
29	146	TTTTTTTTTTTTTTTTTTTTGGTAAATATTGACGGAAGATTGAGG
30	148	TTTTTTTTTTTTTTTTTTTTGGCAGACACCACGGAATAATATAAAAG
31	150	TTTTTTTTTTTTTTTTTTTTCGTAACAAATTTAGGAATACCACATTCAATTACCCAAATCAA
32	151	TTTTTTTTTTTTTTTTTTTTGTTGAAACACCAGAACGAGGCTTGCC
33	169	TTTTTTTTTTTTTTTTTTTTCTCCCGAACCTCCCGACTTCGCGAGGC
34	171	TTTTTTTTTTTTTTTTTTTTAACGGCTTAATTGAGAATCGAACGCTCA
35	175	TTTTTTTTTTTTTTTTTTTTATTACAACATTATTACAGGAACGAACT
36	178	TTTTTTTTTTTTTTTTTTTTCTGGAGAATTAACTGAACAAGCGCAT

4. Handle sequences for SC24H

S.N.	Handle position	Sequence
1	4	TTTTTTTTTTTTTTTTTTTTCACTACGTAGGATTAGAGAGTACCTTTAACAGGGCGATGGCC
2	8	TTTTTTTTTTTTTTTTTTTTAACGTGGATGGTCAATAACGACGTTGTAATCCACTATTAAAG
3	12	TTTTTTTTTTTTTTTTTTTTCGAGATAGCACATTAATTGCGTTGCGCTCCAAAAGAATAGCC
4	17	TTTTTTTTTTTTTTTTTTTTAGGTATCCTGTTTGATGGTCCCCAGCA
5	65	TTTTTTTTTTTTTTTTTTTTCCCTTAGAACATTTTGACGCTCAATCGTCATTAATTAATTTT
6	69	TTTTTTTTTTTTTTTTTTTTCGTTAAATTAAACAGGAGGCCGATTAAAGGTGATAAATAAGG
7	74	TTTTTTTTTTTTTTTTTTTTAATGCTTTAAAATATTCATTGAATCTCCTTTGC
8	79	TTTTTTTTTTTTTTTTTTTTTGCAACAGTCAGATGAATATACAGTAACAGATTAACACCGCC
9	104	TTTTTTTTTTTTTTTTTTTTCTCAGTACGCAGCACCGTAATCAGTAGCGTAGCGGGGTTTTG
10	109	TTTTTTTTTTTTTTTTTTTTAGTATAGCCCGGAATAGGAGAAAATTCATATGGTTTACCATA
11	113	TTTTTTTTTTTTTTTTTTTTGCCTCAGAACCGCCACCCTTTTAGTAC
12	124	TTTTTTTTTTTTTTTTTTTTTTATCCCGAGAATAGAAAGGAACAACTAAACAGCCATATTA
13	134	TTTTTTTTTTTTTTTTTTTTATCGGAACTCATCGAGAACAAGCAAGCCGAGCGAAAGACAGC
14	144	TTTTTTTTTTTTTTTTTTTTATAGCGAGATCCATGTTACTTAGCCGGAACATAAAAACCAAA
15	153	TTTTTTTTTTTTTTTTTTTTGTGAATGGTTTAATTTCAACTGCAGATAG
16	159	TTTTTTTTTTTTTTTTTTTTATTAAGACGCCACCAGAACCACCACCAGTGAAACATGAAAG
17	164	TTTTTTTTTTTTTTTTTTTTACCGAAATAAAGAAATTGCATTTGCAC
18	180	TTTTTTTTTTTTTTTTTTTTAATATGTGAGTGAATAACCGTACATAA
19	181	TTTTTTTTTTTTTTTTTTTTCATTCTGACCTAAATTTATTTAGTTA
20	184	TTTTTTTTTTTTTTTTTTTTCCAGACGGTAATAGTAAAATGTTTAGACTAAAGTAATTCTG
21	186	TTTTTTTTTTTTTTTTTTTTAAGGCGGAACAAAGAAACCGTAACATT
22	188	TTTTTTTTTTTTTTTTTTTTAGAGAATACCAAGTTACAATTCGCCTG
23	189	TTTTTTTTTTTTTTTTTTTTGAGCAATAGTGAATTTATCAGACGCTG
24	192	TTTTTTTTTTTTTTTTTTTTAGTATCATTCCAAGAACGGGGCTGTCT

5. Handle sequences for SC12H

S.N.	Handle position	Sequence
1	4	TTTTTTTTTTTTTTTTTTTTCACTACGTAGGATTAGAGAGTACCTTTAACAGGGCGATGGCC
2	12	TTTTTTTTTTTTTTTTTTTTCGAGATAGCACATTAATTGCGTTGCGCTCCAAAAGAATAGCC
3	74	TTTTTTTTTTTTTTTTTTTTAATGCTTTAAAATATTCATTGAATCTCCTTTGC
4	79	TTTTTTTTTTTTTTTTTTTTTGCAACAGTCAGATGAATATACAGTAACAGATTAACACCGCC
5	104	TTTTTTTTTTTTTTTTTTTTCTCAGTACGCAGCACCGTAATCAGTAGCGTAGCGGGGTTTTG
6	113	TTTTTTTTTTTTTTTTTTTTGCCTCAGAACCGCCACCCTTTTAGTAC
7	144	TTTTTTTTTTTTTTTTTTTTATAGCGAGATCCATGTTACTTAGCCGGAACATAAAAACCAAA
8	153	TTTTTTTTTTTTTTTTTTTTGTGAATGGTTTAATTTCAACTGCAGATAG
9	180	TTTTTTTTTTTTTTTTTTTTAATATGTGAGTGAATAACCGTACATAA
10	181	TTTTTTTTTTTTTTTTTTTTCATTCTGACCTAAATTTATTTAGTTA
11	189	TTTTTTTTTTTTTTTTTTTTGAGCAATAGTGAATTTATCAGACGCTG
12	192	TTTTTTTTTTTTTTTTTTTTAGTATCATTCCAAGAACGGGGCTGTCT

6. Handle sequences for SC1H

S.N.	Handle position	Sequence
1	12	TTTTTTTTTTTTTTTTTTTTCGAGATAGCACATTAATTGCGTTGCGCTCCAAAAGAATAGCC

APPENDIX D

COPYRIGHT CLEARANCE FOR FIGURES IN CHAPTER 1

CCC Marketplace™

This is a License Agreement between Swechchha Pradhan ("User") and Copyright Clearance Center, Inc. ("CCC") on behalf of the Rightsholder identified in the order details below. The license consists of the order details, the CCC Terms and Conditions below, and any Rightsholder Terms and Conditions which are included below.

All payments must be made in full to CCC in accordance with the CCC Terms and Conditions below.

Order Date	17-Dec-2021	**Type of Use**	Republish in a journal/magazine
Order License ID	1169802-2		
ISSN	1098-5514	**Publisher**	AMERICAN SOCIETY FOR MICROBIOLOGY
		Portion	Image/photo/illustration

LICENSED CONTENT

Publication Title	Journal of virology : JVI	**Publication Type**	e-Journal
Article Title	Natural antibody and complement mediate neutralization of influenza virus in the absence of prior immunity.	**Start Page**	3487
		End Page	3494
		Issue	7
		Volume	81
Author/Editor	American Society for Microbiology.	**URL**	https://journals.asm.org/journal/jvi
Date	12/31/1970		
Language	English		
Country	United States of America		
Rightsholder	American Society for Microbiology - Journals		

REQUEST DETAILS

Portion Type	Image/photo/illustration	**Distribution**	Worldwide
Number of images / photos / illustrations	1	**Translation**	Original language of publication
Format (select all that apply)	Electronic	**Copies for the disabled?**	No
		Minor editing privileges?	No
Who will republish the content?	Author of requested content	**Incidental promotional use?**	No
Duration of Use	Life of current edition	**Currency**	USD
Lifetime Unit Quantity	Up to 499		
Rights Requested	Main product		

NEW WORK DETAILS

Title	A foray into the knowledge landscape of virus aggregation: The knowns and unknowns	**Publisher imprint**	N/A
		Expected publication date	2022-01-01
Author	Swechchha Pradhan	**Expected size (number of pages)**	24

CCC Marketplace™

This is a License Agreement between Swechchha Pradhan ("User") and Copyright Clearance Center, Inc. ("CCC") on behalf of the Rightsholder identified in the order details below. The license consists of the order details, the CCC Terms and Conditions below, and any Rightsholder Terms and Conditions which are included below.

All payments must be made in full to CCC in accordance with the CCC Terms and Conditions below.

Order Date	17-Dec-2021	**Type of Use**	Republish in a journal/magazine
Order License ID	1169802-3		
ISSN	1098-5514	**Publisher**	AMERICAN SOCIETY FOR MICROBIOLOGY
		Portion	Image/photo/illustration

LICENSED CONTENT

Publication Title	Journal of virology : JVI	**Rightsholder**	American Society for Microbiology - Journals
Article Title	Dissection of Epitope-Specific Mechanisms of Neutralization of Influenza Virus by Intact IgG and Fab Fragments.	**Publication Type**	e-Journal
		Issue	6
		Volume	92
Author/Editor	American Society for Microbiology.	**URL**	https://journals.asm.org/journal/jvi
Date	12/31/1970		
Language	English		
Country	United States of America		

REQUEST DETAILS

Portion Type	Image/photo/illustration	**Distribution**	Worldwide
Number of images / photos / illustrations	1	**Translation**	Original language of publication
Format (select all that apply)	Electronic	**Copies for the disabled?**	No
		Minor editing privileges?	No
Who will republish the content?	Author of requested content	**Incidental promotional use?**	No
Duration of Use	Life of current edition	**Currency**	USD
Lifetime Unit Quantity	Up to 499		
Rights Requested	Main product		

NEW WORK DETAILS

Title	A foray into the knowledge landscape of virus aggregation: The knowns and unknowns	**Publisher imprint**	N/A
		Expected publication date	2022-01-01
Author	Swechchha Pradhan	**Expected size (number of pages)**	24
Publication	Viruses	**Standard identifier**	N/A
Publisher	MDPI		

CCC Marketplace™

Order Date	17-Dec-2021	**Type of Use**	Republish in a journal/magazine
Order License ID	1169802-1		
ISSN	1098-6596	**Publisher**	AMERICAN ASSOCIATION FOR MICROBIOLOGY
		Portion	Image/photo/illustration

LICENSED CONTENT

Publication Title	Antimicrobial agents and chemotherapy : AAC	**Publication Type**	e-Journal
		Start Page	1810
Article Title	Identification of the minimal active sequence of an anti-influenza virus peptide.	**End Page**	1813
		Issue	4
		Volume	55
Author/Editor	American Society for Microbiology.	**URL**	https://journals.asm.org/journal/aac
Date	12/31/1971		
Language	English		
Country	United States of America		
Rightsholder	American Society for Microbiology - Journals		

REQUEST DETAILS

Portion Type	Image/photo/illustration	**Distribution**	Worldwide
Number of images / photos / illustrations	1	**Translation**	Original language of publication
Format (select all that apply)	Electronic	**Copies for the disabled?**	No
		Minor editing privileges?	No
Who will republish the content?	Author of requested content	**Incidental promotional use?**	No
Duration of Use	Life of current edition	**Currency**	USD
Lifetime Unit Quantity	Up to 499		
Rights Requested	Main product		

NEW WORK DETAILS

Title	A foray into the knowledge landscape of virus aggregation: The knowns and unknowns	**Publisher imprint**	N/A
		Expected publication date	2022-01-01
Author	Swechchha Pradhan	**Expected size (number of pages)**	24

CCC Marketplace™

This is a License Agreement between Arizona State University ("User") and Copyright Clearance Center, Inc. ("CCC") on behalf of the Rightsholder identified in the order details below. The license consists of the order details, the CCC Terms and Conditions below, and any Rightsholder Terms and Conditions which are included below.

All payments must be made in full to CCC in accordance with the CCC Terms and Conditions below.

Order Date	17-Dec-2021	**Type of Use**	Republish in a journal/magazine
Order License ID	1169800-1		
ISSN	1098-5530	**Publisher**	AMERICAN SOCIETY FOR MICROBIOLOGY
		Portion	Image/photo/illustration

LICENSED CONTENT

Publication Title	Journal of bacteriology : JB	**Publication Type**	e-Journal
Article Title	Effect of particle aggregation on the survival of irradiated vaccinia virus.	**Start Page**	1138
		End Page	1142
		Issue	4
Author/Editor	American Society for Microbiology.	**Volume**	90
		URL	https://journals.asm.org/journal/jb
Date	12/31/1915		
Language	English		
Country	United States of America		
Rightsholder	American Society for Microbiology - Journals		

REQUEST DETAILS

Portion Type	Image/photo/illustration	**Distribution**	Worldwide
Number of images / photos / illustrations	1	**Translation**	Original language of publication
Format (select all that apply)	Electronic	**Copies for the disabled?**	No
		Minor editing privileges?	No
Who will republish the content?	Publisher, not-for-profit	**Incidental promotional use?**	No
Duration of Use	Life of current edition	**Currency**	USD
Lifetime Unit Quantity	Up to 499		
Rights Requested	Main product		

NEW WORK DETAILS

Title	A foray into the knowledge landscape of virus aggregation: The knowns and unknowns	**Publisher imprint**	N/A
		Expected publication date	2022-01-01
		Expected size (number of pages)	24
		Standard identifier	N/A

CCC Marketplace™

This is a License Agreement between Arizona State University ("User") and Copyright Clearance Center, Inc. ("CCC") on behalf of the Rightsholder identified in the order details below. The license consists of the order details, the CCC Terms and Conditions below, and any Rightsholder Terms and Conditions which are included below.

All payments must be made in full to CCC in accordance with the CCC Terms and Conditions below.

Order Date	17-Dec-2021	**Type of Use**	Republish in a journal/magazine
Order License ID	1169800-2	**Publisher**	AMERICAN SOCIETY FOR MICROBIOLOGY
ISSN	1098-660X	**Portion**	Image/photo/illustration

LICENSED CONTENT

Publication Title	Journal of clinical microbiology : JCM	**Publication Type**	e-Journal
Article Title	Frequency of preclumped virus in routine fecal specimens from patients with acute nonbacterial gastroenteritis.	**Start Page**	982
		End Page	988
		Issue	5
		Volume	13
Author/Editor	American Society for Microbiology.	**URL**	https://journals.asm.org/journal/jcm
Date	12/31/1974		
Language	English		
Country	United States of America		
Rightsholder	American Society for Microbiology - Journals		

REQUEST DETAILS

Portion Type	Image/photo/illustration	**Distribution**	Worldwide
Number of images / photos / illustrations	1	**Translation**	Original language of publication
Format (select all that apply)	Electronic	**Copies for the disabled?**	No
		Minor editing privileges?	No
Who will republish the content?	Publisher, not-for-profit	**Incidental promotional use?**	No
Duration of Use	Life of current edition	**Currency**	USD
Lifetime Unit Quantity	Up to 499		
Rights Requested	Main product		

NEW WORK DETAILS

Title	A foray into the knowledge landscape of virus aggregation: The knowns and unknowns	**Publisher imprint**	N/A
		Expected publication date	2022-01-01

CCC Marketplace™

Order Date	17-Dec-2021	**Type of Use**	Republish in a journal/magazine
Order License ID	1169800-3		
ISSN	1098-5336	**Publisher**	AMERICAN SOCIETY FOR MICROBIOLOGY
		Portion	Image/photo/illustration

LICENSED CONTENT

Publication Title	Applied and environmental microbiology : AEM	**Publication Type**	e-Journal
		Start Page	523
Article Title	Membrane-associated viral complexes observed in stools and cell culture.	**End Page**	526
		Issue	2
		Volume	50
Author/Editor	American Society for Microbiology.	**URL**	https://journals.asm.org/journal/aem
Date	12/31/1975		
Language	English		
Country	United States of America		
Rightsholder	American Society for Microbiology - Journals		

REQUEST DETAILS

Portion Type	Image/photo/illustration	**Distribution**	Worldwide
Number of images / photos / illustrations	3	**Translation**	Original language of publication
Format (select all that apply)	Electronic	**Copies for the disabled?**	No
		Minor editing privileges?	No
Who will republish the content?	Publisher, not-for-profit	**Incidental promotional use?**	No
Duration of Use	Life of current edition	**Currency**	USD
Lifetime Unit Quantity	Up to 499		
Rights Requested	Main product		

NEW WORK DETAILS

Title	A foray into the knowledge landscape of virus aggregation: The knowns and unknowns	**Publisher imprint**	N/A
		Expected publication date	2022-01-01
		Expected size (number of pages)	24

CCC Marketplace™

This is a License Agreement between Arizona State University ("User") and Copyright Clearance Center, Inc. ("CCC") on behalf of the Rightsholder identified in the order details below. The license consists of the order details, the CCC Terms and Conditions below, and any Rightsholder Terms and Conditions which are included below.

All payments must be made in full to CCC in accordance with the CCC Terms and Conditions below.

Order Date	17-Dec-2021	**Type of Use**	Republish in a journal/magazine
Order License ID	1169800-4		
ISSN	1098-5514	**Publisher**	AMERICAN SOCIETY FOR MICROBIOLOGY
		Portion	Image/photo/illustration

LICENSED CONTENT

Publication Title	Journal of virology : JVI	**Publication Type**	e-Journal
Article Title	Vectorial release of poliovirus from polarized human intestinal epithelial cells.	**Start Page**	4274
		End Page	4282
		Issue	7
Author/Editor	American Society for Microbiology.	**Volume**	67
		URL	https://journals.asm.org/journal/jvi
Date	12/31/1970		
Language	English		
Country	United States of America		
Rightsholder	American Society for Microbiology - Journals		

REQUEST DETAILS

Portion Type	Image/photo/illustration	**Distribution**	Worldwide
Number of images / photos / illustrations	1	**Translation**	Original language of publication
Format (select all that apply)	Electronic	**Copies for the disabled?**	No
		Minor editing privileges?	No
Who will republish the content?	Publisher, not-for-profit	**Incidental promotional use?**	No
Duration of Use	Life of current edition	**Currency**	USD
Lifetime Unit Quantity	Up to 499		
Rights Requested	Main product		

NEW WORK DETAILS

Title	A foray into the knowledge landscape of virus aggregation: The knowns and unknowns	**Publisher imprint**	N/A
		Expected publication date	2022-01-01
		Expected size (number of pages)	24
		Standard identifier	N/A

CCC Marketplace™

Order Date	17-Dec-2021	**Type of Use**	Republish in a journal/magazine
Order License ID	1169800-5		
ISSN	1098-5336	**Publisher**	AMERICAN SOCIETY FOR MICROBIOLOGY
		Portion	Image/photo/illustration

LICENSED CONTENT

Publication Title	Applied and environmental microbiology : AEM	**Publication Type**	e-Journal
		Start Page	159
Article Title	Aggregation of poliovirus and reovirus by dilution in water.	**End Page**	167
		Issue	1
		Volume	33
Author/Editor	American Society for Microbiology.	**URL**	https://journals.asm.org/journal/aem
Date	12/31/1975		
Language	English		
Country	United States of America		
Rightsholder	American Society for Microbiology - Journals		

REQUEST DETAILS

Portion Type	Image/photo/illustration	**Distribution**	Worldwide
Number of images / photos / illustrations	1	**Translation**	Original language of publication
Format (select all that apply)	Electronic	**Copies for the disabled?**	No
		Minor editing privileges?	No
Who will republish the content?	Publisher, not-for-profit	**Incidental promotional use?**	No
Duration of Use	Life of current edition	**Currency**	USD
Lifetime Unit Quantity	Up to 499		
Rights Requested	Main product		

NEW WORK DETAILS

Title	A foray into the knowledge landscape of virus aggregation: The knowns and unknowns	**Publisher imprint**	N/A
		Expected publication date	2022-01-01
		Expected size (number of pages)	24

CCC Marketplace™

This is a License Agreement between Arizona State University ("User") and Copyright Clearance Center, Inc. ("CCC") on behalf of the Rightsholder identified in the order details below. The license consists of the order details, the CCC Terms and Conditions below, and any Rightsholder Terms and Conditions which are included below.

All payments must be made in full to CCC in accordance with the CCC Terms and Conditions below.

Order Date	16-Dec-2021	**Type of Use**	Republish in a journal/magazine
Order License ID	1169502-1		
ISSN	0022-1317	**Publisher**	Microbiology Society
		Portion	Image/photo/illustration

LICENSED CONTENT

Publication Title	The Journal of general virology	**Rightsholder**	Microbiology Society
		Publication Type	Journal
Article Title	Flavivirus infection enhancement in macrophages: an electron microscopic study of viral cellular entry.	**Start Page**	1969
		End Page	1982
		Issue	9
		Volume	66 (Pt 9)
Author/Editor	SOCIETY FOR GENERAL MICROBIOLOGY, FEDERATION OF EUROPEAN MICROBIOLOGICAL SOCIETIES.		
Date	12/31/1966		
Language	English		
Country	United Kingdom of Great Britain and Northern Ireland		

REQUEST DETAILS

Portion Type	Image/photo/illustration	**Distribution**	Worldwide
Number of images / photos / illustrations	1	**Translation**	Original language of publication
Format (select all that apply)	Electronic	**Copies for the disabled?**	No
		Minor editing privileges?	No
Who will republish the content?	Publisher, not-for-profit	**Incidental promotional use?**	No
Duration of Use	Current edition and up to 10 years	**Currency**	USD
Lifetime Unit Quantity	Up to 499		
Rights Requested	Main product		

NEW WORK DETAILS